

# Middle Ear Replication for Otological Studies

A Major Qualifying Project



Submitted to the Faculty of Worcester Polytechnic Institute  
In partial fulfilment of the requirements for the  
Degree in Bachelor of Science In  
Mechanical Engineering/Biomedical Engineering

By:

Sonya DeLorie  
Mickaela Gunnison  
Shannon O'Connor  
Sarah Piela  
Mary Scrivanich

Advisors:

Professor Sarah Wodin-Schwartz  
Professor Zoe Reidinger

Submitted on: March 3, 2022

*This report represents the work of WPI undergraduate students submitted to the faculty as evidence of a degree requirement. WPI routinely publishes these reports on its website without editorial or peer review. For more information about the projects program at WPI, see <http://www.wpi.edu/Academics/Projects>.*

## **Acknowledgements**

The authors thank and recognize Dr. Ivo Dobrev, who served as the project sponsor; Professors Sarah Wodin-Schwartz and Zoe Reidinger who served as project advisors; and the Universitätsspital Zürich Department of Otorhinolaryngology research team who supported project work.

## **Abstract**

The middle ear is a complex sensory organ crucial to the sensation of hearing. Current models of the middle ear used in otological studies display static anatomy. These models fail to capture dynamic sound propagation mechanisms, and thus fail to properly replicate the middle ear. This type of replication is a challenging task that requires an understanding of anatomy and physiology, digital three-dimensional modeling, materials science, additive manufacturing, and instrumentation. The following report discusses steps taken to begin accomplishing this task.

## **Authorship**

The authors have equally contributed to the report below. Sonya DeLorie, Shannon O'Connor, and Mary Scrivanich take the primary authorship roles for all sections related to digital modeling and reconstruction. Mickaela Gunnison and Sarah Piela take the primary authorship roles for all sections related to synthetic materials selection and testing instrumentation.

## Table of Contents

<b>Acknowledgements</b>	<b>1</b>
<b>Abstract</b>	<b>2</b>
<b>Authorship Page</b>	<b>3</b>
<b>Table of Contents</b>	<b>4</b>
<b>Table of Figures</b>	<b>6</b>
<b>Table of Tables</b>	<b>8</b>
<b>1.0 Introduction</b>	<b>9</b>
<b>2.0 Background</b>	<b>11</b>
2.1 Anatomy and Physiology of the Human Ear	11
2.1.1 The Middle Ear	12
2.1.1.1 The Tympanic Membrane (The Ear Drum)	12
2.1.1.2 The Ossicular Chain	12
2.1.1.3 The Oval Window	14
2.1.1.4 Support Structures	14
2.1.1.5 Role in Sound Perception	16
2.2 Sound Mechanics	17
2.3 Modeling and Reconstructing the Middle Ear	18
2.3.1 Current Methods for Teaching and Visualizing the Middle Ear	18
2.3.2 Process of Modeling and Reconstruction	19
2.4 Current Model	20
2.4.1 Review of Previous WPI Team's Work	20
<b>3.0 Project Strategy</b>	<b>22</b>
3.1 Initial Client Statement	22
3.2 Revised Client Statement	22
3.3 Design Requirements	23
3.3.1 Engineering Standards	26
3.4 Project Approach	27
<b>4.0 Design Process</b>	<b>28</b>
4.1 Needs Analysis	28
4.1.1 Static Model	28
4.1.2 Dynamic Model	29
4.2 Design Concept Prototyping	29
4.2.1 CAD Prototyping	29
4.2.2 Data Acquisition for Material Selection	31
4.2.2.1 Replicating the Ossicular Chain	33
4.2.2.2 Replicating the Ligaments, Tendons, Joints, and Membranes	38
4.3 Alternative Designs	43
4.3.1 Static Model	43
4.3.1.1 Design 1	43
4.3.1.2 Design 2	44
4.3.1.3 Design 3	45

4.3.1.4 Design 4 .....	46
4.3.1.5 Design 5 .....	47
4.3.2 Dynamic Model .....	49
4.3.2.1 First Iteration Digital Dynamic Model .....	50
4.3.2.2 Second Iteration Digital Dynamic Model .....	52
4.4 Final Design Selection .....	53
4.4.1 Dynamic Model Assembly .....	57
<b>5.0 Design Verification .....</b>	<b>61</b>
5.1 Materials Selection in the Dynamic Physical Model .....	61
5.1.1 Ossicular Chain Selection .....	62
5.1.2 Joint, Tendon, Ligament, and Membrane Selections .....	66
5.2 Verification of Static Model .....	70
5.3 Verification of Dynamic Model .....	71
<b>6.0 Design Validation .....</b>	<b>72</b>
6.1 Digital Modeling .....	72
<b>7.0 Discussion .....</b>	<b>74</b>
7.1 Static and Dynamic Model Limitations .....	74
7.2 Materials Selection in the Dynamic Physical Model .....	75
7.2.1 Hard Plastic Testing in Ossicular Chain Replication .....	75
7.2.2 Soft Plastic Testing in Compliant Primary Body Replication .....	76
7.2.3 Ligaments and Tendons in Physical Model Assembly .....	77
<b>8.0 Conclusion and Recommendations .....</b>	<b>81</b>
8.1 Material Selection .....	81
8.2 Dynamic Physical Model Assembly .....	81
8.3 Instrumenting the Dynamic Physical Model .....	82
8.4 Pathology Modeling .....	84
8.5 Broader Impacts .....	84
8.5.1 Environmental Impacts .....	84
8.5.2 Societal Influence .....	85
8.5.3 Ethical Concerns .....	85
8.5.4 Health and Safety Issues .....	85
8.5.5 Manufacturability .....	85
8.5.6 Sustainability .....	86
<b>References .....</b>	<b>87</b>
<b>Appendix A .....</b>	<b>92</b>
<b>Appendix B .....</b>	<b>93</b>
<b>Appendix C .....</b>	<b>99</b>
<b>Appendix D .....</b>	<b>100</b>
<b>Appendix E .....</b>	<b>103</b>
<b>Appendix F .....</b>	<b>104</b>
<b>Appendix G .....</b>	<b>107</b>

## Table of Figures

2.1 Anterior View of the Ear .....	11
2.2 Cadaver Ossicles .....	13
2.3 Anterior View of the Ossicular Chain .....	14
2.4 Ligament Locations .....	16
2.5 Pressure Variation of a Sound Wave .....	17
2.6 Longitudinal Wave Properties .....	18
2.7 2020 MQP Team Model .....	21
3.1 Objective and Sub-Objective Overview .....	23
3.2 Gantt Chart Example .....	27
4.1 Middle Ear Anatomy in Geomagic .....	30
4.2 Temporal Bone in Geomagic .....	30
4.3 Block Diagram for Replicating the Ossicular Chain .....	35
4.4 Experimental Set-Up for Replicating the Ossicular Chain .....	35
4.5 Waveform and FFT Graphs .....	36
4.6 Bode Plots for the Aluminum Beam .....	37
4.7 Experimental Set-Up for Replicating the Ligaments, Tendons, Joints, and Membranes .....	39
4.8 Raw Data for TPU Specimen .....	41
4.9 Processed Data for TPU Specimen .....	42
4.10 Static Model Design 1 in Geomagic .....	44
4.11 Static Model Design 1 in SolidWorks .....	44
4.12 Static Model Design 2 in Geomagic .....	45
4.13 Static Model Design 3 in Geomagic .....	46
4.14 Static Model Design 4 in Geomagic with and Without Surgical Cover .....	47
4.15 Isometric View of Final Static Model Without Surgical Cover .....	48
4.16 Surgical View of Final Static Model with Surgical Cover .....	48
4.17 Isometric View of Printed Final Static Model Without Surgical Cover .....	49
4.18 Surgical View of Printed Final Static Model with Surgical Cover .....	49
4.19 LEGO Hinge Clasp Mechanism .....	51
4.20 Dynamic Model Iteration 1 .....	52
4.21 Dynamic Model Iteration 2 .....	53
4.22 Dynamic Model Final Design in Geomagic .....	54
4.23 Physical Dynamic Model .....	55
4.24 Physical Connection of IMJ .....	56
4.25 Physical Connection of Membranes: Tympanic Membrane .....	56
4.26 Physical Connection of Membranes: Cochlea .....	57
4.27 Joint Connection of Malleus and Incus .....	59
4.28 Cochlea Membrane Connection with Magnets .....	59
4.29 Ear Canal Membrane Connection with Magnets .....	60
5.1 Marked PLA and ABS Beams .....	62
5.2 Bode Plots for First Trial PLA .....	63
5.3 Bode Plots for First Trial ABS .....	64

5.4 3D Printing Filaments Q Factors .....	65
5.5 MATLAB Generated Trendline to Calculate TPU Time Constant .....	66
5.6 MATLAB Generated Trendline to Calculate Silicone Time Constant .....	67
5.7 TPU and Silicone Q Factors Versus Compliant Primary Bodies .....	68
7.1 Experimental Set-Up for Compliant Materials Testing .....	77
8.1 Test Set-Up for Acoustically Stimulating the Dynamic Physical Model .....	83
8.2 Block Diagram of the Hardware to Measure Acoustic Stimulation .....	83

## Table of Tables

2.1 Common Ligaments .....	15
3.1 Objective 1: Digital and Physical Static Models .....	23
3.2 Objective 2: Digital Model for Dynamical Physical Model .....	24
3.3 Objective 3: Material Selection for Dynamic Physical Model .....	24
3.4 Objective 4: Dynamic Physical Model Assembly .....	24
3.5 Objective 5: Dynamic Physical Testing .....	25
3.6 Anatomical Lengths, Diameters, and Angles of Orientation for Primary Bodies .....	25
4.1 Material Properties of Primary Bodies .....	32
4.2 Material Properties for Traditional Printing Materials .....	33
4.3 Material Properties of Softer Materials .....	38
4.4 Pugh Concept Selection Matrix for Static Model .....	46
4.5 Pugh Concept Selection Matrix for Connection Points .....	50
5.1 Q Factors of Primary Bodies .....	61
5.2 Q Factor Data for All PLA and ABS Testing Trials .....	64
5.3 Pugh Concept Selection Matrix for Ossicle Replication .....	65
5.4 Pugh Concept Selection Matrix for the IMJ and Membranes .....	68
5.5 Pugh Concept Selection Matrix for Stiffer Ligaments and Tendons .....	69
5.6 Pugh Concept Selection Matrix for Softer Ligaments and Tendons .....	70
7.1 Stiffness Values for Each Compliant Primary Body .....	78
7.2 Stiffness Values for Each Compliant Primary Body based on Material Selection at 15:1 .....	79
7.3 Target Cross-Sectional Area and Diameter Based on Native Tissue Stiffness .....	79

## 1.0 Introduction

The Universitätsspital Zürich is a respected teaching hospital located in Zürich, Switzerland. The Department of Otorhinolaryngology (ORL) has an established academic partnership with Worcester Polytechnic Institute (WPI) to develop and improve dynamic models of the ear for their otology students. The ear is a complex, crucial sensory organ in the peripheral hearing system with three main segments: the outer ear, the middle ear, and the inner ear. The middle ear is the primary focus for the ORL research team. Through mechanical vibrations of three small auditory bones and surrounding connective tissue in the middle ear cavity, this system effectively transmits sound from the outer ear to the inner ear to generate the sensation of hearing (De Greef, 2016).

In 2020, a previous WPI undergraduate team completed a model of the middle ear at 15:1 scale which interchangeably modeled healthy and diseased hearing states (Kane et al., 2020). This project sought to address identified model limitations and advance promising design aspects. Due to time constraints, project scope was limited to healthy middle ear anatomy and physiology. The objectives below realize the overall goal of more accurate healthy middle ear replication.

1. Replicate healthy middle ear anatomy in a static format through digital and physical models
2. Design a digital model which can realize a physical model that dynamically demonstrates healthy middle ear anatomy and physiology
3. Identify suitable synthetic materials to replicate native tissue
4. Assemble a physical dynamic model of a healthy middle ear from the corresponding digital design and material selections
5. Acoustically stimulate the assembled, dynamic physical model to replicate healthy middle ear physiology

The first and second project objectives focused on creating digital models of the middle ear in both a static and dynamic state. Objective one also includes printing the static model. These models were designed in Geomagic based on a  $\mu$ CT scan and a digital anatomical middle ear model. Each model iteration was evaluated based on client feedback and budget constraints.

The third project objective aimed to choose synthetic materials that matched the mechanical properties and sound propagation mechanics of corresponding native tissues. It was thought that similar material selections would improve both the anatomical and physiological accuracy of the dynamic physical model. The evaluations were limited to materials in the plastic family. Stiffer plastics were identified for bone replication while softer plastics were considered for connective tissue replication. The mechanical properties of each identified plastic were evaluated using peer-reviewed literature databases while sound propagation mechanisms were experimentally determined. Testing analysis on the sound propagation mechanisms verified hard plastic selection. Geometry dependent properties validated soft plastic selection.

The fourth project objective was a culmination of the previous three aims: assembling the physical dynamic model of a healthy middle ear. Following the design and validation of the

digital design as well as material selection, the digital model was printed and assembled. The physical dynamic model gives a representation of the functionality and movement of the middle ear which can later be tested.

Due to time constraints, the project did not address the fifth project objective. Instead, a preliminary testing procedure for the dynamic physical model is thoroughly outlined in the final chapter. It is recommended that future projects investigate instrumenting and acoustically stimulating the dynamic physical model using this outlined procedure. Though the team did not consider pathology modeling, it is also recommended that future projects follow the project objectives listed above to accurately demonstrate common middle ear diseases and their associated hearing states.

## 2.0 Background

The following chapter reviews concepts relevant to replicating the middle ear as a dynamic, stimuli-sensitive model for the Universitätsspital Zürich.

### 2.1 Anatomy and Physiology of the Human Ear

The human ear is an essential sensory organ in the peripheral hearing system. The three primary sections of the ear, shown in Figure 2.1, are the outer, middle, and inner ears. The outer ear captures external acoustic vibrations and transmits them to the middle ear. The middle ear converts purely acoustic vibrations to acousto-mechanical vibrations. Three small auditory bones in the middle ear – the malleus, incus, and stapes – carry the vibrations to the inner ear, specifically the cochlea. Once the vibrations enter the cochlea, hair cells in the cochlear fluid convert them to electrochemical signals. The cochlear nerve carries the electrochemical signals to the central nervous system, thus generating the sensation of hearing (De Greef, 2016; I. Dobrev, personal communication, 2020).

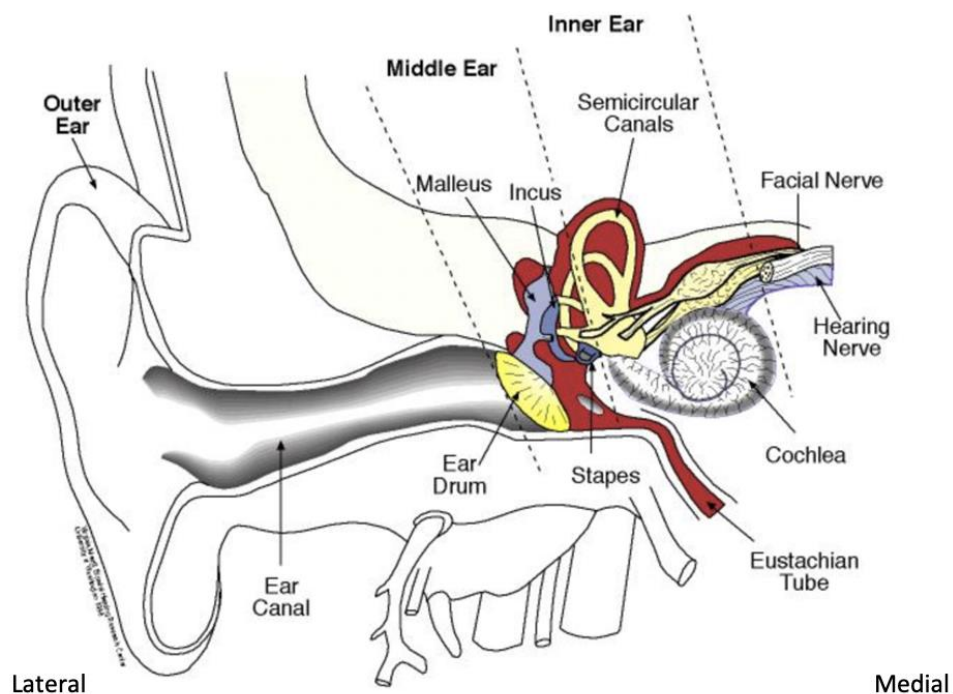


Fig. 2.1. The anterior, of the front view, of the three ear primary sections – the outer ear, middle ear, and inner ear (adapted from Brockmann et al., 2005).

The following section reviews the anatomy and physiology of a human ear, with a specific focus on the middle ear.

### *2.1.1 The Middle Ear*

The middle ear sits in the tympanic cavity of the temporal bone. It transmits sound from the outer ear to the inner ear by interfacing with the ear canal and cochlea, respectively. The following section reviews the primary components of the middle ear.

#### *2.1.1.1 The Tympanic Membrane (The Ear Drum)*

The tympanic membrane, or ear drum, connects the ear canal to the middle ear. The tympanic annulus, a thick ring of cartilage, connects the tympanic membrane to the temporal bone. A smaller, multi-layered membrane, the pars tensa, sits within the annulus. The lateral, or external, layer is continuous with the cells lining the ear canal. The middle layer is primarily dense connective tissue organized into radial and circumferential fibers originating from the center of the membrane, or the umbo. The medial, or inner, layer is continuous with mucosal lining of the tympanic cavity. The overall membrane thickness is between 50  $\mu\text{m}$  and 150  $\mu\text{m}$ , but the thickness decreases dramatically from the annulus to the umbo (De Greef, 2016; I. Dobrev, personal communication, 2020). The tympanic membrane is elliptically shaped, approximately 7.5 mm in length and 7.8 mm in width. In three-dimensional space, the membrane is conical, with an average height between 1.5 and 2.0 mm. The apex of the cone points into the tympanic cavity. The apex of this cone is the umbo. The membrane is oriented with the ear canal at an angle varying between  $0^\circ$  and  $60^\circ$  (De Greef, 2016; I. Dobrev, personal communication, 2020).

When the tympanic membrane is stimulated by acoustic vibrations from the ear canal, the pars tensa mechanically vibrates. At low frequencies, below 1 kHz, it is assumed the tympanic membrane executes piston-like motions into the tympanic cavity. At higher frequencies, however, the pattern is far more complex, exhibiting a traveling wave motion that follows the contours of the radial and circumferential fibers (I. Dobrev, personal communication, 2020). The umbo articulates, or connects, with the first ossicle in the ossicular chain, thus transferring the mechanical vibrations through the middle ear.

#### *2.1.1.2 The Ossicular Chain*

The ossicular chain contains three small auditory bones that span across the tympanic cavity. The first ossicle in the chain is the largest. The malleus, or the hammer, is located medially to the tympanic membrane. The handle, or manubrium, follows the radius of the pars tensa. The tip of the manubrium, the spatulate process, articulates with the pars tensa through loose connective tissue to form the umbo. The head of the malleus articulates with the head of the incus through the incudomalleor joint. The second ossicle is the incus, or the anvil. The lenticular process articulates with the head of the stapes through the incudostapedial joint. The final ossicle is the stapes, or the stirrup. The tympanostapedial syndesmosis, a primarily cartilage-based connection, articulates the stapes footplate to the oval window. (Ossika, 2021). Figure 2.2 shows isolated images of the malleus, incus, and stapes, respectively, with relevant dimensions and densities. (Ossika, 2021; De Greef, 2016).

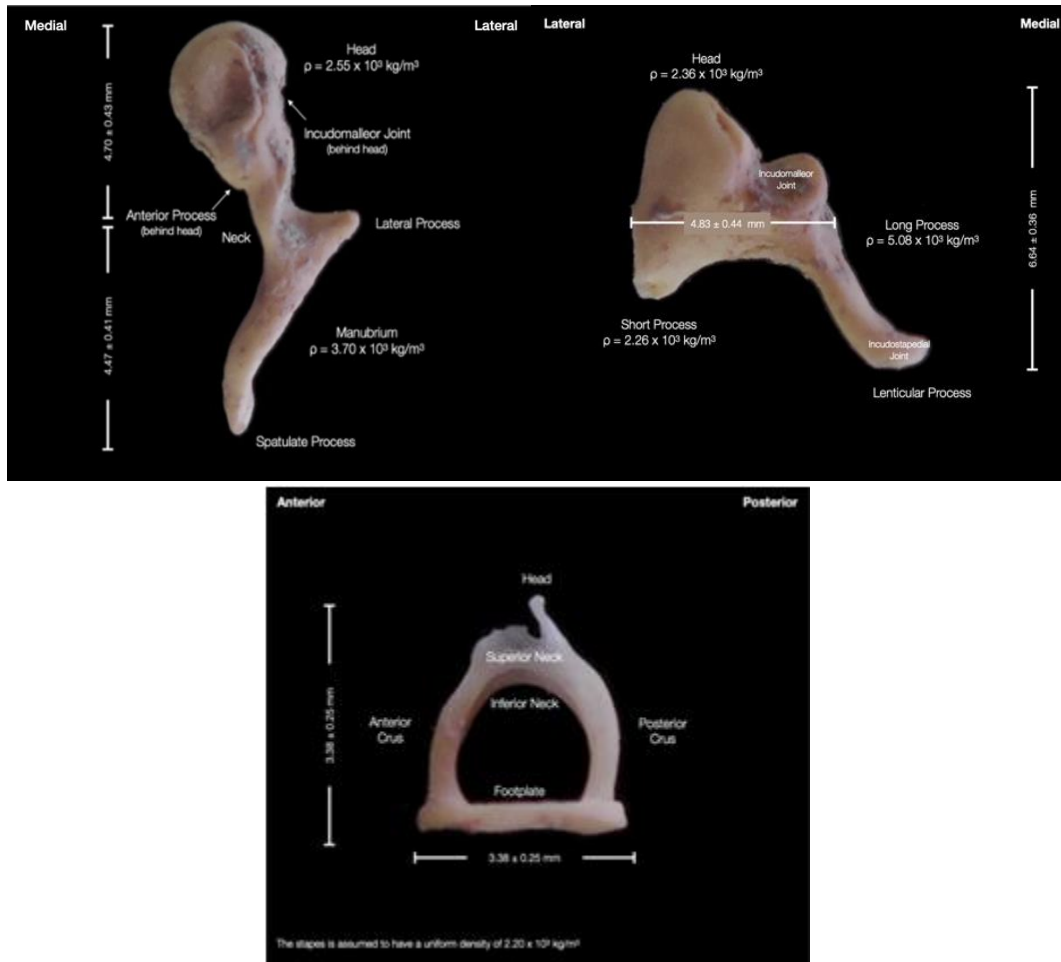


Fig. 2.2. Recovered cadaver ossicles. Top Left: Anterior view of the malleus. Top Right: Anterior view of the incus. Bottom: Lateral view of the stapes (adapted from Sirak et al., 2020; Homma et al., 2009; Gentil et al., 2012; Sodhi et al., 2017; Ossika, 2021).

The ossicular chain transfers mechanical vibrations of the tympanic membrane to the fluid-filled inner ear. Figure 2.3 shows the orientation of the ossicular chain within the tympanic cavity. The vibrations from the tympanic membrane displace the malleus, which in turn moves the incus and stapes. At low frequencies, below 1 kHz, both the incus and malleus display rigid body motion with the same axes of rotation, and the stapes acts as a piston, pushing the mechanical vibrations of the tympanic membrane to the fluid-filled inner ear. At frequencies above 1 kHz, the incus and malleus have different axes of rotation, while the stapes exhibits a rocking-like motion into the oval window (I. Dobrev, personal communication, 2020; De Greef, 2016).

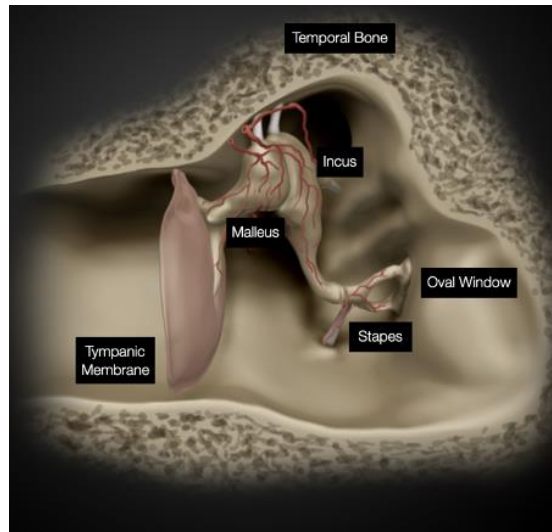


Fig. 2.3. Anterior view of the ossicular chain in the tympanic cavity (adapted from Gassler, 2019).

### 2.1.1.3 The Oval Window

The oval window is a kidney-shaped, membrane-covered opening that connects the middle ear to the inner ear. In adult populations, the average membrane width is 2.63 mm, the average membrane height is 1.50 mm, and the approximate thickness is 0.1 mm (Zdilla et al., 2018; Tang et al., 2017). The tympanostapedial syndesmosis fixes the membrane to the footplate of the stapes on the lateral side. Loose connective tissue fixes the membrane to the cochlea on the medial side. The membrane vibrates when the ossicular chain is stimulated and transmits the vibrations into the cochlear fluid (Tang et al., 2017). It should be noted, the ossicular support structure is equally important in sound transmittance to the inner ear (I. Dobrev, personal communication, 2020).

### 2.1.1.4 Support Structures

The support structure is a system of joints, ligaments, and tendons that suspend and articulate the ossicular chain. The joints interface between the ossicles and provide basic mobility. The ligaments connect the ossicles to the walls of the tympanic cavity. The tendons connect the select ossicles to muscles running through the tympanic cavity (De Greef, 2016; Ossika, 2021).

There are two primary joints in the middle ear: the incudomalleor joint (IMJ) and the incudostapedial joint (ISJ). A joint in the middle ear connects two ossicles with a layer of dense connective tissue. The connective tissue creates a capsule in between the two adjoining ossicles for synovial fluid, which acts as a shock absorber. The saddle shaped IMJ articulates the head of the malleus to the head of the incus (Gottlieb, 2018). IMJ flexibility and mobility is frequency dependent with mobility starting at 1 to 2 kHz. This phenomenon may explain which the malleus-incus complex behaves as a rigid body below 1 kHz (De Greef, 2016; Gottlieb, 2019; Homma et al., 2009). The ISJ connects the tip of the incus, the lenticular process, to the head of

the stapes. The ISJ is comparatively more flexible, and mobility is seen at low frequencies i.e., frequencies below 1 kHz (Gottlieb, 2019).

Ligaments are equally important connective tissues in the middle ear. They are primarily composed of collagen and elastin, which provides support and flexibility. The exact number and location of middle ear ligaments is highly contested (Ossika, 2021; Homma et al., 2009). De Greef's 2016 thesis considers ligament locations in six cadaver models. Table 2.1 details the ligaments found in at least five of the six cadaver samples and their location in the middle ear. Figure 2.4 also shows the common ligaments' locations in two views. (De Greef, 2016).

Table 2.1. Common Ligaments (adapted from De Greef, 2016; Homma et al., 2009)

Ligament	Number in Figure 4	Origin	Direction of Attachment to Tympanic Cavity Wall
Anterior Malleolar	5	Anterior process and neck of the malleus	Anterior (Front)
Medial Anterior Malleolar	6	Anterior surface of the malleolar head	Anterior-medial (Front-towards the middle)
Lateral Malleolar	9	Neck of the malleus	Lateral-posterior (Side-towards the back)
Posterior Malleolar	Not Shown	Posterior side of the manubrium	Posterior (Back)
Superior Malleolar	2	Superior-posterior-medial head of the malleus	Superior-posterior (Top-towards the back)
Posterior Incudal	1	Medial and lateral side of the incudal short process	Medial and lateral (Middle and side)
Lateral Incudal	8	Lateral side of the incudal long process midpoint	Lateral (Side)
Stapedial Annular	Not Shown	Around the stapes footplate	Around the stapes footplate

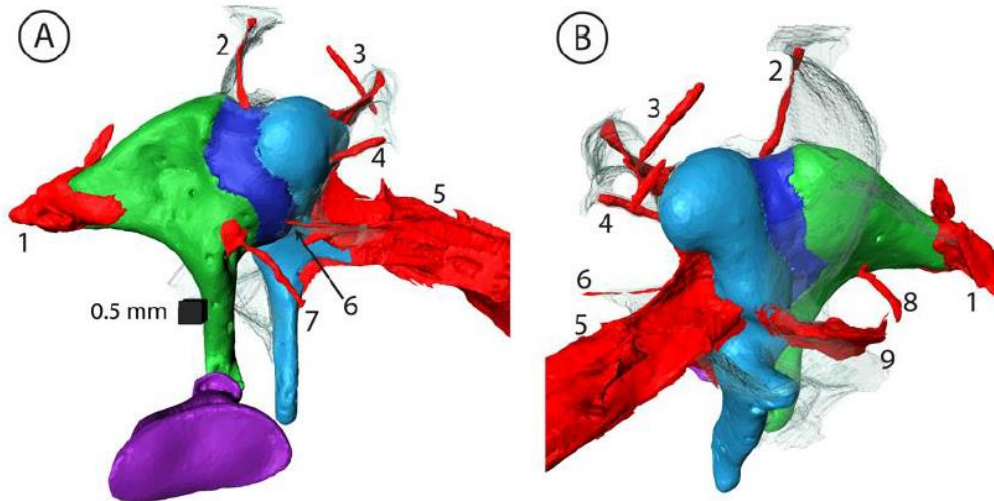


Fig. 2.4. Location of ligaments in the middle ear from (A) the medial view and (B) the superior-lateral view. The ligaments are shown in red. The malleus is shown in turquoise. The incus is shown in green. The stapes is shown in purple. The IMJ is shown in dark blue. Note, ligaments 3 and 4 are not represented in Table 1 because they occurred in less than five of the six cadavers (De Greef, 2016).

The final component of the support system involves the tendons. Like ligaments, tendons are a combination of collagen and elastin. However, tendons connect bone to muscle. The first tendon in the middle ear is the tensor tympani tendon, which originates from the medial side of the upper manubrium (De Greef, 2016). The tendon transitions to muscle as it approaches the wall of the tympanic cavity from the medial direction. The muscle proceeds out of the tympanic cavity and follows the contours of the eustachian tube, as shown in Figure 2.1 (Ossika, 2021; De Greef 2016). The second tendon is the stapedial tendon, which articulates with the posterior side of the stapes head, transitions to muscle, and approaches the tympanic cavity wall from the medial-anterior direction (De Greef, 2016; Ossika, 2021).

#### 2.1.1.5 Role in Sound Perception

The structure of the middle ear supports its function. As acoustic and acousto-mechanical vibrations reach the outer and middle ears, respectively, they travel through air. The stapes transmits the mechanical vibrations to the inner ear through the oval window. An image of the cochlea can be referenced in Fig. 2.1. After the vibrations pass through the oval window, the medium changes from air to cochlear fluid. The medium change underscores the importance of the middle ear. The acoustic impedance in air, or the resistance to sound propagation, is significantly reduced compared to the acoustic impedance in the cochlear fluid, which can be approximated as water. Therefore, the air pressure in the outer ear is significantly higher than the air pressure in the inner ear. Without the middle ear, the boundary between the air and water acts as a mirror, mirroring over 99% of the air pressure back to the outer ear and preventing mechanical vibrations from reaching the inner ear. Because the middle ear acts as a pressure amplifier, the mechanical vibrations can enter the cochlear fluid and reach the cochlear hair cells. This process helps convert the mechanical vibrations into an electrical signal. The hearing, or cochlear, nerve carries the electrical signal to the brain. This process creates the sensation of hearing (I. Dobrev, personal communication, 2020).

## 2.2 Sound Mechanics

Sound mechanics refer to how sound is perceived. Sound is a mechanical wave that results from the back-and-forth vibration of the particles. The vibration propagates the particles through a medium. Both the particles and the medium are instrumental in this process. Without a medium to carry the sound, no sound can travel, but it is important to note that the medium itself is not vibrating (Oxenham, 2016).

In the human ear, the acoustic vibrations of a sound wave are transferred to mechanical vibrations, as described in Section 2.1.1.5. Primary properties of sound waves are wavelength, frequency, and amplitude. Frequencies are the number of wave cycles, or oscillations, which passes per unit of time. The sound frequency range for the human ear is 20 to 20,000 Hz (Silva, 2017). Amplitude is the maximum displacement of the wave relative to its position which can be seen in Fig. 2.5. Overall, the frequency and amplitude are independent of each other but together make up a sound wave. Another property of sound waves is the wavelength. The wavelength, also known as a period, is the distance it takes to complete one cycle of a wave. The wavelength, frequency, and amplitude properties are key in determining the timbre, pitches, and loudness of a sound respectively (Wave Variables, n.d).

Sound waves in air are characterized as longitudinal waves (Cooper et al., 2018). A longitudinal wave is a series of disturbances through a medium, in this case air, where the particles vibrate in paths parallel to the directions of the disturbances of the wave traveling. The longitudinal motion of the air particles cause regions of the air particles to be compressed and other regions to be spread apart which are known as compressions and rarefactions respectively. The compression regions are regions of high pressure, and the rarefactions are regions of low pressure as seen in Fig. 2.5. As the pressure varies throughout the wave, the density varies in parallel as seen in the graph in Fig. 2.5. As the pressure increases, the density increases and vice versa. Due to this repeating pattern of high- and low-pressure changes, sound waves are further characterized as pressure waves.

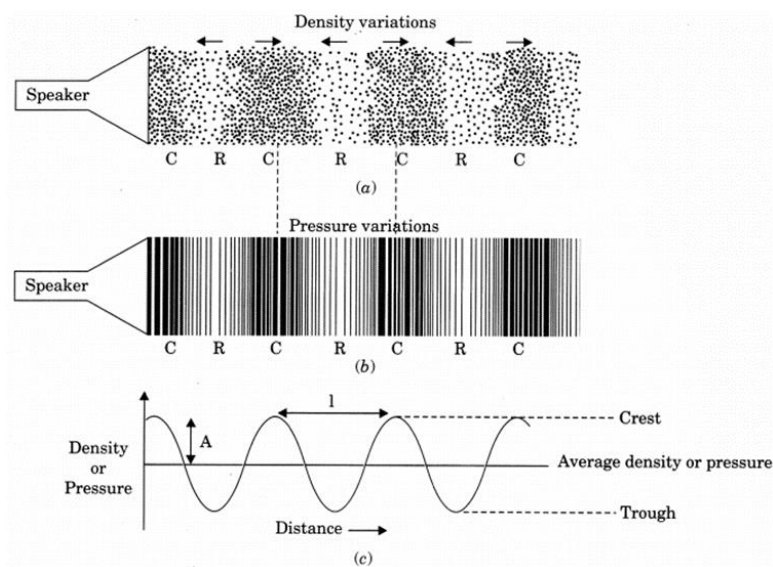


Fig. 2.5. The Pressure Variation of a Sound Wave (Anum, 2021).

To measure a longitudinal wave, its wavelength can be measured using the distance from one compression to the next compression or one rarefaction to the next adjacent rarefaction as seen in Fig. 2.6. Since these waves consist of changes in pressure, the wave can be detected using a pressure detector. The detector theoretically can detect the high and low pressure which in turn will produce a sine curve for the pressure versus time graph as seen in Fig. 2.6 below. Therefore, the amplitudes of longitudinal waves are measured in terms of the increase and decrease in pressure.

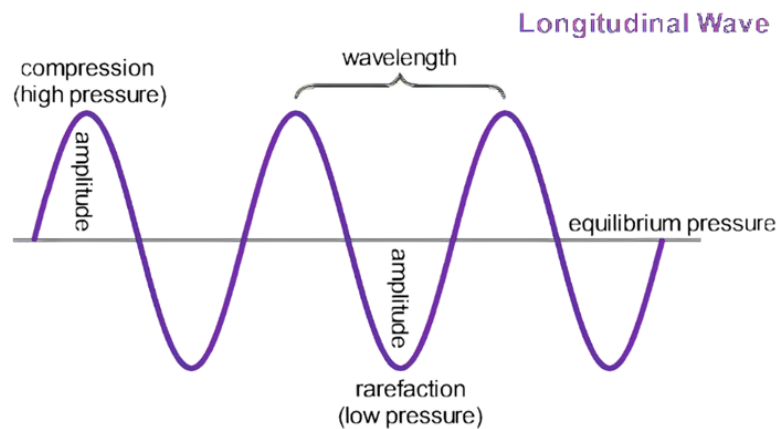


Fig. 2.6. A graph of the Properties of a Longitudinal Wave (Colwell, n.d).

In the human ear, the amount of sound that reaches each primary ear can be quantified with acoustic impedance. Acoustic impedance is the opposition to the passage of sound and the magnitude of the resistance is dependent on the mass and stiffness of the membrane and the ossicular chain. The impedance is measured with the volume velocity which determines how many particles move past a certain plane (Withnell et al., 2013).

### 2.3 Modeling and Reconstructing the Middle Ear

The anatomy of the middle ear is often poorly understood without proper visuals and learning techniques (Ng et al., 2015). Someone studying the middle ear should be able to spatially visualize the middle ear under both healthy conditions as well as with common pathologies. The structures within the middle ear are hidden, which prevents students and researchers from being able to gain a deep understanding of how each individual part connects and functions without proper resources (Anschuetz et al., 2019). Middle ear anatomy is generally taught by using two-dimensional (2D) diagrams, cadaver specimens, animal specimens, and three-dimensional (3D) computer models (Jenks et al., 2021).

#### 2.3.1 Current Methods for Teaching and Visualizing the Middle Ear

2D diagrams are used to teach a simple overview of the parts of the middle ear. Although this method is sufficient to teach vocabulary as well as the general location and layout of the middle ear, it lacks the spatial aspect that is necessary for students to learn, especially if they are working towards performing middle ear surgery (Luers & Hüttenbrink, 2016). A more robust teaching method is needed for students to understand not only anatomy, but also physiology and

common pathologies. This cannot be done by simply looking at a flat diagram of a complex structure.

Cadaveric dissection can properly display 3D relationships between anatomical structures and appreciating anatomical variations (Ghazanfar et al., 2018). However, cadaver specimens are becoming less prevalent in some medical schools due to the ethical question of how temporal bone specimens are obtained (Leong & Aldren, 2007). Therefore, this teaching method is not practical for routine teaching or use (Jenks et al., 2021). Countries such as the United States have a temporal bone donor bank, but there is not a steady influx of cadaveric temporal bone specimens (Leong & Aldren, 2007). Animal cadaveric specimens are used in place of human temporal bones to increase accessibility and exposure to surgical practice. Although we can approximate the human ear with another animal's temporal bone, the main limitation is that the anatomy is only comparable to an extent. Both human and animal cadaveric dissection serve as a great teaching tool as well as valuable practice for surgeons, as they allow them to gain competence and confidence with difficult middle ear procedures (Bergin et al., 2013).

3D modeling has grown to be a viable alternative to cadaveric experiments as it provides a resource that is more accessible while providing similar benefits to students (Jenks et al., 2021). One of the most popular methods for creating 3D computer models of the middle ear is using  $\mu$ CT scans, which involves taking scans of the object slice by slice at a high resolution on a microscale, giving a view of the inside of an object such as a temporal bone (Micro Photonics Inc., 2021). 2D images are acquired using X-ray and are then reconstructed into a 3D model. Since the scan is constructed slice by slice, the  $\mu$ CT scan reveals the internal features that are obscured by the temporal bone. This tool's increased resolution allows the capture of necessary components despite the bones within the middle ear being small and delicate. (Elsevier B.V., n.d.). The process is nondestructive which allows temporal bone sample used to obtain these images to be preserved in the process, enabling researchers to use the sample later for additional scans or future purposes (Lee et al., 2010).  $\mu$ CT scans also introduce the possibility of creating physical replicas of the middle ear for surgeons to practice on or use to gain a spatial understanding of the structure. Unlike cadavers, which are an expensive and scarce resource, 3D printed models are reproducible, reusable, and inexpensive. When the digital 3D model of the middle ear is obtained using  $\mu$ CT scans, the point clouds from the model can be converted to STL files. These files are subsequently sent to a 3D printer and constructed into a physical model (Micro Photonics Inc., n.d.). 3D printing in combination with  $\mu$ CT scanning has created the opportunity to manufacture new high-fidelity tools to display anatomy, physiology, and common pathologies.

### *2.3.2 Process of Modeling and Reconstruction*

These physical 3D models can be created with a higher degree of design freedom by using additive manufacturing. Additive manufacturing, also known as 3D printing, is the process of combining layers of a material to create objects from a computer aided design (CAD) model data. This technology is used in rapid prototyping to print parts as it enables the redesign of individual parts that other manufacturing processes do not offer (Bikas et al., 2015).

Additive manufacturing is an integral technological tool for basic rapid prototyping of lightweight parts. Common printing technologies include fused deposition modeling (FDM) and stereolithography (SLA) which print a part layer by layer. FDM printers extrude melted thermoplastic material by running it through a heated nozzle. The thermoplastic then cools to a solid state to create the final part. SLA printers use thermosets, which cannot melt and instead use ultraviolet light for part curing and formation. Because there is no cooling process and associated dimension change, SLA printers create high-accuracy prototypes with tight tolerances and smooth surfaces. FDM printing is used for lower-level parts that have a constrained resolution determined by the size of the extrusion nozzle (Formlabs, 2022).

Additive manufacturing techniques can replicate complex geometries and systems. Hence, these technologies are frequently utilized to build anatomical models, like the middle ear. Individual components of the model can be made through additive manufacturing of synthetic materials that simulate the material properties of native tissue. Two synthetic materials, polylactic acid (PLA) and acrylonitrile butadiene styrene (ABS), are particularly popular printing filaments because their material properties can be tailored to tissue type. A more compliant printing filament, like thermoplastic polyurethane (TPU), can be processed using FDM technology to replicate softer tissues. Another option for reconstructing softer tissues is silicone rubber casting. The liquid silicone rubber is poured into a mold, which can be made using FDM. After the rubber silicone is heat cured, it is removed from the mold to create the final part (Protolabs, 2022). These various materials and methods can be used in tandem to accurately recreate the various tissues in the middle ear.

#### *2.4 Current Model*

A previous team of Worcester Polytechnic Institute (WPI) undergraduates created a physical dynamic model of the middle ear for the Universitätsspital Zürich. They displayed the translation of vibration through the ossicular chain in both healthy and diseased states. While the current model was an excellent step in replicating middle ear anatomy and physiology, it is not able to meet all the hospital's teaching needs. The following section provides an overview of the previous team's primary deliverables and starts to review potential improvements.

##### *2.4.1 Review of Previous WPI Team's Work*

In 2020, a previous WPI team completed their senior capstone, or Major Qualifying Project (MQP), with Dr. Ivo Dobrev, a post-doctorate student at the Universitätsspital Zürich. The previous team created a dynamic middle ear model to serve as a visual aid for students. They replicated middle ear anatomy at a 15:1 scale using additive manufacturing technology and manual assembly techniques. They assembled the model to interchangeably display healthy and diseased middle ears and stimulated both display states acoustically. They measured the resultant vibrations using accelerometers attached to the ossicula chain and analyzed the data. Their final model displaying healthy middle ear anatomy is shown in Fig. 2.7 (Kane et al., 2020).

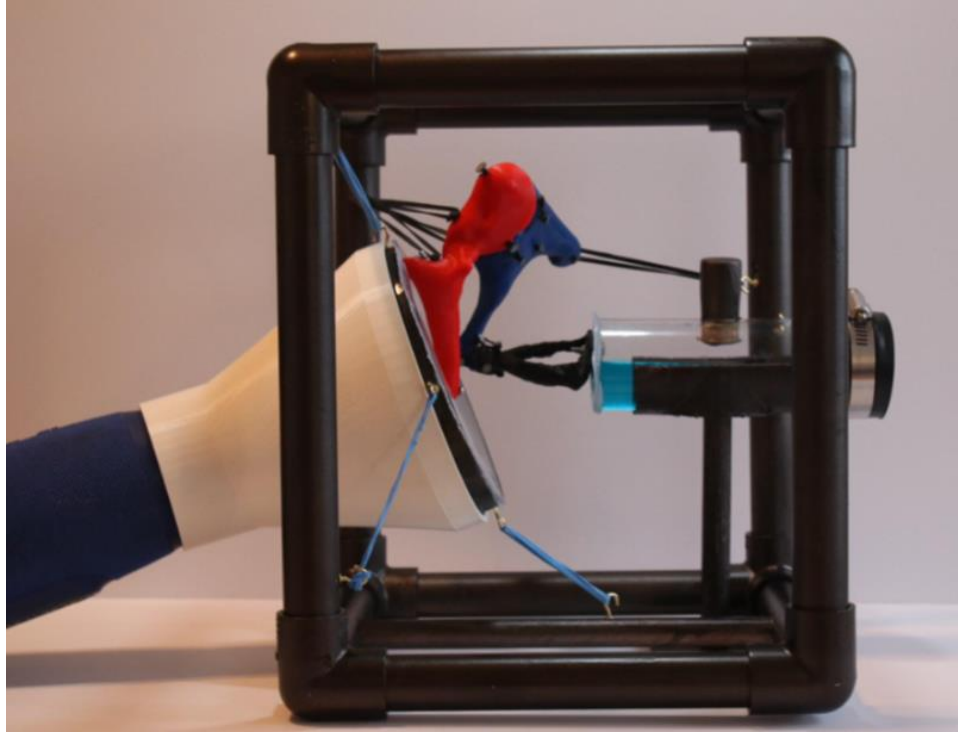


Fig. 2.7. Final model created by 2020 Zurich MQP team. Components include ear canal, tympanic membrane, malleus, incus, stapes, select ligaments, the oval window, and cochlear tube (Kane et al., 2020).

They accurately replicated the geometries of each ossicle using FDM techniques and they began to investigate how replication material would affect ossicular chain vibrations. For example, they experimented with printing infill percentages, favoring more porous options that better mimicked the porosity of native bone. Due to time constraints, they were not able to test these options. While material choices were an interesting part of their research, the current model has some more impacting limitations. For example, model assembly relied on estimating the approximate articulations between each ossicle and local attachment points for each ligament and tendon. The pins in each ossicle were manually drilled after the parts were printed and the connections to the tympanic cavity walls were limited by the material available on the cuboidal support structure. Additionally, the frame gives a false impression of middle ear openness *in vivo*.

The model also has complications related to assembly. Dr. Dobrev struggled to interchange healthy and damaged ossicles without compromising anatomical accuracy and mechanical stability. Interchangeability required multiple people to remove and re-attach articulation materials. The primary materials used to represent articulations were soft thermoplastics and elastomers (e.g., rubber bands). After a year and a half of use, the softer plastics have weathered, and some have broken altogether. Replacing the damaged parts was difficult, as the model had to be almost completely disassembled to fix one component (I. Dobrev, personal communication, January 5, 2022).

### 3.0 Project Strategy

Based on the 2020 WPI middle ear model, there is a clear need to address concerns related to anatomical accuracy and model assembly. There are also opportunities to advance their work on materials selection in replicating native tissue. The following chapter outlines the next steps for this model creation and advancement.

#### 3.1 Initial Client Statement

Dr. Dobrev expressed interest in the following avenues to address the limitations of the previous model:

1. Design a digital model of the full middle ear, which can interchangeably demonstrate healthy and diseased hearing states
2. Use the digital files to create a physical model, again interchangeably demonstrating healthy and diseased hearing states
3. Select materials for the physical model that mimic native tissue and ensure selected materials are durable and easily replaceable
4. Design a support system for the physical model which allows for correct, anatomical alignment of primary bodies in the middle ear
5. Measure the physical model's healthy and diseased hearing states in a quantitative and reproducible manner

Although these avenues were effective in initially determining the project scope, the team segmented Dr. Dobrev's interests into time sensitive objectives to better understand the work breakdown, reviewed below.

#### 3.2 Revised Client Statement

The team assigned a ranking system to Dr. Dobrev's initial interests and asked him to score each item on a scale of 1 to 5, with 5 being the most important and 1 being the least important. Dr. Dobrev's feedback can be reviewed in Appendix A. From his feedback, the project scope was adjusted to only model healthy middle ear anatomy and physiology. The primary modeling elements include: the medial portion of the ear canal, the tympanic membrane, the ossicular chain, the Incudomalleolar joint<sup>1</sup>, both tendons, five mechanically important ligaments<sup>2</sup>, the oval window, and proper attachment points on the tympanic cavity walls. The listed elements will be referred to as "primary bodies" throughout the report. The objectives below should be completed in their listed order to realize the project goal and address Dr. Dobrev's interests. The static models are meant to be figures that only demonstrate anatomy. The work towards the static model will also help in dynamic model creation. The dynamic model should move in response to an external stimulus and replicate the motion of the middle ear.

1. Replicate static healthy middle ear anatomy in digital and physical models
2. Design a digital model to realize a dynamic physical model
3. Identify suitable synthetic materials to replicate native tissue
4. Assemble a physical dynamic model of a healthy middle ear from the corresponding digital design and material selections

5. Demonstrate healthy middle ear physiology on the assembled physical dynamic model

The section below discusses the project objectives and their accompanying requirements in more detail.

3.3 Design Requirements

Sub-objectives and quantitative specifications were attached to each project objective. Figure 3.1 shows an overview of the objective and sub-objective relationships.

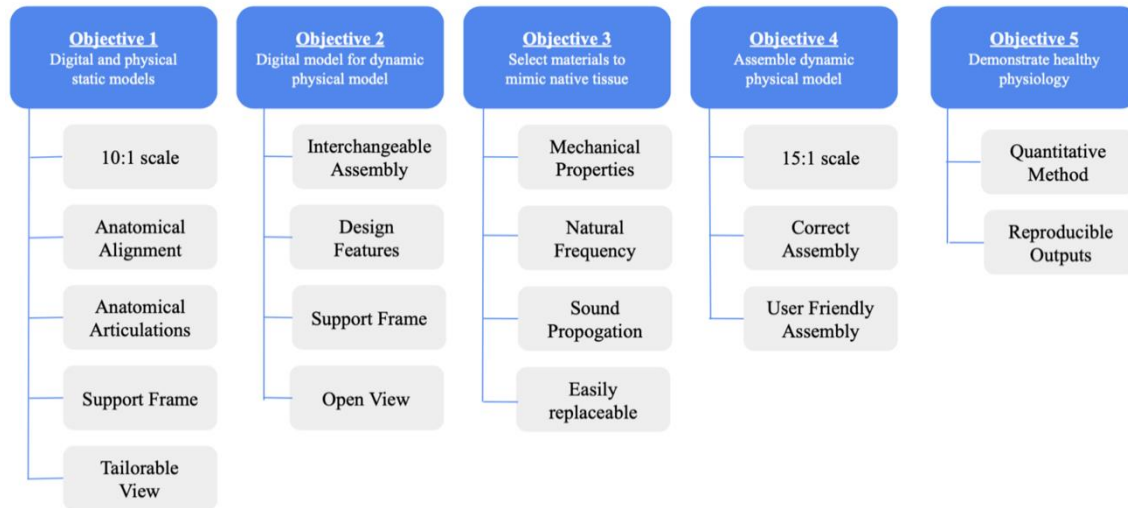


Fig 3.1. Objective and Sub-Objective Overview

Tables 3.1 through 3.5 correspond to Objectives 1 through 5. The tables define each sub-objective and the associated design specifications.

Table 3.1. Objective 1, Digital and Physical Static Models

Sub Objective	Definition	Specifications and Constraints
10:1 Scale	All primary bodies will be scaled up by a factor of 10 in digital and physical formats.	Refer to Table 3.6
Anatomical Alignment	Primary bodies must be aligned in an anatomically correct fashion.	Refer to Table 3.6
Anatomical Articulations	The articulation points are where ligaments connect bone to bone and where tendons connect bone to muscle. The attachment points must be anatomically correct.	Refer to Table 3.6
Support Frame	Due to the complex geometry of the ossicular chain and surrounding membranes, joints, ligaments, and tendons, the models require a mechanically stable support frame.	The support frame must stand on its own and support the full weight of the model.
Tailorable View	The support frame should allow viewers to selectively view portions of the middle ear, specifically a surgery incision site. With user manipulation, the support frame should also allow full view of the middle ear.	The primary bodies and articulations point should be easily visible. At least 50% of the USZ research teams needs to agree that the view is acceptable.

Table 3.2. Objective 2, Digital Model for Dynamical Physical Model

Sub Objective	Definition	Specifications and Constraints
Interchangeable Assembly	All primary bodies should be separate, distinct entities in the digital model	Bodies can be loaded separately in digital modelling software.
Design Features	The design features used to represent the physical connections between two bones (ligaments) or between a bone and muscle (tendon) must match the mechanical functions of the native connective tissues.	The connections must only allow rotation on one axis. The connections must also allow some shear force transfer.
Support Frame	See Table 3.1 Definition.	Follows the Support Frame Specification in Table 3.1
Open View	The support frame should allow the most open view of all primary bodies.	Follows the Tailorable View Specification in Table 3.1

Table 3.3. Objective 3, Material Selection for Dynamic Physical Model

Sub Objective	Definition	Specifications and Constraints
Mechanical Properties	The mechanical properties of the selected materials should mimic native tissue	No set specifications, quantified with the Young's Modulus and density. Further reviewed in Section 4.2.2.
Natural Frequency	The natural frequency of the materials should be scaled to the intended size of the dynamic physical model (15:1 scale).	Because natural frequency is inversely proportional to system size, the selected materials should have a natural frequency between 53 Hz and 80 Hz, one fifteenth of the middle ear natural frequency range (Homma et al., 2009).
Sound Propagation	The sound propagation mechanisms should mimic corresponding native tissues.	No set specifications, quantified with material loss factor. Further reviewed in Section 4.2.2.
Easily Replaceable	Material durability cannot be assessed within the project timeline, but materials chosen should be easily replaceable.	No set specifications, the sources and SKU numbers (if applicable) must be listed for all final materials

Table 3.4. Objective 4, Dynamic Physical Model Assembly

Sub Objective	Definition	Specifications and Constraints
15:1 Scale	All primary bodies will be scaled up by a factor of 15 in physical formats.	Refer to Table 3.6
Correct Assembly	The assembly should produce anatomically correct alignment of primary bodies.	Refer to Table 3.6

User Friendly Assembly	The assembly should be quick and simple for one person, and each primary body should be an interchangeable part.	Assembly must be accomplished by one person. The process should last between 1 minute and 5 minutes. The process must not take longer than 5 minutes (I. Dobrev, personal communication, January 13., 2022).
------------------------	--	--

Table 3.5. Objective 5, Dynamic Physical Model Testing

Sub Objective	Definition	Specifications and Constraints
Quantitative Method	Physical demonstration of physiology will involve acoustically stimulating the dynamic physical model. The inputs can be continuous signals or pulses. The signals should be simultaneously measured from two distinct locations on the model.	Like the specification in Table 3.3., the entire model's natural frequency must be between 53 Hz and 80 Hz (Homma et al., 2009). From the tympanic membrane to oval window, there should be a pressure drop between 10 and 15 dB re 1 V (I. Dobrev, personal communication, Jan. 18, 2022).
Reproducible Method	The outputs should be quantitative and reproducible. When a part is interchanged or the model is re-assembled, the model should give similar frequency and pressure readings.	Each measured value should not deviate by more than one standard deviation.

Table 3.6 shows the anatomical lengths, diameters, and angles of orientation for primary bodies. The measurements were taken on cadaver models and serve as the specifications and constraints for sub-objectives relating to model scale, anatomical alignment, and anatomical articulations. The static model's length and diameter ranges will be multiplied by a factor ten while the dynamic model's length and diameters will be multiplied by a factor of fifteen. When completing design verification for the physical models, the ranges below will be expanded by  $\pm 0.5$  mm, the worst case FDM printing tolerance (Redwood, 2022).

Table 3.6. Anatomical Lengths, Diameters, and Angles of Orientation for Primary Bodies.

Primary Body	Measurements
Tympanic Membrane (Pars Tensa)	Angle between membrane and ear canal is between 40° and 60° (I. Dobrev, personal communication, 2020). Length between 7.0 mm and 7.5 mm, width between 7.8 mm and 8.0 mm, height from apex to base between 1.5 mm and 2.0 mm (De Greef, 2016)
Oval Window	Length between 1.31 mm and 1.69 mm, width between 2.40 mm and 2.86 mm, approximate thickness between 0.1 mm and 0.5 mm (Zdilla et al., 2018).

Malleus	Total length between 7.50 mm and 8.24 mm, length of the manubrium between 4.06 mm and 4.80 mm, length of the head and neck between 4.26 mm and 5.13 mm (Sondhi et al., 2017). Manubrium must be flush with the slant height of the pars tensa and parallel to the long process of the incus (De Greef, 2016).
Incus	Total length between 6.28 mm and 7.00 mm, width from the end of the short process to the end of the body between 4.39 mm and 5.27 mm, length between the tip of the short process and tip of the lenticular process between 4.99 mm and 5.79 mm (Sondhi et al., 2017). The lenticular process of the incus and the head of stapes must form an angle between 67° and 90° (Gottlieb, 2018).
Stapes	Total length from between 3.13 mm and 3.63 mm, footplate length between 2.63 mm and 3.01 mm, footplate width between 1.23 mm and 1.51 mm (Sodhi et al., 2017).
Tensor Tympani Tendon	Diameter between 0.7 mm and 0.9 mm and length between 2.06 mm and 2.34 mm (Sim & Puria, 2008).
Stapedial Muscle/Tendon	Diameter between 0.46 mm at the tympanic cavity wall and 0.47 mm at the stapes head (Wojciechowski et al., 2020).
Anterior Malleolar Ligament	Diameter between 0.80 mm and 1.0 mm and length between 1.74 mm and 2.46 mm (Sim & Puria, 2008).
Lateral Malleolar Ligament	Diameter between 0.5 mm and 0.6 mm and length between 1.57 mm and 2.43 mm (Sim & Puria, 2008).
Superior Malleolar Ligament	Diameter between 0.2 mm and 0.3 mm and a length between 0.96 mm and 1.64 mm (Sim & Puria, 2008).
Posterior Incudal Ligament	Width on the medial side between 0.8 mm and 1.16 mm, width on the lateral side between 0.53 mm and 0.84 mm (Sim & Puria, 2008).
Stapedial Annular Ligament	Thickness between 0.06 mm and 0.08 mm, height between 0.18 mm and 0.26 mm, follows the perimeter of the stapes footplate (Sim & Puria, 2008).

### 3.3.1 Engineering Standards

While the exact design process for each objective will be reviewed in the following chapter, this section presents the engineering standards relevant to each objective. The first and second objectives (and, by extension, the fifth objective) involved digital modeling. The team based the digital models on  $\mu$ CT scans of human cadaver middle ears. The process for obtaining the  $\mu$ CT scans protected patient identity and therefore remained HIPPA compliant. Because the team is working not working with biological materials, ethical considerations regarding material sourcing and safety considerations regarding biological toxins were not made. The actual printing was outsourced to professional companies, and the signal processing hardware ran at currents below 5 Amperes. Therefore, the team did not consider risk assessments related to printing and signal acquisition.

### 3.4 Project Approach

To accomplish the project objectives and deliverables on time, the team developed a week-by-week Gantt chart. Each task had an assigned resource to ensure equal contribution from all team members. Within the week-by-week breakdown, the tasks were color coordinated to easily differentiate between the different action item types. The green tasks represented design deliverables, the blue tasks represented MQP deliverables, and the orange represented slack time for either deliverable. The slack time was built into the Gantt chart to account for variability in the progress of design deliverables and advisor feedback. Once a task was completed, it was filled in with an “X” for clarity. For reference, the first week of the Gantt chart is shown below in Fig. 3.2.

Task	Resource	Week 1				
		3-Jan	4-Jan	5-Jan	6-Jan	7-Jan
Research Middle Ear Anatomy & Physiology	Sarah		X	X	X	X
Research Middle Ear Pathology	Mickaela		X	X	X	X
Research Sound and Signal Processing	Mary		X	X	X	X
Research Current Models and Visualization Techniques	Shannon		X	X	X	X
Research Materials that best replicate Anatomy	Sarah, Mickaela		X	X	X	X
Research Materials that are available for 3D Models	Mary, Shannon, Sonya		X	X	X	X
Research on the 3D Model Tools and Print Shops	Sonya		X	X	X	X
Discuss Limitations of Current Model	Shannon	X	X	X	X	X
Develop Project Scope and Create Draft Client Statement	All			X	X	X

Fig. 3.2. One week example of the project Gantt Chart

## 4.0 Design Process

The following chapter will review the needs analysis of the client, data acquisition of materials, the static model iterations and dynamic model iterations. The needs analysis evaluates the needs, wants, and physical limitations defined by the project's objectives. The analysis will incorporate skills, time, and resources available to best satisfy the client's needs and wants. The static model was designed to focus on an anatomical visual representation of the middle ear while the dynamic model was intended to be a functional model that replicates the movement of the middle ear. The following chapter describes the static and dynamic model's digital iterations in chronological order including their individual benefits and drawbacks. The transition from how the static model transitioned into the dynamic model is further described. A final design was created and presented to Dr. Dobrev. To prepare for realization of the dynamic model in physical form, procedures to quantitatively compare synthetic materials to corresponding native tissues were designed. The outlined procedures have a specific focus on the sound propagation mechanisms of synthetic materials, as these properties will define model movement in response to acoustic stimulation in Objective 5.

### 4.1 Needs Analysis

The following analysis further identifies and evaluates the needs, wants, and physical limitations defined by the project's objectives. The analysis incorporates skills, time, and resources available to best satisfy the client statement.

#### 4.1.1 Static Model

The static model is encompassed by Objective 1. The needs for Objective 1, the replication of the static healthy middle ear anatomy in digital and physical models, are as follows:

1. Modifiable digital model
2. Primary bodies can be seen with the naked eye
3. Anatomically correct primary bodies
4. Each primary body must be distinguishable from others and from support structure
5. Support at ligaments
6. Open view
7. Can be held in hands
8. Easily transportable
9. Durable materials
10. 10:1 scale from the original 1cm<sup>3</sup> size
11. Transparent tympanic membrane

The wants for Objective 1 are as follows:

1. Easily printable
2. Least amount of material possible
3. Shape of temporal bone
4. Surgical view

## 5. Ear canal support

The physical limitations for Objective 1 are as follows:

1. Easily transportable
2. Minimize amount of material used for printing
3. 10:1 scale from the original 1cm<sup>3</sup> size
4. Must be able to be held in hands

### *4.1.2 Dynamic Model*

The dynamic model is encompassed by Objectives 2 and 4. These objectives describe the replication of the healthy middle ear in digital and physical formats to display the physiology of the middle ear. The needs for Objectives 2 and 4 are as follows, in addition to static needs 1 through 9:

1. Anatomically correct attachment mechanisms for primary bodies
2. Interchangeable/detachable parts
3. 15:1 scale from the original 1cm<sup>3</sup> size

The wants for Objectives 2 and 4 are as follows, in addition to static wants 1 and 2:

1. Transparent tympanic membrane
2. Able to be assembled by one person
3. Quick assembly
4. Easily replaceable parts

The physical limitations for Objectives 2 and 4 are as follows, in addition to static physical limitations 1 and 2:

1. 15:1 scale from the original 1cm<sup>3</sup> size

### *4.2 Design Concept Prototyping*

The following sections detail the two main steps that were taken to begin prototyping the model: the process of creating the digital middle ear models and the material selection process.

#### *4.2.1 CAD Prototyping*

The digital models for both the static and dynamic middle ear models were designed in Geomagic. Both models heavily relied on a  $\mu$ CT scan of the temporal bone in Geomagic which included the temporal bone itself as well as the stapes, incus, and malleus as seen in Fig. 4.1. These models also used a digital middle ear anatomy model created by Dr. Jae Hoon Sim, seen in Fig. 4.2., which depicts all the primary bodies deemed necessary (Sim & Puria, 2008). This digital middle ear anatomy model can be uploaded into Geomagic, used for reference, and edited for future use.

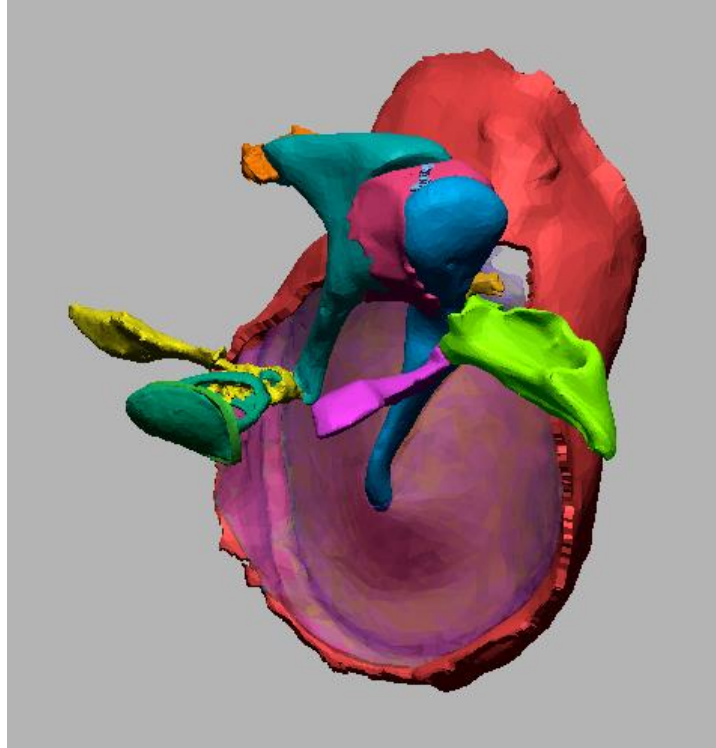


Fig. 4.1. Middle ear anatomy model created by Dr. Jae Hoon Sim viewed in Geomagic

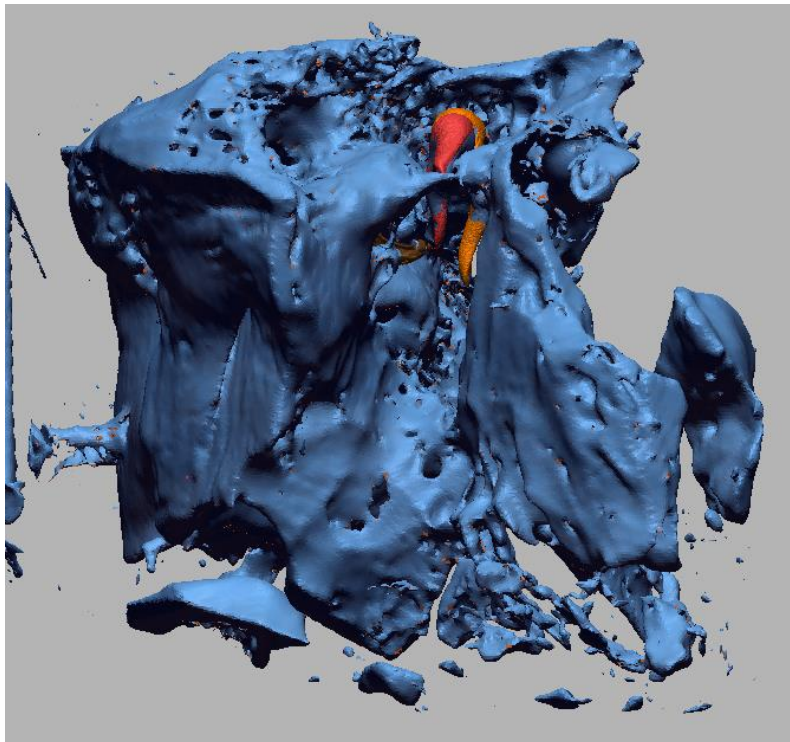


Fig. 4.2.  $\mu$ CT scan of the temporal bone viewed in Geomagic. Temporal bone can be seen in blue, stapes in brown, incus in red, and malleus in orange.

One of the largest criticisms of the previous MQP group's design was the lack of accurate articulation points. The first challenge was to determine the direction of the ligaments since

accurate movement and depiction of the middle ear relies heavily on direction. To obtain these articulation points for each ligament on both sides, the digital middle ear anatomy model was rotated, translated, and scaled to be aligned with the  $\mu$ CT scan of the temporal bone and ossicular chain. Once the digital middle ear anatomy model was aligned properly, each ligament was turned into a vector in Geomagic, and a point was placed where the vector intersects with the temporal bone. This was determined to be the most suitable option because ligament location and geometry are still widely disputed. Although the digital middle ear anatomy model and the  $\mu$ CT scan were obtained from different ears, these two models together give an approximation of the length and direction of the ligaments. Ligament lengths could have been approximated based on literature values, but per the client's requests, they were extracted from the  $\mu$ CT scan as described above.

In Geomagic, points are defined by an X, Y, and Z coordinate location. In SolidWorks, a point must be placed at a specific graphics area. Points cannot be inserted by typing in a coordinate location. Additionally, to process models with complicated surface geometry in SolidWorks, more computing power is necessary, therefore opening files of the ossicular chain would not transfer to SolidWorks correctly due to improper computing power. Since the reference points are an integral aspect of this new model, it was ultimately decided to use Geomagic to complete the CAD modeling to increase efficiency.

To create the static model, a support structure was designed to replicate the attachment points on the temporal bone. After a few iterations, this model was printed, and the digital version was transformed into a dynamic model. This dynamic model allows the user to remove and replace parts easily and display the movement of the middle ear. These iterations and the design process will be described in detail in sections 4.3 and 4.4.

For both models, client feedback served as the main design verification factor. Main specifications changed from ligament diameter and length to solely having the model based on the  $\mu$ CT scan and diameters selected by the client.

#### *4.2.2 Data Acquisition for Material Selection*

The physical dynamic model requires durable materials that resemble the structure and function of native middle ear tissues. Table 4.1, below, shows relevant material properties for the primary bodies. The Young's Modulus can be approximated as the material stiffness, while the material loss factor,  $\eta$ , describes the fraction of energy transmitted over energy stored. In sound mechanics, a high material loss factor indicates sound dampening. So, structures in the middle ear crucial to sound conduction display low, constant material loss factors, i.e., the ossicular chain and IMJ. Structures not directly associated with sound conduction have comparatively higher loss factors, i.e., smaller joints, ligaments, tendons, and membranes. These support structures primarily serve a protective function. Their material loss factors increase linearly with frequency to control the intensity of high-pitched sound delivered to the inner ear (Homma et al., 2009; [Sherif & Almufadi, 2020](#)).

Table 4.1. Material Properties of Primary Bodies (adapted from Homma et al., 2009, Gentil et al., 2012, Caminos et al., 2008, [Zhang & Gan, 2012](#))

Primary Body	Young's Modulus (Pa)	Density (kg/m <sup>3</sup> )	$\eta$
Malleus	1.41 x 10 <sup>10</sup>	Head: 2.55 x 10 <sup>3</sup>	0.01
		Neck: 4.53 x 10 <sup>3</sup>	
		Manubrium: 3.70 x 10 <sup>3</sup>	
Incus	1.41 x 10 <sup>10</sup>	Body: 2.36 x 10 <sup>3</sup>	0.01
		Short Process: 2.26 x 10 <sup>3</sup>	
		Long Process: 5.08 x 10 <sup>3</sup>	
Stapes	1.41 x 10 <sup>10</sup>	2.20 x 10 <sup>3</sup>	0.01
Incudomalleol Joint (IMJ)	1.41 x 10 <sup>10</sup>	2.39 x 10 <sup>3</sup>	0.01
Tensor Tympani Tendon	1.9 x 10 <sup>7</sup>	1.2 x 10 <sup>3</sup>	0.15 at 1 kHz
Stapedial Tendon	3.8 x 10 <sup>5</sup>	1.2 x 10 <sup>3</sup>	0.15 at 1 kHz
Pars Tensa (Tympanic Membrane)	3.0 x 10 <sup>7</sup>	1.2 x 10 <sup>3</sup>	0.15 at 1 kHz
Oval Window (Membrane)	4.0 x 10 <sup>7</sup>	1.2 x 10 <sup>3</sup>	Not Found
Anterior Malleolar Ligament	1.5 x 10 <sup>7</sup>	1.2 x 10 <sup>3</sup>	0.15 at 1 kHz
Lateral Malleolar Ligament	5.0 x 10 <sup>5</sup>	1.2 x 10 <sup>3</sup>	0.15 at 1 kHz
Superior Malleolar Ligament	4.9 x 10 <sup>4</sup>	1.2 x 10 <sup>3</sup>	0.15 at 1 kHz
Posterior Incudal Ligament	4.8 x 10 <sup>6</sup>	1.2 x 10 <sup>3</sup>	0.15 at 1 kHz
Stapedial Annular Ligament	4.12 x 10 <sup>5</sup>	1.2 x 10 <sup>3</sup>	0.25 at 1 kHz

Perhaps the most important native tissue material property for the model is the loss factor. Because this model will be acoustically stimulated to demonstrate middle ear physiology, it is important to consider how sound will propagate in synthetic materials at a 15:1 scale. Based on Table 4.1, the primary bodies can be split into two main categories: stiff materials with a constant loss factor and compliant materials with a variable loss factor.

The manufacturing technique for the stiff materials, i.e., the ossicles, involves 3D printing. Due to material availability of local print shops within the project budget, the potential materials were limited to the plastic family. Traditional printing filaments, e.g., ABS and PLA, are considered in Section 4.2.2.1. Softer thermoplastics and elastomers are considered in Section 4.2.2.2 for compliant body replication. Though the IMJ has a similar stiffness and density to the ossicular chain, it will be considered a compliant primary body in the dynamic physical model. A

compliant material is needed to act as shock absorber and ensure more correct motion of the IM complex (I. Dobrev, personal communication, February 4, 2022).

#### 4.2.2.1 Replicating the Ossicular Chain

The ossicular chain should be replicated using stiff plastics. Table 4.2 lists select material properties of traditional printing filaments considered in ossicular chain replication. It should be noted that Table 4.2 displays the material properties of virgin plastics. The presence of additives may change the values listed below (Granta EDUPack, 2022).

Table 4.2. Material Properties for Traditional Printing Materials (Granta EDUPack, 2022)

Material	Printing Technology	Young's Modulus (Pa)	Density (kg/m <sup>3</sup> )
ABS	FDM	$1.99 \times 10^9 - 2.89 \times 10^9$	$1.02 \times 10^3 - 1.06 \times 10^3$
PLA	FDM	$3.30 \times 10^9 - 3.85 \times 10^9$	$1.24 \times 10^3 - 1.27 \times 10^3$

The stiffness and density of the listed filaments are well-reported. Each filament's stiffness and density are similar to the ossicular chain. However, the material loss factors for each traditional printing filament vary significantly across sources (Granta EDUPack, 2022). Additionally, the literature reported values do not address the effect, if any, of material processing. For example, FDM technologies do not procedure isotropic materials. To better understand these relationships, the material loss factor for each selected filament was determined experimentally.

The experiment directly determined each printing filament's first natural frequency, or the lowest frequency at which elastic deformation begins. The material loss factor is then calculated from this property. For the experiment, each material was shaped into a thin beam, where the length is at least fifteen times the width. Under this geometry, it is assumed any wavelengths travel along the length of the beam instead of through the bulk of the material (I. Dobrev, personal communication, February 2, 2022). 15 cm by 2 cm by 0.5 cm beams of ABS and PLA at 30% infill were ordered from the HanCon 3D Printing service. The length dimension represents the approximate length of the largest ossicle, the malleus, on a 15:1 scale. The width and height dimensions satisfy the requirements for a thin beam. The 30% infill was chosen because 3D printed parts with 20-40% infill are cost efficient, functional, and withstand low forces (3DPros, 2021). It should be noted, the calculations below assume the beams are solid, i.e., not porous or hollow.

In the set-up, each beam was clamped at one end between two metal plates and free at the other. An Adafruit ADXL335 accelerometer was taped to the free end of the beam. In the calculations below, the mass of the accelerometer is considered negligible. A Visitation FRS8M speaker, connected to a Kenmo 12-Watt amplifier, was placed under the beam, flush with the metal support structure, as shown in Fig. 4.4. A polyurethane foam rectangle was taped to the membrane of the speaker and placed flush against the beam. The foam protected the speaker membrane and ensured enough signal was delivered to the beam to elastically deform it. When the speaker played a stimulus frequency, the resultant sound wave was assumed to travel along

the length of the beam to the accelerometer, causing beam deformation perpendicular to its length. To sense the deformation, the accelerometer's  $Z_{out}$  pin was used. The accelerometer's GND (ground) and  $V_{in}$  pins were also wired to complete the circuit.

The accelerometer was connected to the third Analog input channel, AI2, in a National Instrument's USB-4431 analog to digital converter, or ADC. Note, this report uses ADC and DAQ synonymously. The speaker and amplifier were connected to the analog output channel. The DAQ was connected to a 64-bit computer. The computer executed a MATLAB code which can be referenced in Appendix B, sending 0.5 seconds of a continuous signal through the speaker for a user-selected frequency range. Frequency ranges were dependent on the material being evaluated. To test the code and hardware, a rectangular aluminum beam was used. To determine the appropriate stimulus frequency range, the first natural frequency was approximated using the Young's Modulus and moment of inertia for a rectangular beam in Equation 4.1, below.

$$f(Hz) = \frac{3.516}{2\pi L^2} \sqrt{\frac{ELwh^3}{12m}} \quad (4.1)$$

The Young's Modulus of aluminum is  $69 \times 10^9$  Pa. The length of the beam,  $L$ , was 30.0 cm. The width,  $w$ , was 1.905 cm. The height,  $h$ , was 0.3185 cm. The distributed mass,  $m$ , was 0.0997 kg. Solving the equation above gives an approximate first natural frequency of 100 Hz. So, the stimulus frequency range was programmed to span one octave below this frequency and one octave above this frequency. The exact inputs were programmed to fall within the frequency resolution, which is 1 over the time block of 0.5 seconds. For the frequency resolution of 2 Hz, the stimulus frequency range was [26, 54, 78, 94, 100, 122, 188, 286, 400]. By manipulating the MATLAB linspace function, the stimulus range had smaller intervals around the estimated natural frequency. The amplitude of each stimulus frequency was 0.2 V to prevent signal clipping when stimulus frequencies approached the estimated natural frequency.

To monitor the signal input and signal output, the speaker and amplifier were also connected back to the AI0 and AI1 analog input channels, respectively. A block diagram for this set-up can be referenced in Fig. 4.3, while a test set-up using an aluminum beam is shown in Fig. 4.4 (I. Dobrev, personal communication, 2021; I. Dobrev, personal communication, February 4, 2022).

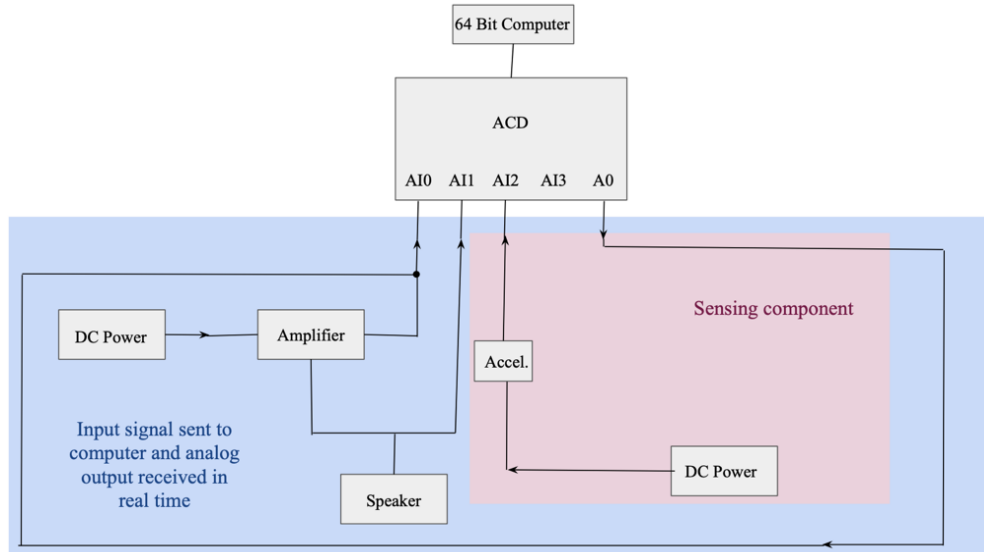


Fig. 4.3. Block diagram of DAQ, inputs, and output used to experimentally determine the first natural frequency and material loss factors

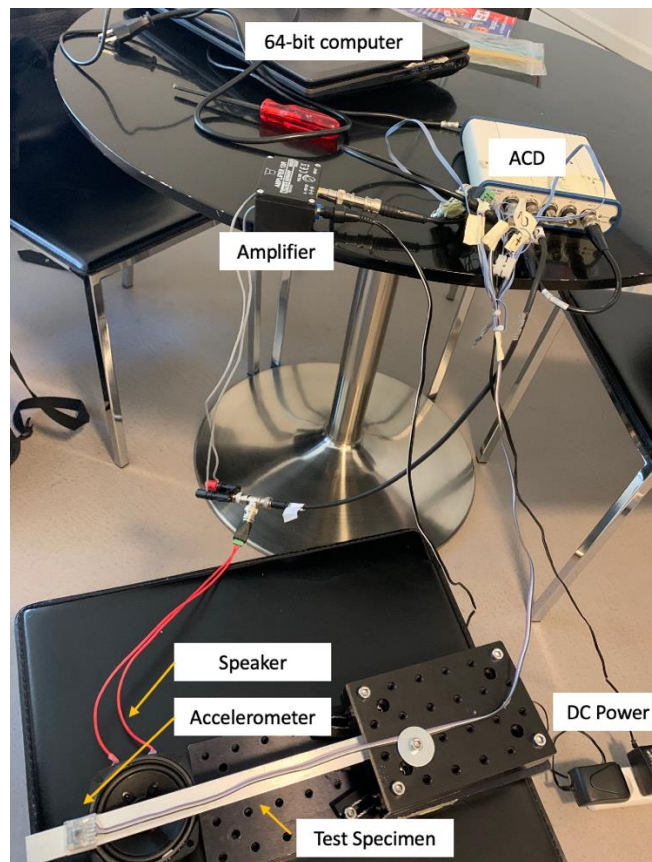


Fig. 4.4. Experimental set-up to determine first natural frequency and material loss factors

Figure 4.5 was produced in MATLAB and represents the data for one stimulus frequency in the user-selected range. Both a waveform and Fast Fourier Transform (FFT) were produced for the signal programmed to the amplifier (called “Amp In” in Fig. 4.5), the signal outputted by

the amplifier (called “Amp Out” in Fig. 4.5), and the signal measured by the accelerometer (called “Accelerometer” in Fig. 4.5).

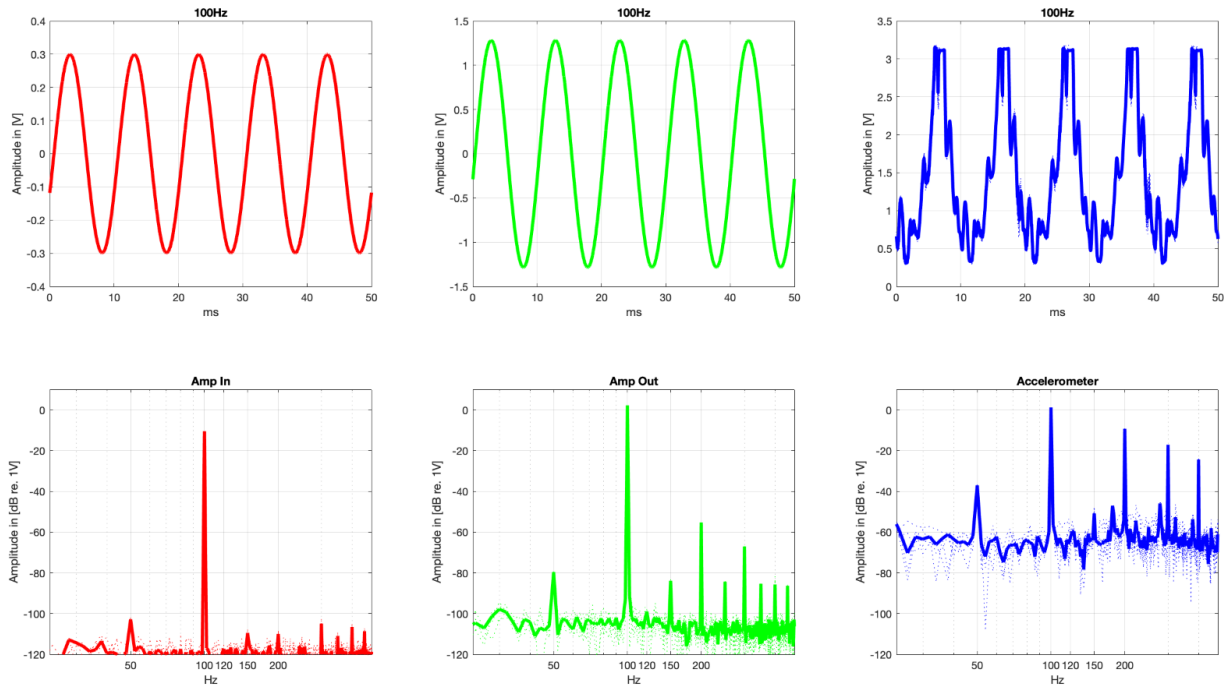


Fig. 4.5. Waveform data on the top row and FFT data on the bottom row for Amp In, Amp Out, and Accelerometer channels at a 100 Hz stimulus frequency. The waveform data for the accelerometer indicates the beam is resonating, which is confirmed by the smaller peaks in the FFT corresponding to harmonics of 100 Hz (e.g., 200 Hz, 300 Hz).

The magnitude of the frequency response measured by accelerometer was considered for each input signal. Using the FFT generated for the accelerometer at each input signal, the peak amplitude and corresponding frequency were extracted to generate a Bode magnitude plot using MATLAB. The angle of the magnitude was then taken to generate a Bode phase plot, again created in MATLAB. This process was done for channels AI1 and AI2. This was done to ensure the accelerometer was measuring beam vibration not speaker membrane vibration. Then, the ratio from AI2 to AI1 was taken to generate the transfer function.

Figure 4.6, below, shows the magnitude and phase plots for the transfer function. The magnitude plot for the transfer function was used to determine the first natural frequency of the aluminum beam. The peak corresponds to the first natural frequency,  $f_N$ , and the full width of the peak at half of its height represents the resonance width,  $\Delta f$  (Burwell & Strang, 1951).

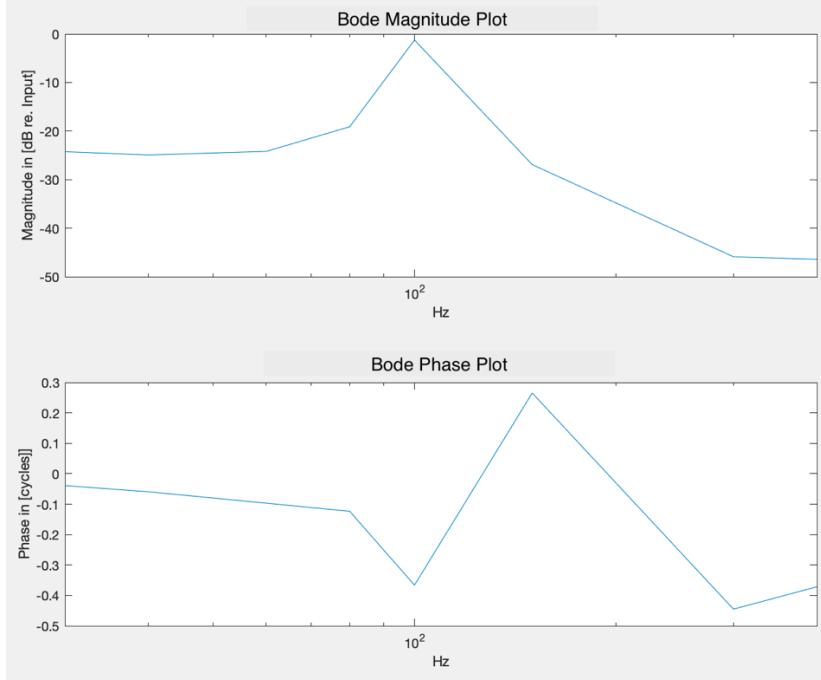


Fig. 4.6. Bode magnitude and phase plot for the aluminum beam used in the test set-up, showing a natural frequency of 100 Hz at -1.25 dB reference 1 V. The phase plot suggests there may be a second natural frequency around 150 Hz.

Both the natural frequency and resonance width can be used to determine the Q factor, a dimensionless parameter that relates the energy stored versus energy dissipated by the material for one radian of vibration. Equation 4.2 relates the three variables (Burwell & Strang, 1951).

$$Q = \frac{f_N}{\Delta f} \quad (4.2)$$

The peak frequency and corresponding amplitude were given in Figure 4.6. The resonance width was approximated by drawing a horizontal line 6 dB re 1 V down from the peak amplitude. The frequency values for each intersection point between the horizontal line and Bode plot were determined. The smaller frequency value was subtracted from the larger frequency value to give the resonance width. This procedure was repeated three times to determine the associated uncertainty of the resonance width measurement (I. Dobrev, personal communication, February 10, 2022). For the aluminum beam, the resonance width was calculated to be  $13 \text{ Hz} \pm 0.8 \text{ Hz}$ . The resonance width uncertainty was propagated when calculating the Q factor. Equation 4.3 indicates the propagation calculation for a generic equation  $Z = \frac{X}{Y}$  (Lindberg, 2000).

$$\frac{\Delta Z}{Z} = \sqrt{\left(\frac{\Delta X}{X}\right)^2 + \left(\frac{\Delta Y}{Y}\right)^2} \quad (4.3)$$

For the aluminum beam used in the test set-up, the Q factor was calculated to be  $7.7 \pm 0.5$ . The Q factor can be related to the damping the entire system experiences, expressed by the damping ratio,  $\zeta$ . Equation 4.4 relates the two parameters (Burwell & Strang, 1951).

$$\zeta = \frac{1}{2Q} \quad (4.4)$$

For the aluminum beam, the damping ratio was calculated to be  $0.07 \pm 0.004$ . The associated uncertainty comes from the Q factor and was calculated using equation 4.3. To relate the damping ratio to the material loss factor, the system was assumed to follow the Rayleigh Method. This method assumes the material loss factor linearly increases with the stimulus frequency,  $f_0$ , by some constant,  $c$ . Equation 4.5 shows the governing equation for the Rayleigh Method, and Equation 4.6 shows how the damping ratio is used to calculate  $c$  from the natural frequency (Alipour & Zareian, 2008).

$$\eta(f_0) = c \times 2\pi f_0 \quad (4.5)$$

$$c = \frac{\zeta}{\pi f_0} \quad (4.6)$$

For the aluminum beam, the material loss factor at 100 Hz is  $0.13 \pm 0.01$ , the uncertainty comes from the damping ratio and was calculated using equation 4.3. Calculations on the aluminum beam were performed to better understand sound mechanics theory. This method is far more suitable for viscous and—to a limited extent—viscoelastic materials. Homma et al. assumed this model when calculating the material loss factors for native middle ear tissues (2009). This method is also used for the thin beams of 3D printed PLA and ABS. The results can be reviewed in Section 5.1.

#### 4.2.2.2 Replicating the Ligaments, Tendons, Joints, and Membranes

Table 4.3 lists select material properties for common, flexible plastics to replicate compliant primary bodies, i.e., the ligaments, joints, and tendons. The primary soft materials within project budget include silicone elastomers and thermoplastic elastomers.

Table 4.3. Material Properties of Softer Materials (Granta EDUPack, 2022)

Material	Young's Modulus (Pa)	Density (kg/m <sup>3</sup> )
Silicone	$5.0 \times 10^5 - 5.0 \times 10^7$	$1.02 \times 10^3 - 1.20 \times 10^3$
Thermoplastic Polyurethane Elastomer (TPU)	$2.85 \times 10^7 - 3.97 \times 10^7$	$1.18 \times 10^3 - 1.20 \times 10^3$

The stiffness and density of the materials listed above are like the compliant primary bodies in Table 4.1. Again, the most important parameter to consider in replicating middle ear physiology is the material loss factor. The material loss factors for each soft plastic were determined experimentally.

The materials listed above were not stiff enough to be tested in a cantilever beam structure. Instead, the material loss factor was determined by considering each material as a first order spring. A 32 cm TPU tube with a 2.5 mm inner diameter and 4.0 mm outer diameter (SKU Number 0724310200) and 30 cm silicone string at 3 mm diameter (SKU Number 1026210603)

were purchased from APSO parts. Because the listed Elastic Modulus range for VMQ silicone is so large, the modulus for the specimen ordered was approximated. APSO lists the silicone as a Shore Hardness of 8 on the A scale, indicating a very soft material. The hardness value can be converted to the Young's Modulus in Megapascals,  $10^6$  Pa, using equation 4.7, below (Computer Aided Technology, 2022).

$$E = e^{(Shore\ A\ Durometer \times 0.0235 - 0.6403)} \quad (4.7)$$

Equation 4.7 gives a Young's Modulus of  $6.3 \times 10^5$  Pa for VMQ silicone. A similar procedure was not completed for TPU because no Shore Hardness value was given and the listed Modulus in Table 4.3 does not vary significantly. Fig. 4.7 displays the experimental set-up for both strings. Both ends of the string were pinned using metal support structures, the string was oriented along its length, and the string length was measured. The center of the string was measured and marked in pen for ease of seeing the exact location. The string was then stretched by 0.9 cm, and the metal support structures were fastened to the metal breadboard, shown below. A 30 cm ruler was placed height wise behind the system, and the height of the string in its neutral position was taken.

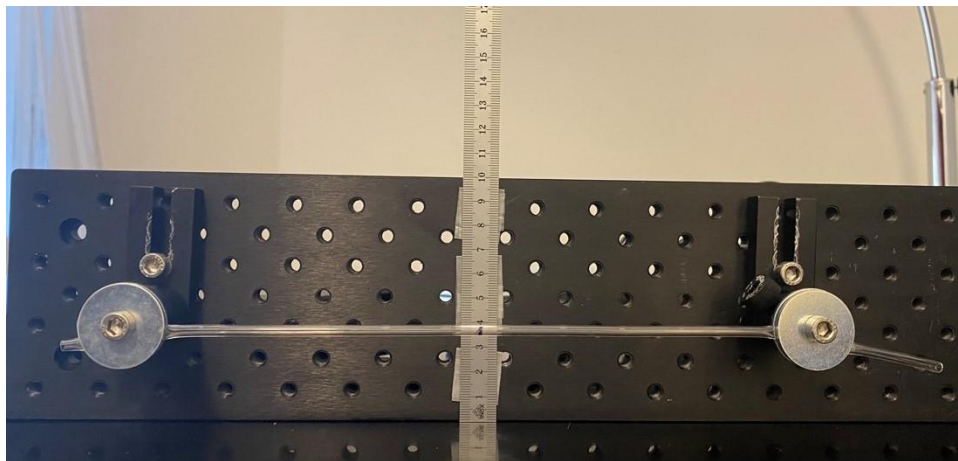


Fig. 4.7. Experimental set-up used in determining system damping and material loss factors

The TPU string was tested first. When the string was properly secured in the support structure pictured above, it was then plucked at its center. Video motion capture using an iPhone 11 was used to capture the vibrations. The video was set on a slow-motion setting pre-programmed to record at 240 frames per second (fps). The motion of the string was evaluated at certain frames, outlined below, and the height of the vibrations were measured using the ruler behind the setup.

To begin the TPU data collection, the slow-motion video was imported into the Windows Media Player and the Play Speed Settings feature under Enhancements was selected. This allows the user to manually advance the video one frame at a time. Then the number of frames were counted from the initial pluck to the end of the vibration, referenced as one full cycle. It was found that one full cycle for TPU was 60 fps. To find the time it took for one full cycle, Equation 4.8 was used.

$$\frac{\text{Number of frames}}{\text{Video frame rate}} \quad (4.8)$$

Then, the percent increments of data collection were determined by the user. The percent increments are how often data is collected within the full time of the sample. 2% increments of data collection were reasonable for the TPU data set because the full cycle was only 0.25 seconds, and 51 data points for 60 frames will give representative data of the full cycle. Using Equation 4.9, this resulted in 1.176 fps per 2% increment, but since the software only allowed for 1 fps increases, the frames were advanced by one for each data point collection.

$$\frac{\text{Number of frames}}{\text{Number of data points}} \quad (4.9)$$

Since the end of the full cycle was extremely dampened and barely oscillated, the 90-100% increments were advanced three frames instead of one frame to result in the full 60 frames.

Testing of the silicone string followed the same procedure, however there were some variations due to the higher time for dampening. It was found that the full cycle was 450 frames and 1.875 seconds long. Because of the high number of frames compared to the TPU sample, the data points had to be collected in 1% increments to get a representative set of data. This resulted in the frames being advanced by four for each increment of data collection, and the 91-100% increments were advanced by nine frames to result in the full 450 frames.

The excel files containing the time and location vectors from the procedure above were loaded into MATLAB. Figure 4.8. plots the raw data with a connecting line, showing the oscillation of the string as it returns to its neutral position. The location vector is represented as amplitude.

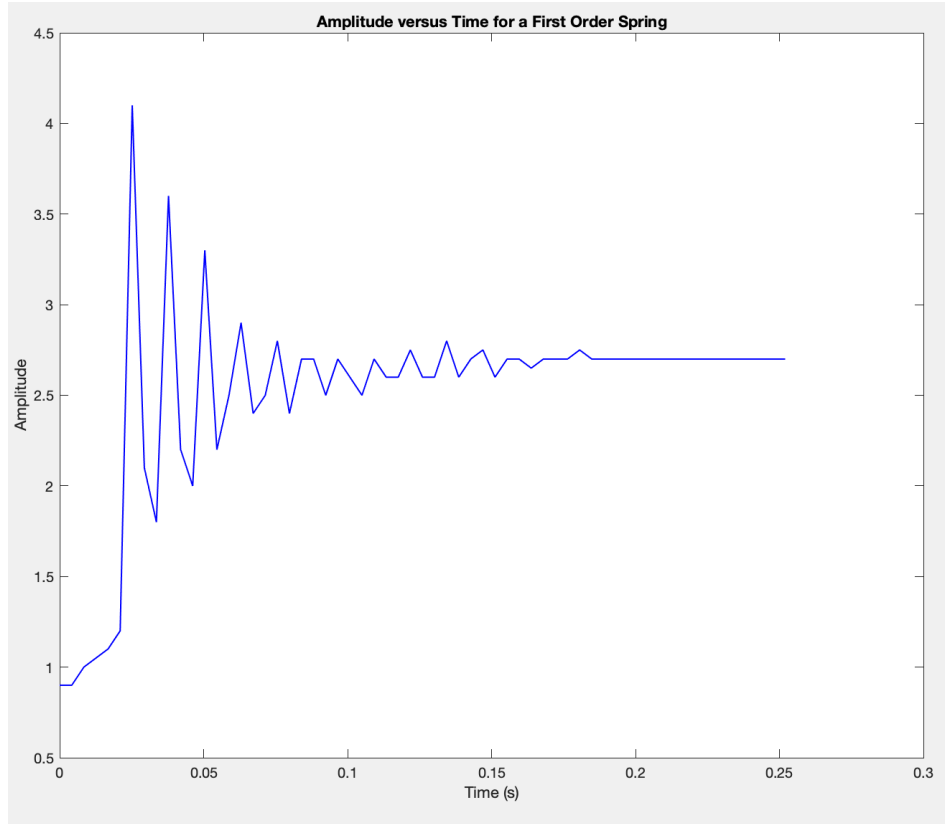


Fig. 4.8. Raw data for the TPU specimen

Because the string is assumed to be a first order system, the amplitude's exponential decay can be approximated using Equation 4.10, which shows amplitude,  $A$ , as a function of time,  $t$ . (Burwell & Strang, 1951).

$$A(t) = A_0 e^{-\frac{t}{\tau}} \quad (4.10)$$

In Equation 4.10, both  $A_0$  and  $\tau$  are constants.  $A_0$  indicates the initial amplitude of the system, and  $\tau$ , the time constant, is defined the amount of time for system's amplitude to decrease by a full step, which can be approximated as 63% (Burwell & Strang, 1951). Of the two constants, only  $\tau$  is needs to calculate the material loss factor. To find the time constant, the midline was first adjusted to 0 by subtracting the mean of the amplitude from the total amplitude. Once the midline was adjusted, the absolute value of the amplitude was taken. Once the absolute value was taken, the signal was trimmed to eliminate noise. For the TPU specimen, the signal was trimmed to begin at 0.05 seconds and end at 0.2 seconds. Figure 4.9 shows the raw data in comparison with the processed data. The final, trimmed signal represented by the red trendline was further processed to determine the time constant.

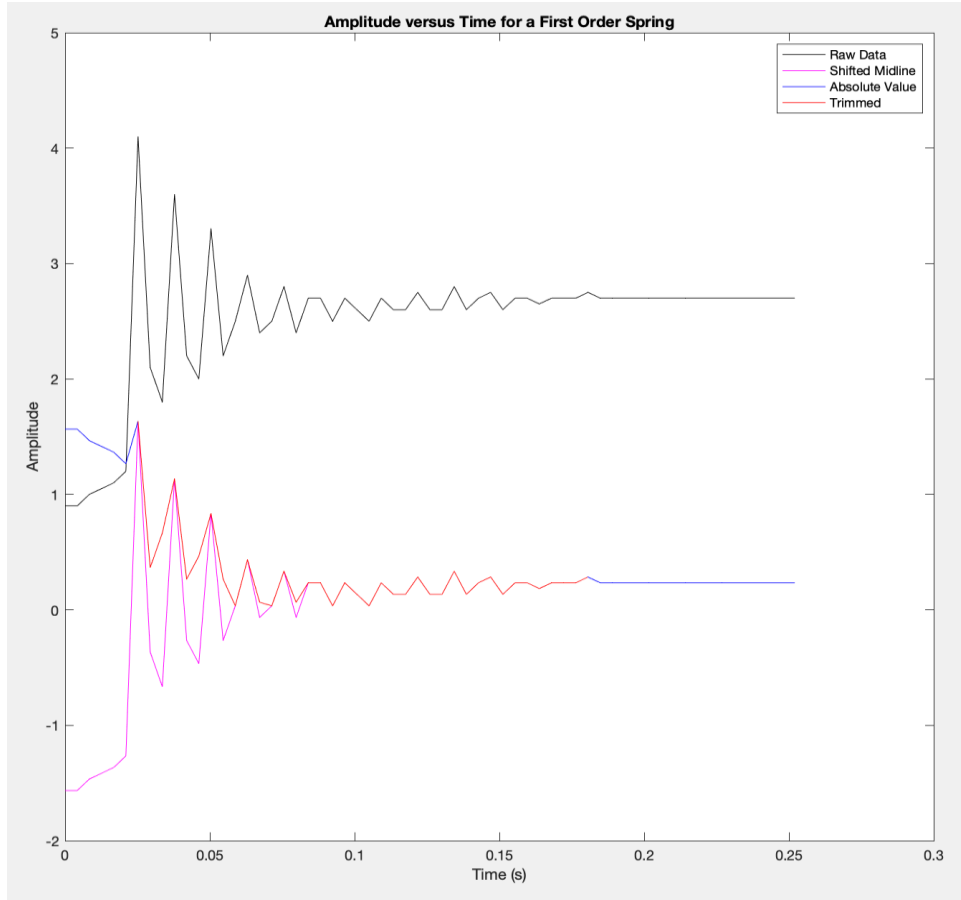


Fig. 4.9. Processed data for the TPU specimen

The local maxima of the trimmed signal were found using the MATLAB function, `findpeaks`. The data points were then plotted, and the MATLAB curve fitter app was used to generate an exponential trendline. The curve fitting app estimates both  $A_0$  and  $\tau$  with 95% confidence bounds and produces an  $R^2$  value to indicate goodness of fit. It should be noted that  $\tau$  is expressed as  $-\frac{1}{\tau}$  and must be re-expressed for further analysis. Similar graphs for the silicone specimen can be found in Appendix C, and the MATLAB code and functions used to process and analyze this data can be referenced in Appendix D.

The generated curves for both TPU and silicone can be found in Section 5.1. The logarithmic decrement, a constant which also indicates the rate of amplitude reduction, can be calculated from the time constant. In Equation 4.11, the logarithmic decrement is represented by  $\delta$ . The period of the damped frequency is represented by the variable  $P$  (Burwell & Strang, 1951). The uncertainty of the time constant was propagated using Equation 4.3.

$$\delta = \frac{P}{\tau} \quad (4.11)$$

The logarithmic decrement was then used to find the damping ratio,  $\zeta$ , as shown in Equation 4.12 (I. Dobrev, personal communication, 2021).

$$\zeta = \frac{\delta}{\sqrt{(2\pi)^2 + \delta^2}} \quad (4.12)$$

The uncertainty in the damping ratio was considered using Equation 4.13, below, which is generalized to consider a function, Z, with independent variables, W, X, and Y (Lindberg, 2000).

$$\Delta Z^2 = \left(\frac{\delta f}{\delta w}\right)^2 \Delta w + \left(\frac{\delta f}{\delta x}\right)^2 \Delta x + \left(\frac{\delta f}{\delta y}\right)^2 \Delta y \quad (4.13)$$

Like the methodology described in Section 4.2.2.1, it is assumed the system undergoes viscous damping governed by Equation 4.5. To use this equation, the natural frequency was calculated from the damped frequency. The damped frequency was determined by taking the inverse of the period, or 1/P. Equation 4.14 related the damped frequency,  $f_D$ , to the natural frequency,  $f_N$  (Burwell & Strang, 1951). Again, uncertainty was considered using Equation 4.13 and propagated from the damping ratio.

$$f_N = \frac{f_D}{\sqrt{1-\zeta^2}} \quad (4.14)$$

Both the experimentally determined natural frequency and damping ratio can be used to solve for the constant, c, in Equation 4.6. These results for TPU and silicone can be referenced in Section 5.1.

### 4.3 Alternative Designs

The static model was designed to focus on an anatomical visual representation of the middle ear while the dynamic model was intended to be a functional model that replicates the movement of the middle ear. The following section describes each model's digital iterations in chronological order including their individual benefits and drawbacks. The transition from how the static model transitioned into the dynamic model is further described.

#### 4.3.1 Static Model

The following sub-section describes the iterations of the static model. Each iteration was evaluated based on client feedback and changed to create the most cost-effective model.

##### 4.3.1.1 Design 1

The goal of this design, as seen in Fig. 4.10 and 4.11, was to mimic the temporal bone by creating a tight shell shape surrounding the middle ear. The surrounding shell was connected to the end of the various ligaments and muscles at their anatomically correct attachment points by extruding material from the end of the ligaments and muscles to the shell. This design was created using the middle ear anatomy represented in Geomagic and transferred into SolidWorks to create the surrounding temporal bone. SolidWorks has more user-friendly features to model the Loft feature, compared to Geomagic, therefore it was ideal to model the temporal bone in SolidWorks. However, it was difficult to edit the middle ear anatomy that was imported from Geomagic when needed because it is imported as one body and its features cannot be changed in SolidWorks. This design was not continued and therefore the cuts into the temporal bone to create an open view were not completed. Overall, this design was an attempt to closely recreate

the temporal bone while having an open view of the middle ear. However, the two software, Geomagic and SolidWorks, were not compatible therefore making modifications difficult.

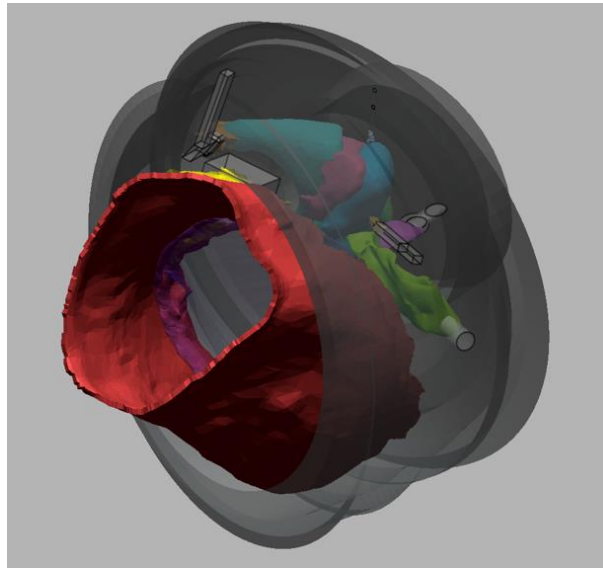


Fig. 4.10. Static model design 1 in Geomagic

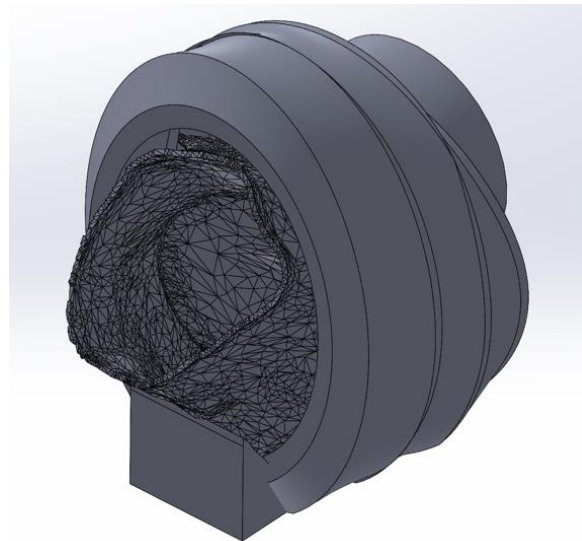


Fig. 4.11. Static model design 1 in SolidWorks

#### 4.3.1.2 Design 2

Design 2, as seen in Fig. 4.12, was created with the goal of replicating the shape of the temporal bone and tympanic cavity. One of the main concerns with the previous project's design was the lack of anatomical accuracy of the attachment points. To address this issue, the shape of the tympanic cavity was extracted from the  $\mu$ CT scan to create a support structure. Having a support structure that replicates the shape of the tympanic cavity allows for more accurate attachment points.

Although this design provides a more accurate visual of the middle ear cavity, the support structure is very dense. A priority with the designs included limiting material cost, therefore this design was not feasible. Additionally, this design would not translate well into a dynamic model. When using the dynamic model, the user should be able to access the ligaments easily to increase the ease of interchangeability of the primary bodies and this design does not allow for this.

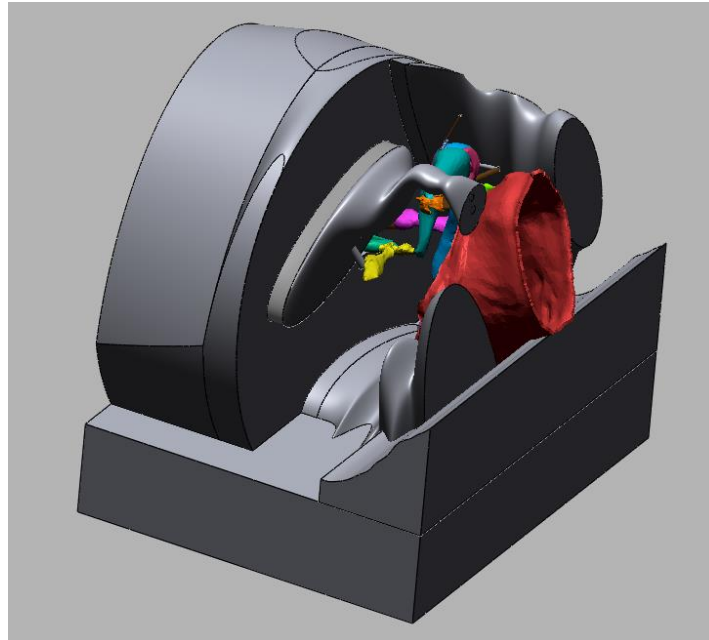


Fig. 4.12. Static model design 2 in Geomagic

#### *4.3.1.3 Design 3*

Design 3, seen in Fig. 4.13, was created with the intention of having the most visibility of the middle ear's primary bodies. A top priority of the client was to have as much visibility while maintaining anatomically accurate supports and extensions of the primary bodies. The design was created using a cage-like structure where the ligaments extend to the support structure that extends from the outside cage. The base structure was created as a separate part, so the cage structure could be removed. The removable structure allows the middle ear to be easily handled and viewed. Design 3 can easily be modified and translated into the dynamic model.

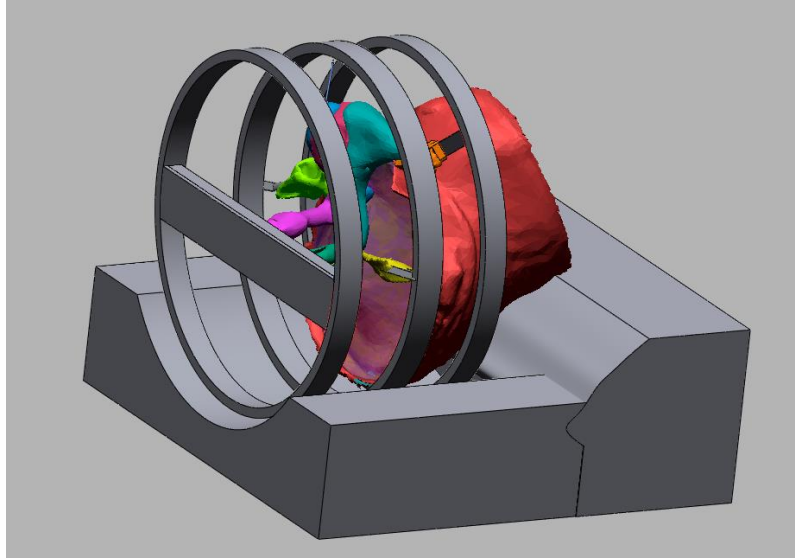


Fig. 4.13. Static model design 3 in Geomagic

#### 4.3.1.4 Design 4

A Pugh concept selection matrix was created to determine which design the team should proceed to modify. The Pugh concept selection matrix considered the needs and wants of the static model which were previously identified in 4.1.1. The features of the three initial designs were evaluated by creating a Pugh concept selection matrix and based on feedback from Dr. Dobrev's team. The Pugh concept selection matrix can be found below in Table 4.4. Each design was ranked on a scale from -1 to 1, where -1 was considered bad, 0 was considered neutral and 1 was considered good.

Table 4.4. Pugh Concept Selection Matrix for Static Model

	<b>Design 1</b>	<b>Design 2</b>	<b>Design 3</b>
Modifiable	-1	0	1
Visible	-1	0	1
Anatomically Correct	1	1	1
Distinguishable Supports	0	-1	1
Support at Ligaments	1	1	1
Open View	-1	0	1
Easily Transportable	1	1	1
Durable Materials	1	1	1
Easily Printable	0	1	-1
Least Material Possible	-1	-1	-1
Shape of Temporal Bone	-1	1	-1
Surgical View	-1	-1	1
<b>Total</b>	<b>-2</b>	<b>2</b>	<b>8</b>

Based on the results of the Pugh concept selection matrix, design 3 was determined to best fit the wants and needs of the client. Design 3 was further modified with improvements discussed with Dr. Dobrev and the team.

Design 4, seen in Fig. 4.14, was modeled after the prior three designs were created. Design 4 used design 3 as a primary influence using the cage-like structure. Further modifications of the cage-like structure included reducing the amount of support around the ear canal, similar to design one. The model consists of two parts that would be printed separately. The first part is the base of the model that supports the primary bodies and shows an open view of the middle ear. The second part is a cover that goes over the primary bodies and slides into the base part on each side. This component shows the surgical view through an opening on the cover. This design was the final approved design by Dr. Dobrev that was imported into the print shop software to calculate the potential cost.

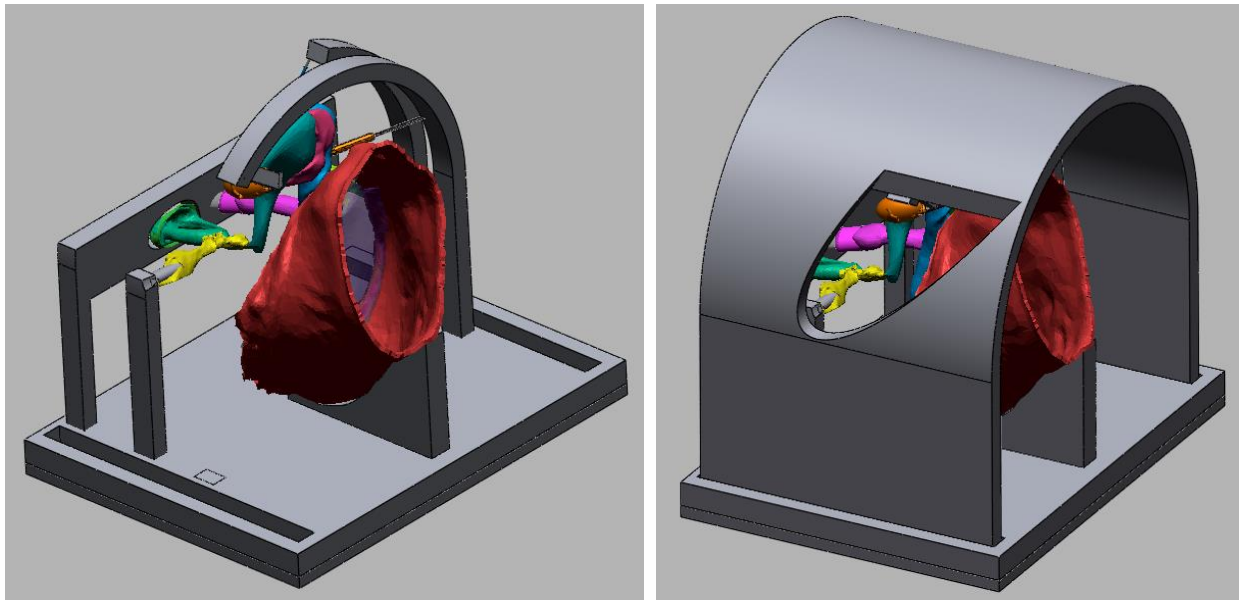


Fig. 4.14. Right: Static model design 4 in Geomagic with surgical view cover. Left: Static model design 4 in Geomagic without surgical view cover.

#### 4.3.1.5 Design 5

After loading Design four into the printing software and discussing the total cost with Dr. Dobrev, the design was modified a final time to reduce material costs. The base was made smaller in every direction and the cover was thinned and shortened. The surgical view cover was secured with extrusions on top of the base instead of extruding into the base. These design changes reduced the cost of the print by nearly half. The surgical view cover was further modified to display a more accurate view and angle, which is displayed in Fig. 4.16. The surgical view was extruded outwards to represent an accurate view and create the illusion of the viewing the middle ear through the temporal bone as seen in Fig. 4.15.

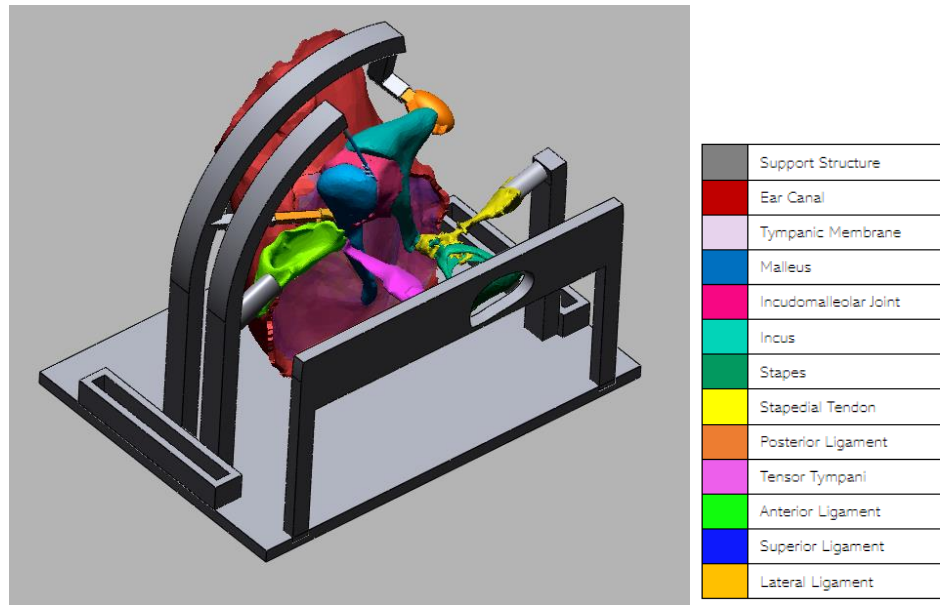


Fig. 4.15. Isometric view of final static model without the surgical view cover

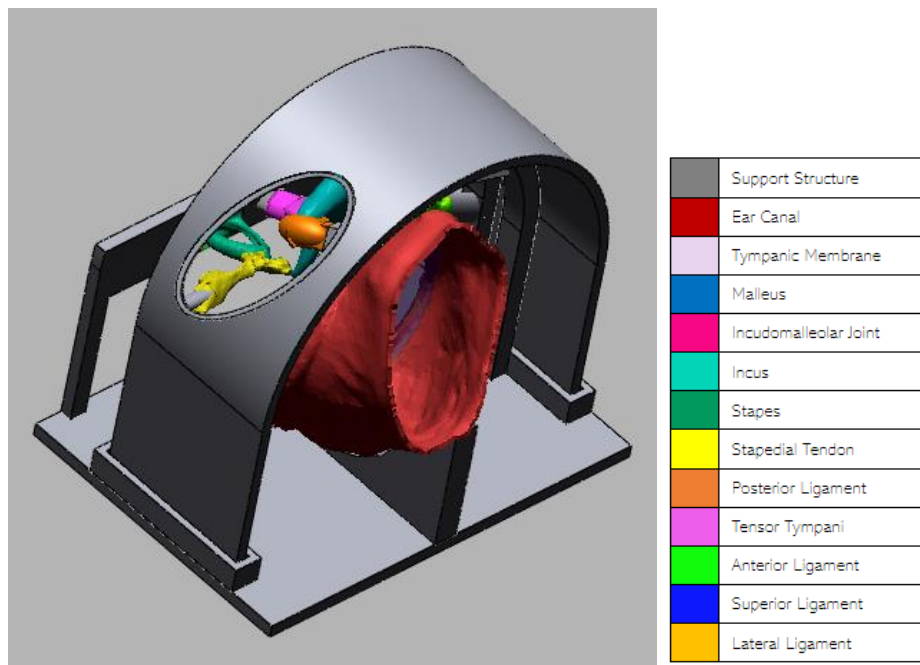


Fig. 4.16. Surgical view of final static model with the surgical view cover

The final model, design 5, was 3D printed in PLA and painted to better visually represent the individual primary bodies. An isometric view of the printed model without the surgical view cover is shown in Fig. 4.17. The printed model with the surgical view cover is shown in Fig. 4.18.

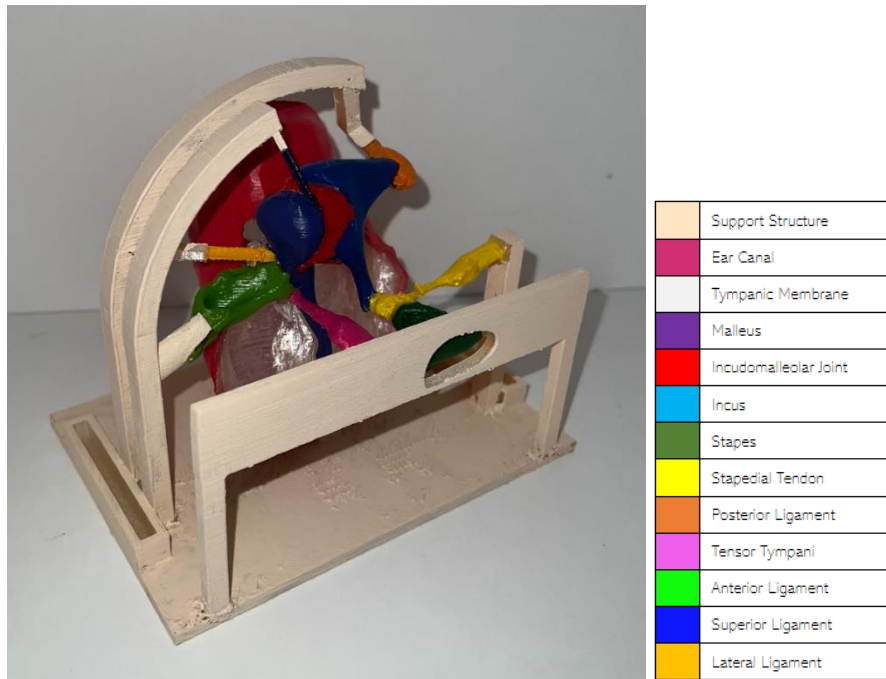


Fig. 4.17. Isometric view of printed final static model without surgical view cover



Fig. 4.18. Surgical view of printed final static model with surgical view cover

#### 4.3.2 Dynamic Model

To create the dynamic model, each iteration was created digitally and reviewed with the client. Based on client feedback, subsequent iterations were created. The following details each

design's features including their individual benefits and drawbacks while creating the most cost-effective dynamic model. A final design was created and presented to Dr. Dobrev.

#### 4.3.2.1 First Iteration Digital Dynamic Model

The goal of the first iteration of the dynamic model was to replicate the anatomy of the middle ear while allowing for movement. This iteration is a continuation of the static model, using the same support structure and anatomically correct attachment points. All the ligaments were changed to be modeled as cylinders and the temporal bone/support structure had extrusions for parts to be attached. The largest change was separating the ligaments, ossicles, and support structure into separate parts and determining the best way to set up the mechanical connection points within the model. Determining the most suitable connections for the ligaments to the ossicles and support structure was decided using a Pugh concept selection matrix. Several options for connections were explored including screws, hooks, buttons, bolts, etc. A decision matrix was created with the most important factors based on client needs and team resources. The factors that influenced the decision were anatomically correct, ease of CAD, accessibility of buying parts, ease of interchangeability, and durability. The scale ranged from 1 to 5, with 1 being considered very bad, 2 being considered bad, 3 being considered neutral, 4 being considered good, and 5 being considered very good. The Pugh concept selection matrix can be found below in Table 4.5.

Table 4.5. Pugh Concept Selection Matrix for Connection Points

	<b>Screws &amp; Rubber bands</b>	<b>Ring/Hole &amp; Hook</b>	<b>2 Hooks</b>	<b>Snap Buttons</b>	<b>Hinge Clasp</b>
Anatomically Correct	5	5	5	1	5
Ease of CAD	5	4	5	5	4
Accessibility of Buying Parts	5	5	5	5	5
Ease of Interchangeability	1	4	4	3	5
Durability	1	5	5	3	5
<b>Total</b>	<b>17</b>	<b>23</b>	<b>24</b>	<b>17</b>	<b>24</b>

Hinge clasp/binder ring and 2 hooks had a tie in ranking therefore, anatomically correct, ease of interchangeability, and durability were viewed at a higher priority when considering the highest rank because they are client wants/needs. Since the ease of CAD and accessibility of buying parts are less of a priority and affect the client less, it was decided to prioritize the client's wants/needs to best satisfy the objectives. Both the hinge clasp and the 2 hooks had a ranking of 5 for anatomically correct and durability, whereas hinge clasp had a ranking of 5 for ease of

interchangeability compared to the 2 hooks which had a ranking of 4. Therefore, the team will proceed with the hinge clasp for the first iteration of the dynamic model.

The mechanical idea of the hinge clasp was tested with LEGOs. The mechanism assembled replicated the connection with hinges and clasps to test if there would be enough movement for the ligament. Fig. 4.19. below shows how the mechanism was set up.



Fig. 4.19. LEGO hinge clasp mechanism

After reviewing the findings with the client, the client expressed to go in a different direction. The client had a strong desire to use wires rather than the metal hinge and clasp since the model will be small, therefore the grip for the clasp may be difficult. The client preferred a wire connection because of easier assembly and the wire's ability to be cut and soldered. The team proceeded with the clients' wants and further proceeded to dimension the connections to have the wires fit.

After brainstorming ideas for connections and confirming the clients' wants, the team proceeded to the Geomagic model. First, the ligaments were separated from the support structure and the ossicles that they are connected to. Each ligament and its corresponding connection to the temporal bone and ossicle had holes added to them, allowing for wires to be fed through to hold the assembly together. This design replicates the pin connection that ligaments can be modeled as.

The design of the stapes muscle and posterior ligament are more complex. In the original anatomy, the posterior ligament wraps around the short process of the incus. This shape was replicated using rectangular extrusions on either side of the incus as well as a football-like shape cap at the end of the short process of the incus. The stapes muscle appears to wrap around the neck of the stapes and the lenticular process of the incus. This was replicated by creating a clamp-like shape that can be tightened around these areas.

Although this iteration strongly replicated the anatomy and geometry of the middle ear, the client desired a more simplified version to emphasize ease of assembly. This iteration included anatomically correct articulation points, ligament lengths, and ligament diameters. The

client expressed concerns regarding the complexity of the stapes muscle design as well as the bulkiness of the posterior ligament design. Another concern was the diameters of the ligaments. The client noted that the diameters may be too large and may cause a difference in stiffness between the ligaments when they are printed. Based on this client feedback, the next iteration was created digitally as shown in Fig. 4.20.

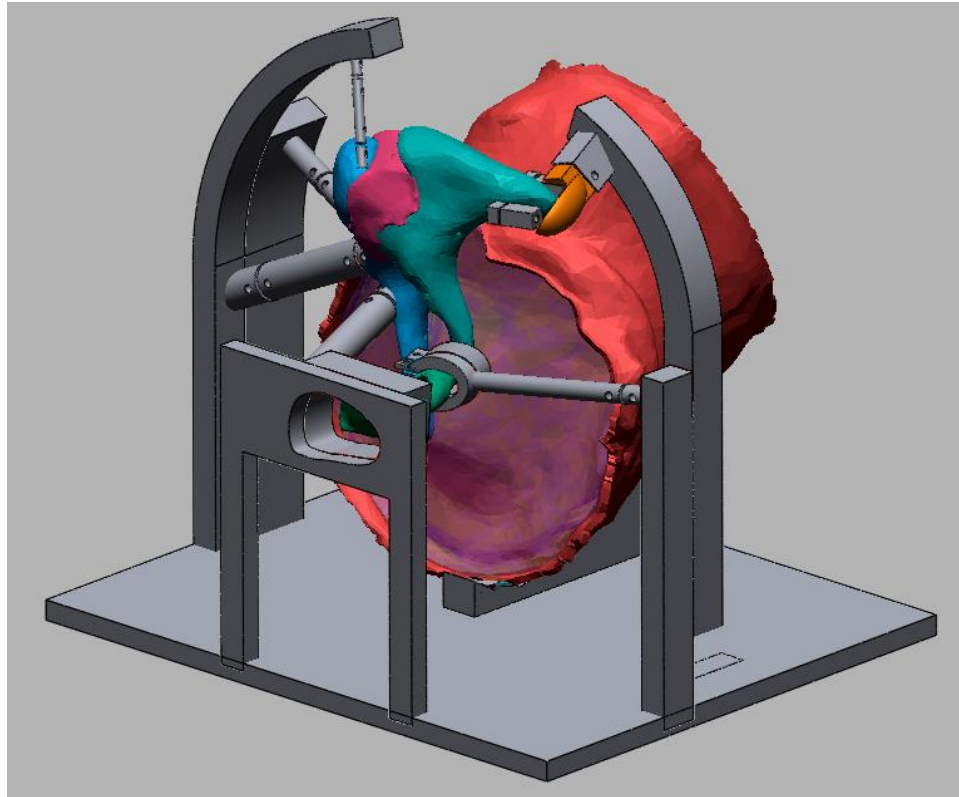


Fig. 4.20. Dynamic model iteration 1

#### 4.3.2.2 *Second Iteration Digital Dynamic Model*

After further communication and considerations with Dr. Dobrev, the decision was made to not consider the entirety of the physical anatomy as an important specification. The overall functionality of the ligaments remained the priority. The distances and vector directions of the ligaments and muscles remained important while the shape and diameters of the ligaments were discarded in the model. The ligaments were all given an equal diameter per the client's request.

Due to the expense of printing, the team and the client decided the entirety of the ear canal was not important for the overall functionality of the middle ear. The ear canal was simplified into a more basic shape and shortened to cut down costs on printing, time, and material. Additionally, to remove as much material as possible without disrupting the functionality and stability of the model, the inner portion of the base was removed. The second iteration, shown in Fig. 4.21., was then shown to and reviewed with the client.

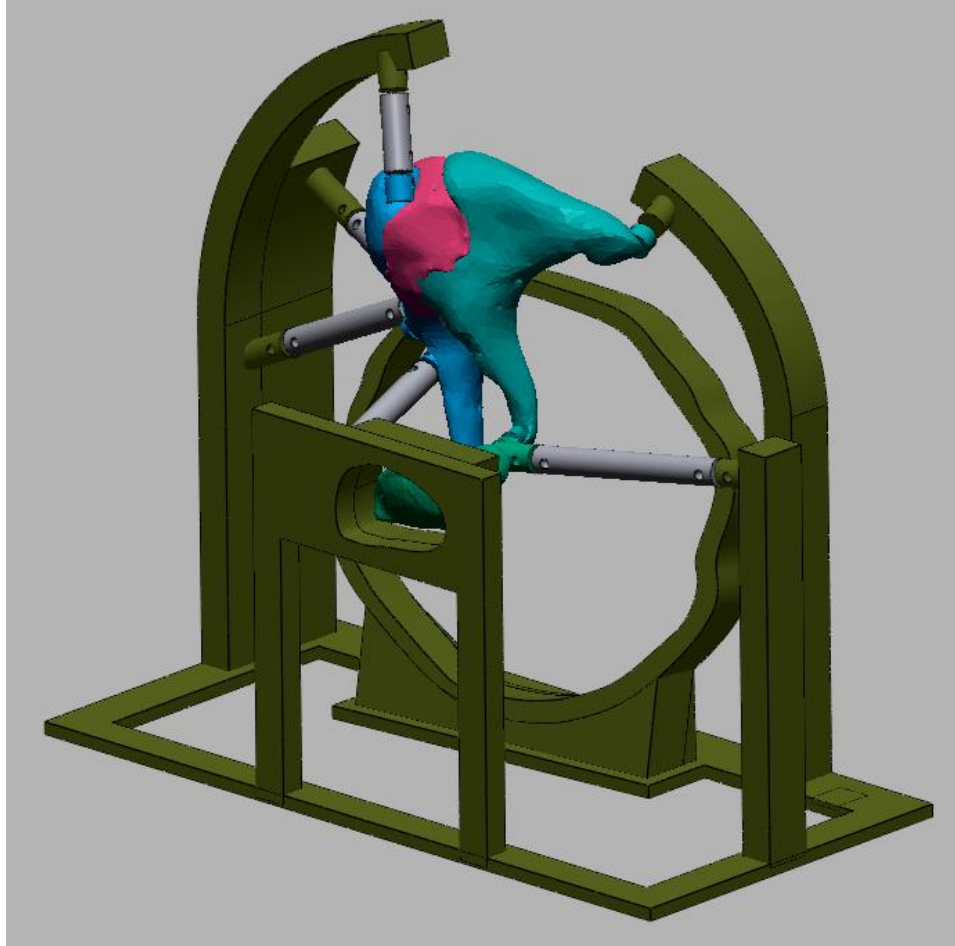


Fig. 4.21. Dynamic model iteration 2

#### *4.4 Final Design Selection*

The final dynamic model was selected by collaborating with Dr. Dobrev through presenting the design, receiving client feedback, and modifying the design to meet these desired changes. This process was repeated multiple times until a final design was agreed upon with the client, as well as ensuring that the model remained within budget. Client feedback was the main factor in evaluating the alternative models. The final model was set to be scaled to 15:1 from the actual size of the middle ear per the client's request. Specific measurements of the ligaments were no longer required by the client as the functionality of the model was prioritized over anatomical correctness. The diameters of the ligaments at a scaled printed version were set at 8.25 mm by the client. The corresponding holes for the attachment points were set at a 3 mm diameter based on the diameters of the ligaments and the necessary space needed when attaching the ligaments to the ossicles and temporal bone.

Initially when the model was set to print, the model was designed so the ligaments would be printed in TPU. However, the ligaments were not printed since it was discovered the scale of the print would not match the stiffness of the ligaments and not allow the proper movement of

the model. The final decision was to model the ligaments with either rubber bands or silicone based on the materials findings. The materials selection process is explained further in Chapter 5.

The minimization of material on the model was a priority for the client, therefore the final model was designed to be attached to a breadboard at the base to ensure proper support, as shown in Fig. 4.22. This required design changes and additional patterned holes to be cut into the base of the model to match the pattern of the breadboard so it can be connected physically with screws. Finally, the ear canal was modified to be a simple, circular shape and made to be removable to ensure ease of assembly. The ear canal structure can be removed from the breadboard independent from the rest of the base so the tympanic membrane can be easily attached. These modifications reduced the cost of the model to be within Dr. Dobrev's budget.

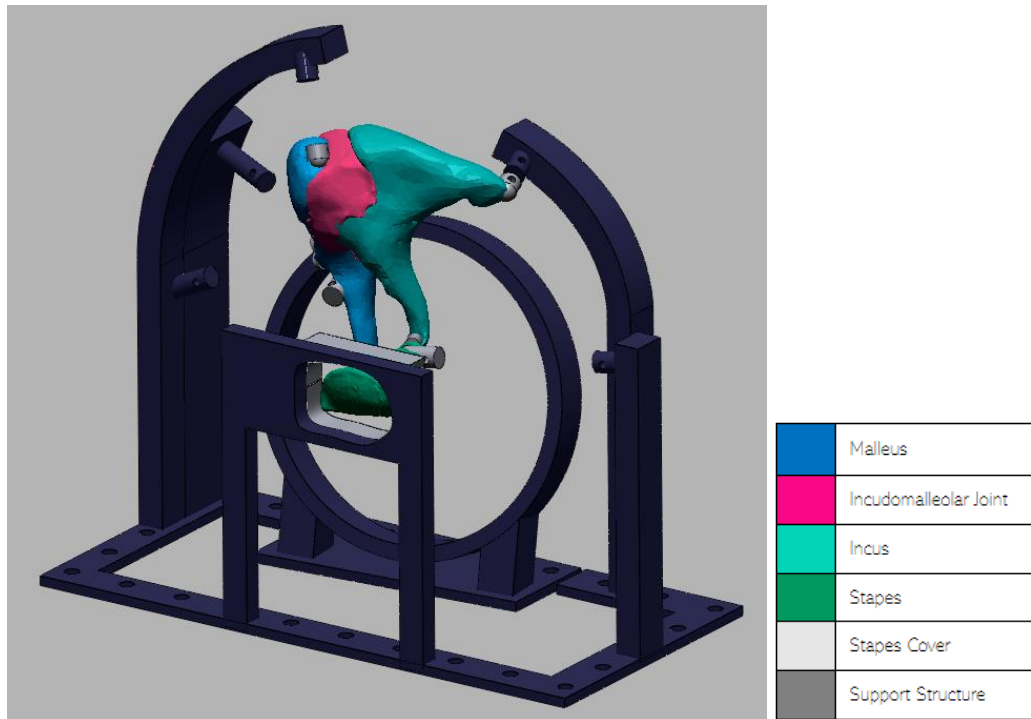


Fig. 4.22. Dynamic model final design in Geomagic. Not pictured: membranes, ligaments, connection mechanisms.

The physical dynamic model can be seen in Fig. 4.23. The features not pictured in the digital dynamic model in Geomagic are the tympanic membrane, the cochlea, their connection mechanisms, and the mechanisms used to connect the joints. As pictured below in Fig. 4.25, magnets are glued around the ring of the 3D printed ear canal. The material used to represent the tympanic membrane will then be placed on these magnets, and another set of magnets will be attached to hold the membrane in place. The malleus will have two magnets glued onto it, one on the anterior process and one on the lateral process. An additional magnet on the opposite side of the tympanic membrane material will secure the malleus to the membrane. The same process will be repeated with the stapes and the cochlea as seen in Fig. 4.26. The cochlea will be attached to the support structure with magnets, and the stapes will be attached to the cochlea with magnets.

The same approach will be used as the last MQP team to secure the joint between the incus and malleus as well as the joint between the incus and stapes as seen in Fig 4.24 (Kane et al., 2020). Nails will be placed around the joint on both the incus and malleus and secured with rubber bands. The IMJ will be printed in TPU as a place holder. Nails will also be placed around the lenticular process of the incus and the neck of the stapes and secured with rubber bands. This will secure these bodies together while also allowing for movement.

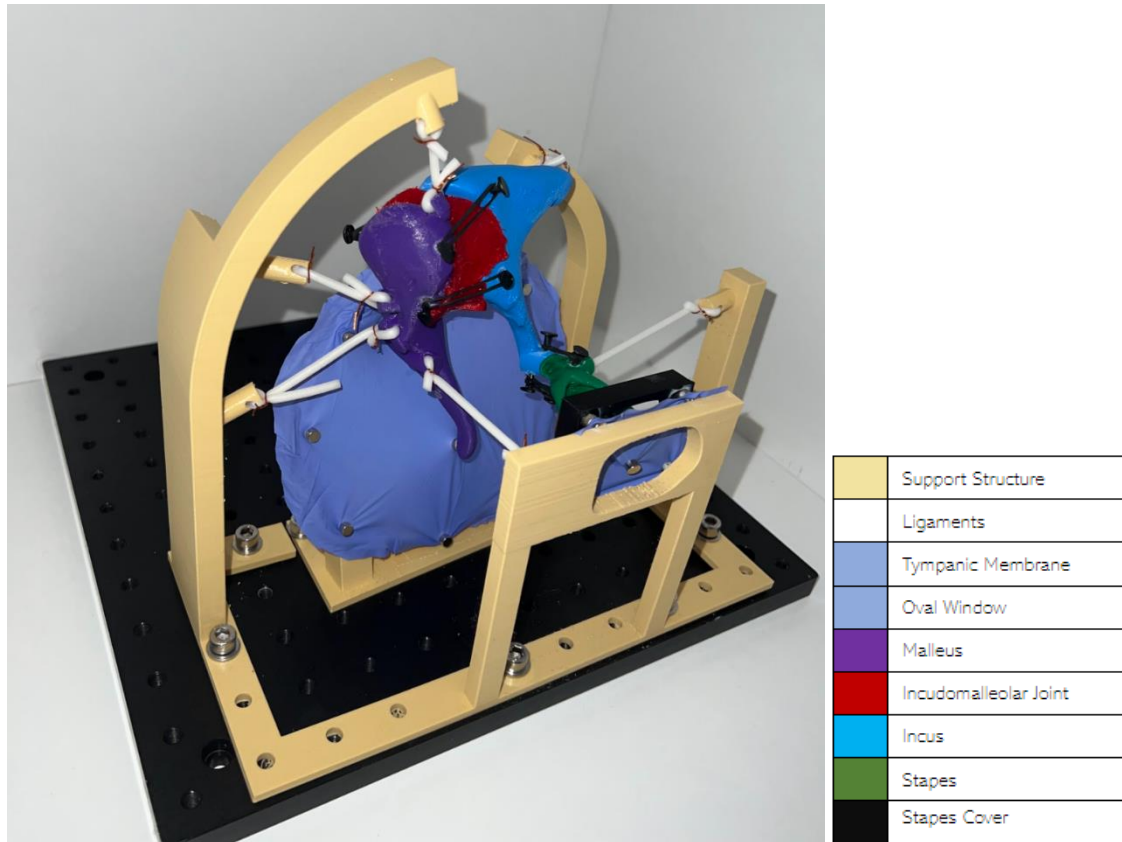


Fig. 4.23. Physical dynamic model

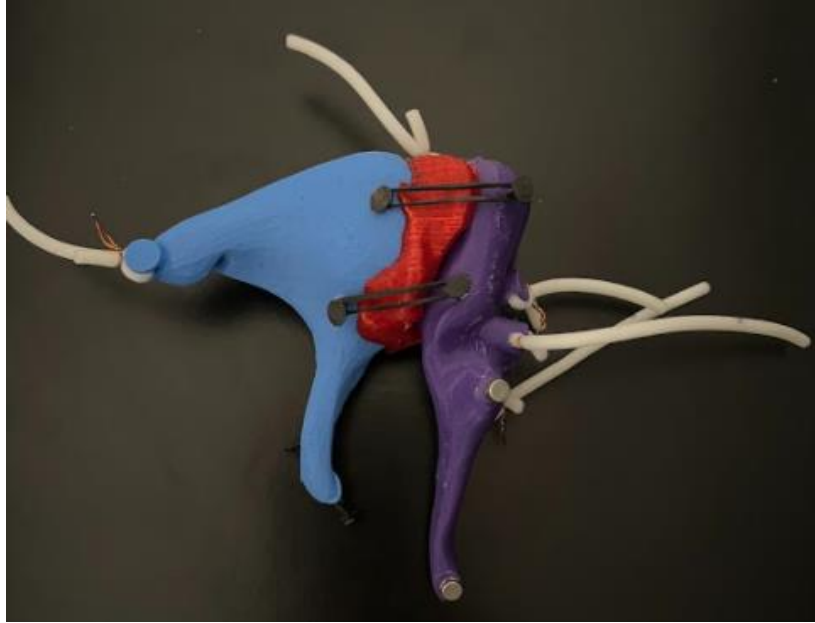


Fig. 4.24. Physical connection of IMJ

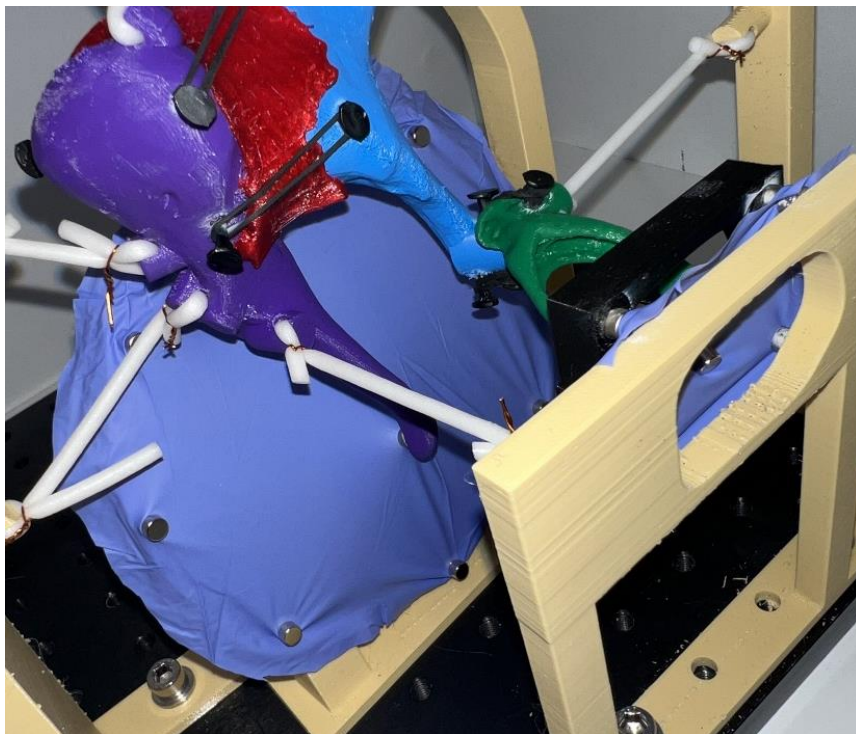


Fig. 4.25. Physical connection of membranes: Tympanic membrane

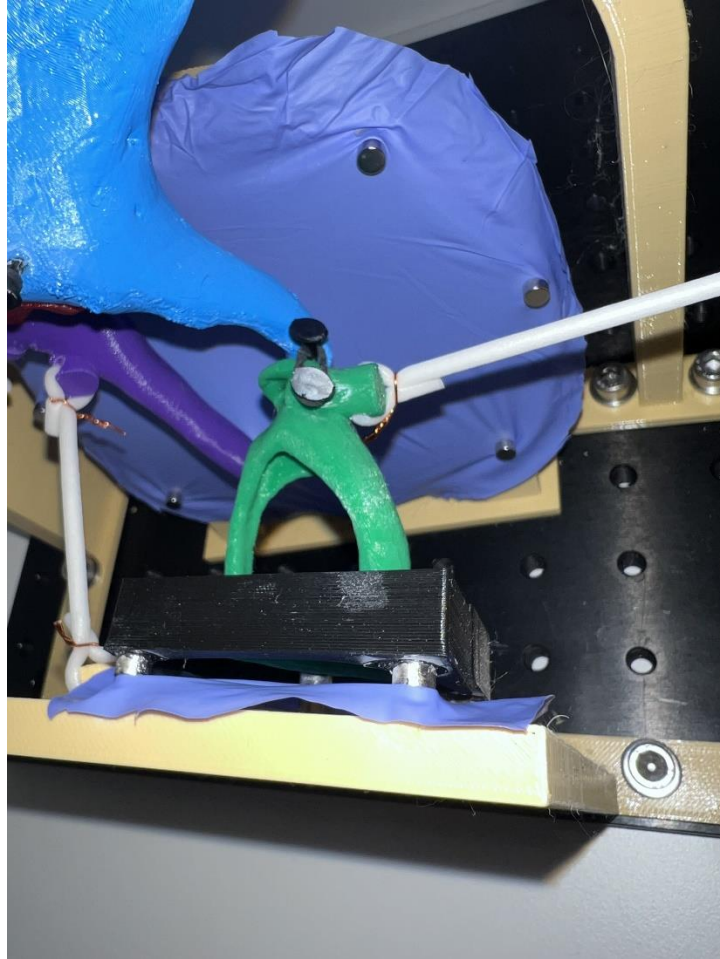


Fig. 4.26. Physical connection of membranes: Cochlea

#### *4.4.1 Dynamic Model Assembly*

The first and second project objective of the static model ultimately led to the fourth project objective, the assembly of the physical dynamic model. After designing and printing the static model, the discovery of the default Boolean subtraction setting in Geomagic enabled the dynamic model to be sent to print without this setting. To fix this problem for the dynamic model, each group of meshes that represented a single primary body was combined in SolidWorks. This ensured that there were no gaps between connecting bodies as mentioned previously. The design of the static model was modified into a dynamic model with accurate mechanical attachment mechanisms for ligaments, joints and membranes. After this model was verified through client feedback, it was printed and assembled.

The model was 3D printed at a local print shop, Teil3. Pins were placed into the malleus, incus, and stapes to attach these ossicles with rubber bands. This attachment mechanism mimics the IMJ as well as the ISJ. The rubber bands were placed at points which would present an accurate angle of all the ossicles in the model. The IMJ, printed in TPU, was placed between the incus and malleus and the rubber bands were placed on the corresponding pin attached, holding

the IMJ in place. The addition and subtraction of the rubber bands can be changed depending on the need for a more stiff or less stiff modeling of the joint.

The materials needed for assembly can be found in Appendix E. The initial design that was sent to print had holes that were intended to have wires fit through the support structure, ossicles, and ligaments holes. The soft material of the soft ligaments was never printed since it was later discovered TPU would not be the most suitable material for ligaments. Instead of using ligaments printed from TPU and wire supports, a silicone cord with a 3 mm diameter was purchased. The holes were slightly too small for the silicone ordered; therefore, a weaving technique was required to pull the silicone cord through the holes. The silicone cord was measured based on the distances of the ligaments in Geomagic with 2 cm of additional length on each end to wrap around the support structure and ossicles. The extra length on each end was then secured with wire as desired by the client. The silicone was first weaved through the holes in the ossicles and secured. Then one by one the silicone cord was weaved through each hole in the support structure to achieve the anatomically correct attachment position of the ossicles to the temporal bone support structure. This process was repeated until all the ligaments were in tension.

The membranes were connected to the temporal bone support structure using small strong magnets ordered online from Supermagnete by the client. The magnets were placed on the support structure that mimics the ear canal and the temporal bone around the stapes. The membranes were made using a latex rubber glove that was cut to mimic the shape of the membrane. Eight magnets were glued to the 3D printed ring that represents the ear canal. The ear canal membrane was secured by attaching eight magnets on the opposite side of the rubber latex. The membrane was pulled taught before attaching the magnets to ensure that it was in tension as shown in Fig. 4.29. The magnets were glued to the anterior process and manubrium of the malleus as seen in Fig. 4.27 on the purple malleus. The malleus magnets were secured to the membrane with a magnet on the opposite side. The membrane that represents the cochlea was attached similarly using magnets. Four magnets were glued around the oval window to the temporal bone support structure. The stapes cover, with four magnets glued around the oval window, was then placed on the other side of the membrane to hold it in place. The membrane sits in between the oval window and the stapes cover. Another magnet was glued to the middle of the stapes footplate and secured to the membrane with a magnet on the opposite side of the rubber latex as shown in Fig. 4.28.

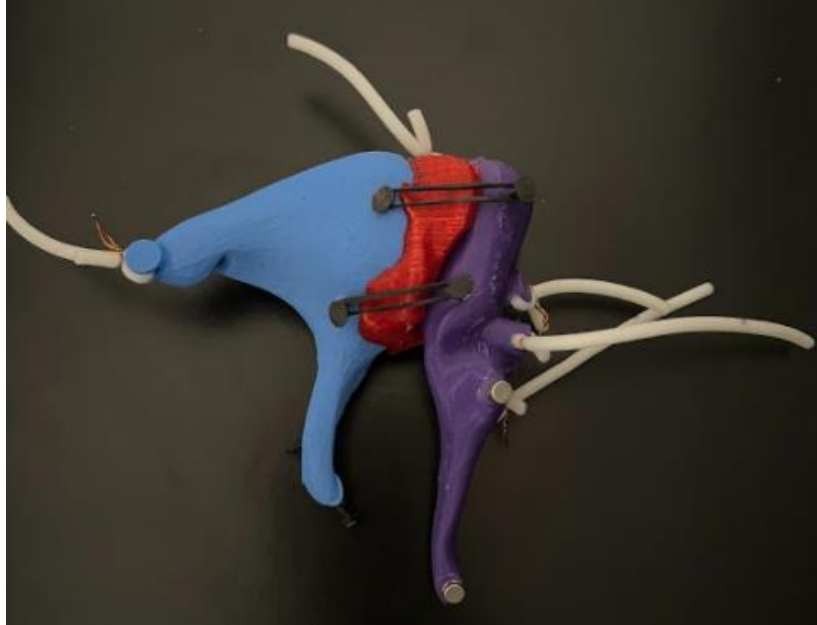


Fig. 4.27. Joint connection of malleus and incus with pins and rubber bands

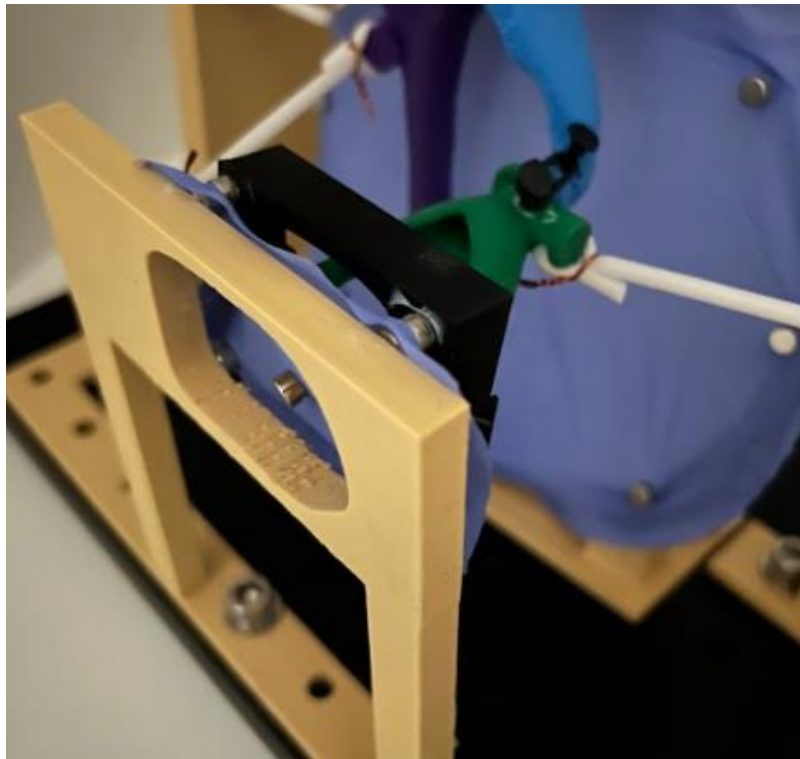


Fig. 4.28. Cochlea membrane connection with magnets



Fig. 4.29. Ear canal membrane connection with magnets

## 5.0 Design Verification

The following chapter provides design verification of the static model, materials selections, and dynamic model. The results of synthetic materials testing are compared to native tissue material properties and sound propagation mechanisms found in primary literature. The static and dynamic model was verified based on client feedback which is further explained below.

### 5.1 Materials Selection in the Dynamic Physical Model

The third project objective states that the materials selected for the dynamic physical model should mimic the material properties of native middle ear tissues. Initially, the Young's Modulus, density, and material loss factor were the three parameters chosen to define material selection. Based on the literature review in Section 4.2.2, the material properties involved in sound propagation and transmittance were prioritized over mechanical properties. So, procedures were designed to experimentally determine material loss factors for each potential synthetic material. Initially, the procedures did not consider how this material property would scale for a larger model. Dr. Dobrev indicated scaling the material loss factors would be complex. He recommended replicating the natural frequencies of native tissues at a 15:1 scale (personal communication, February 8, 2022). The average natural frequency for the middle ear is between 0.8 and 1.2 kHz (Homma et al., 2009). Natural frequency is generally inversely related to system size. Therefore, the natural frequency of the dynamic physical model—and primary materials chosen for the model—should be one fifteenth of the middle ear's natural frequency, i.e., 53 to 80 Hz. Dr. Dobrev also recommended trying to replicate the Q factor of native tissues. Interestingly, Q factors can be directly compared among multiple systems with far less concern about system size (personal communication, February 8, 2022). The Q factors for primary bodies can be found in Table 5.1, below.

Table 5.1. Q Factors of Primary Bodies (Homma et al., 2009; Guelke & Keen, 1952; Halpin et al., 2016)

Primary Body	Q Factor
Malleus	37
Incus	37
Stapes	37
IMJ	Not Found, likely comparable to the ossicular chain Q-factor given similar material loss factors
Tensor Tympani Tendon	6.6
Stapedial Tendon	6.6
Pars Tensa	6.6
Oval Window	0.6
Anterior Malleolar Ligament	6.6
Lateral Malleolar Ligament	6.6
Superior Malleolar Ligament	6.6

Posterior Incudal Ligament	6.6
Stapedial Annular Ligament	4.0

The following sections outline the modifications made to Section 4.2.2 procedures, present an overview of the measured data, and finalize materials selections for each primary body.

### 5.1.1 Ossicular Chain Selection

As reviewed in Section 4.2.2.1, traditional 3D printing filaments PLA and ABS were considered for ossicle replication in the dynamic physical model. Each beam was received from HanCon Printing Services and visually inspected for any warping or damage before testing. Then, each beam was marked in pencil for accelerometer placement and location for clamping. Each beam had a free end of approximately 14 cm. This was done to standardize potential confounding variables. The marked beams can be referenced in Fig. 5.1.

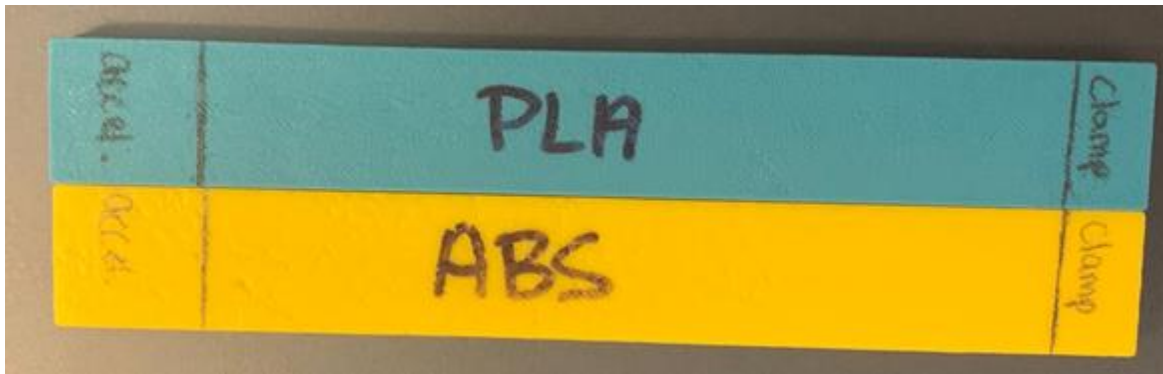


Fig. 5.1. Marked PLA and ABS beams for accelerometer placement and location for clamping

Data acquisition followed the procedure outlined in Section 4.2.2.1. The first natural frequencies for each beam were calculated using Equation 4.1. With an average Young's Modulus of  $3.57 \times 10^9$  Pa, PLA had an estimated first natural frequency of 50 Hz. A calibration test was run with a manually selected stimulus frequency range between 10 Hz and 80 Hz in steps of 10 Hz. Based on the resultant Bode magnitude plot, the estimated first natural frequency was refined to 54 Hz. Using this as the estimated frequency, the final stimulus frequency range was programmed using the manipulated MATLAB linspace function to give [14 Hz, 28 Hz, 42 Hz, 50 Hz, 54 Hz, 66 Hz, 102 Hz, 154 Hz, 216 Hz]. The test was completed in triplicate using this frequency range. The Bode magnitude and phase plots for trial 1 can be referenced in Fig. 5.2, below. Figure 5.2 confirms the accelerometer was measuring beam vibration as opposed to speaker membrane vibration. The input magnitude curve, or AI1, have a significantly smaller amplitude, and the output magnitude curve, AI2, has similar features and scale to the transfer function magnitude curve. The magnitude plot for the transfer function has similar features to a typical Bode plot with one degree of freedom. However, this plot exhibits a ramp up before reaching the natural frequency. This is likely due to the lower frequencies failing to move the beam effectively.

The frequency stimulus range for ABS was similarly determined. With an average Young's Modulus of  $2.44 \times 10^9$  Pa, ABS had an estimated first natural frequency of 45 Hz. A

calibration test was completed using the stimulus range between 10 Hz and 80 Hz in steps of 10 Hz. The Bode plot showed an approximate first natural frequency of 46 Hz. The resultant, final stimulus frequency range was [24 Hz, 34 Hz, 40 Hz, 44 Hz, 52 Hz, 80 Hz, 122 Hz, 172 Hz]. Again, this test was completed in triplicate, and the Bode magnitude and phase plots for trial 1 can be referenced in Fig. 5.3, below. Again, the resultant “ramp up” in the transfer function’s magnitude plot is due to lower frequencies failing to vibrate the beam. Bode magnitude and phase plots for all trials of both ABS and PLA testing can be referenced in Appendix F.

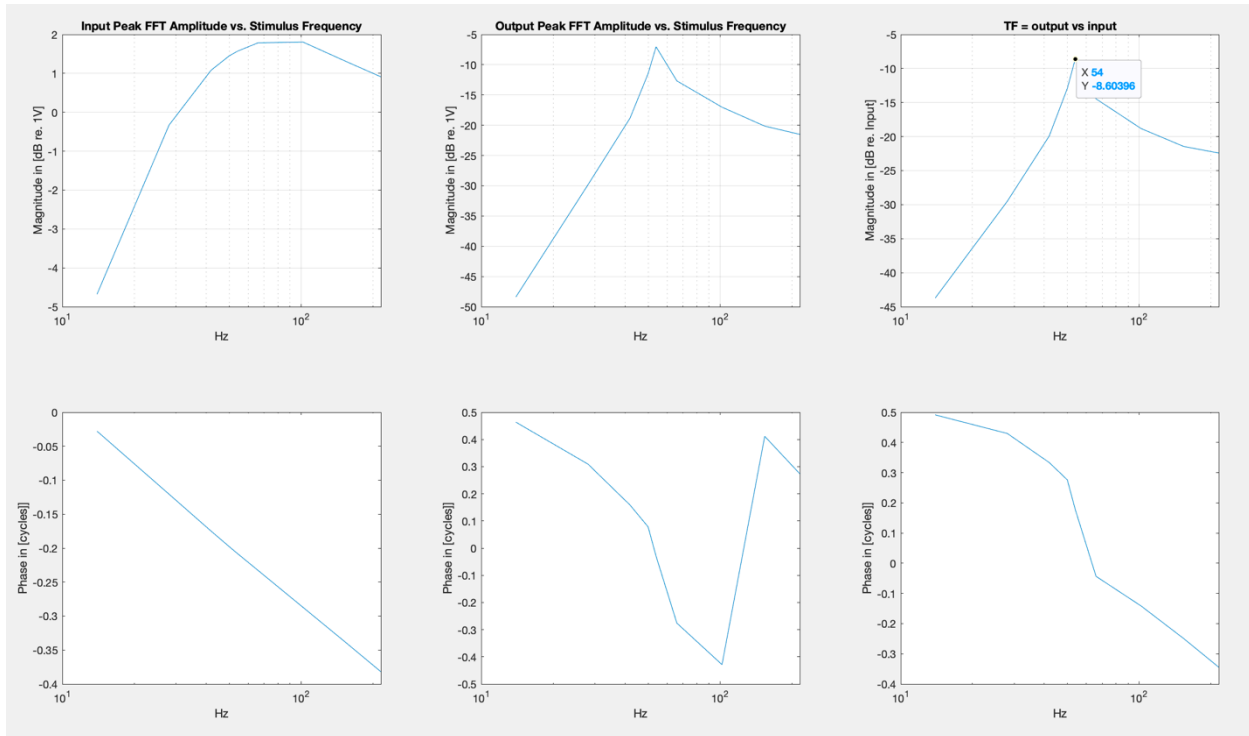


Fig. 5.2. Bode magnitude only plot for PLA trial 1 giving a natural frequency of 54 Hz at -8.60 dB re 1 V

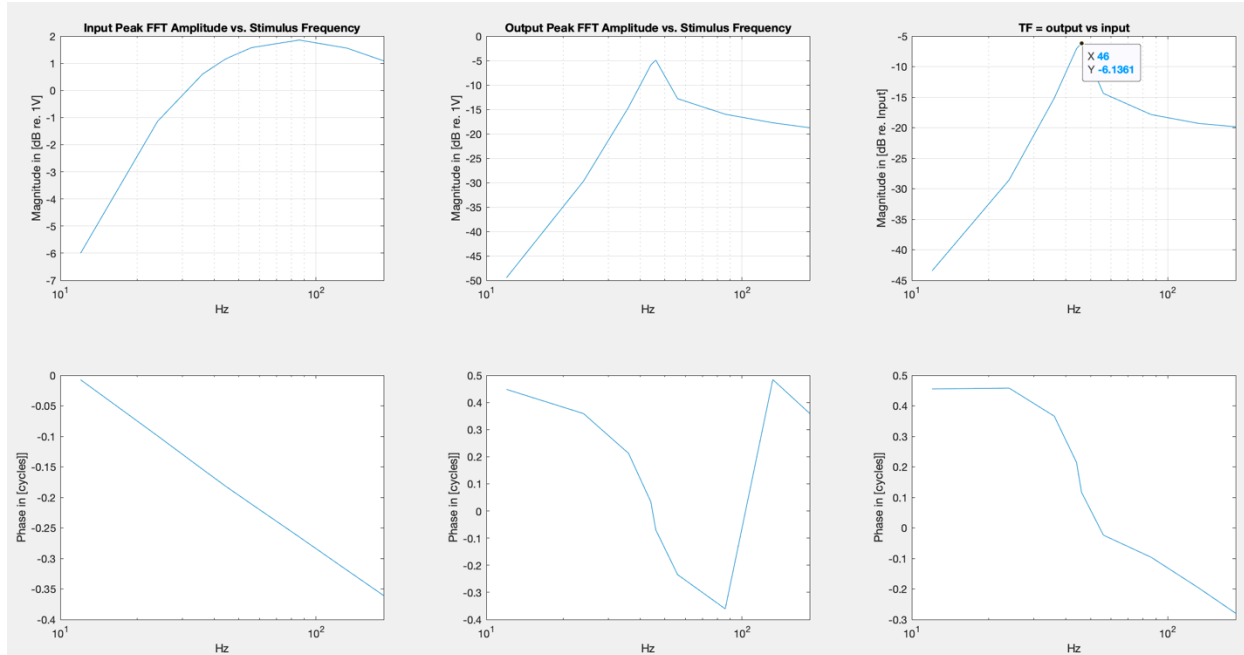


Fig. 5.3. Bode magnitude only plot for ABS trial 1 giving a natural frequency of 46 Hz at -6.13 dB re 1 V

The Q factor was calculated from each Bode plot using the procedure outlined in Section 4.2.2.1. Because the entire procedure was completed in triplicate, the uncertainty of the Q factor is further propagated using Equation 4.3 (Lindberg, 2000).

Table 5.2. Q Factor Data for All PLA and ABS Testing Trials

	ABS	PLA
Trial 1	$2.8 \pm 0.2$	$3.1 \pm 0.2$
Trial 2	$2.8 \pm 0.1$	$3.4 \pm 0.2$
Trial 3	$3.1 \pm 0.2$	$3.2 \pm 0.2$
Mean	2.9	3.2
Sample Standard Deviation	0.3	0.3
T-Test ( $\alpha = 0.05$ )	0.067	

From Table 5.2, there is no statistically significant difference between each material's calculated Q factor. As a deviation from the protocol laid out in Section 4.2.2.1, the material loss factor for each printing filament was not calculated. Instead, the Q factors of each printing filament were directly compared to the reported value for the ossicular chain. Figure 5.4 shows each printing filament's Q factor with their standard deviations against that of the ossicular chain. It should be noted that the Q factor for the ossicular chain contains all three ossicles and some remaining connective tissue, i.e., it is not a fully rigid body. Therefore, it is not a completely fair comparison between native tissue and both printing filaments, which are rigid bodies.

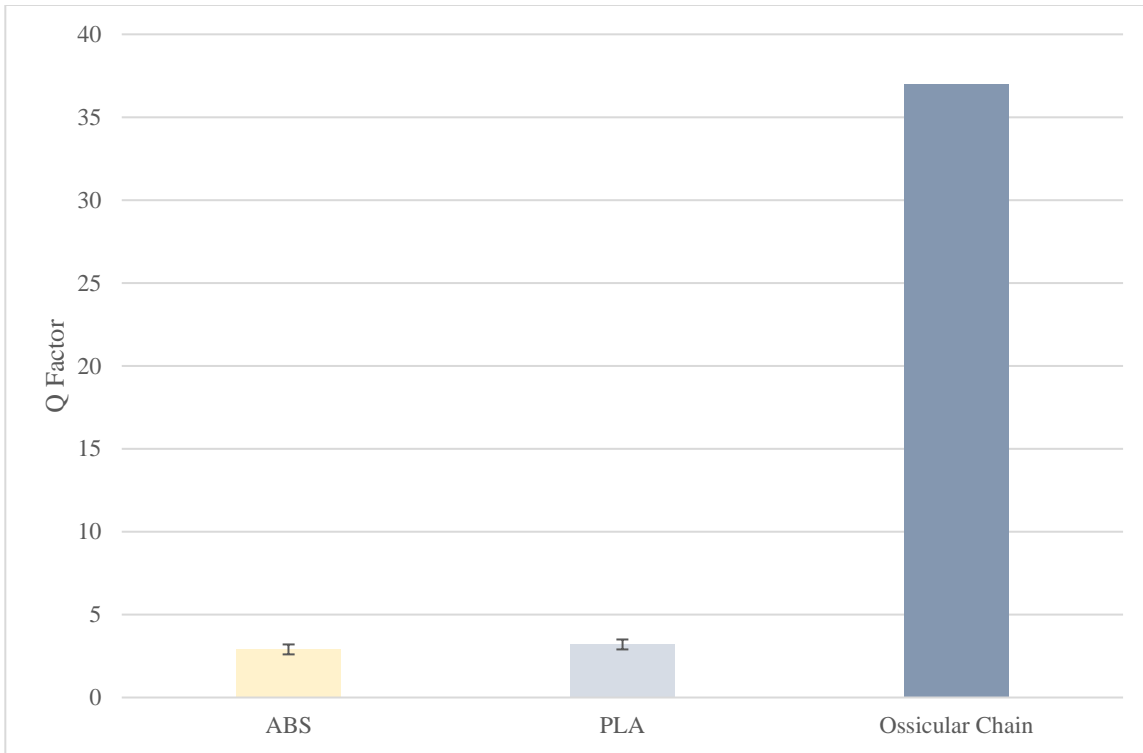


Fig. 5.4. Q Factor of common 3D printing filaments and the ossicular chain (Guelke & Keen, 1952).

The apparent mismatch between printing filament and ossicular chain Q factors will prevent the dynamic physical model from fully replicating the physiology of a healthy middle ear. Based on Table 5.2 and Figure 5.4, either filament can be used to replicate the ossicular chain. However, PLA satisfies the constraint of staying within the 15:1 scaled natural frequency. ABS is close to the low end of the specified range, 53 Hz. Table 5.3 weighs these factors in addition to the mechanical properties and accessibility of the printing filaments in Zurich, Switzerland. The weights are organized on a scale of 1 to 5, with 1 being the least important and 5 being the most important. Similarly, the scores for each material are organized on a scale of 1 to 5 with 1 indicating poor satisfaction and 5 indicating total satisfaction. The total is 95, representing complete satisfaction in all factors, or  $(5 \times 5) + (3 \times 5) + (1 \times 5) + (5 \times 5) + (5 \times 5)$ .

Table 5.3. Pugh Concept Selection Matrix for Ossicle Replication

Factor	Weight	ABS	PLA
Mimics Q-Factor	5	2	2
Mimics Young's Modulus	3	2	3
Mimics Average Density	1	4	4

Within Specified Natural Frequency Range	5	3	5
Printing Filament is Readily Accessible	5	4	5
Total (Out of 95)		55	73

Based on Table 5.3, PLA is the more suitable material for ossicle replication. In vivo, ossicle density is variable and thought to assist in propagating vibrations (Homma et al., 2009). Density variations in a 15:1 model should not affect the overall function; thus, the ossicles in the dynamic model can be assumed to have a constant density (I. Dobrev, personal communication, January 18, 2022). To satisfy this assumed constant density, the ossicular chain should be printed at a constant 30% infill.

5.1.2 Joint, Tendon, Ligament, and Membrane Selections

As reviewed in Section 4.2.2.2, softer thermoplastics and elastomers were considered compliant primary body replication. Both silicone and TPU cylinders from APSO parts were tested as first order springs. Following the procedure outlined in Section 4.2.2.2, the calculated time constants for both TPU and silicone can be referenced in Figures 5.5 and 5.6, respectively.

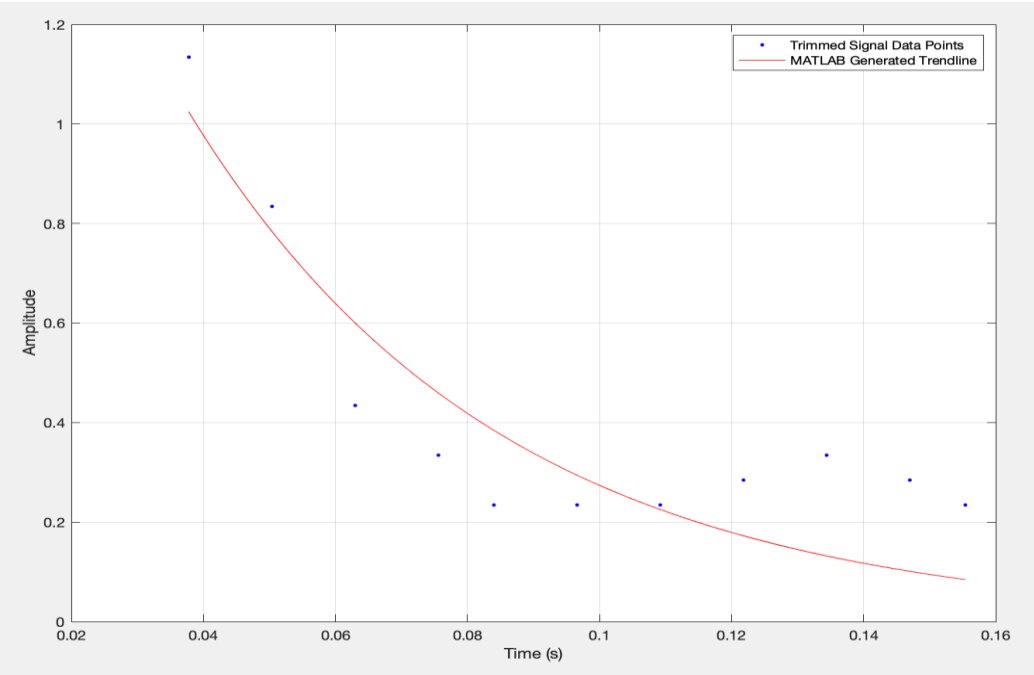


Fig. 5.5. MATLAB generated trendline to calculate TPU time constant

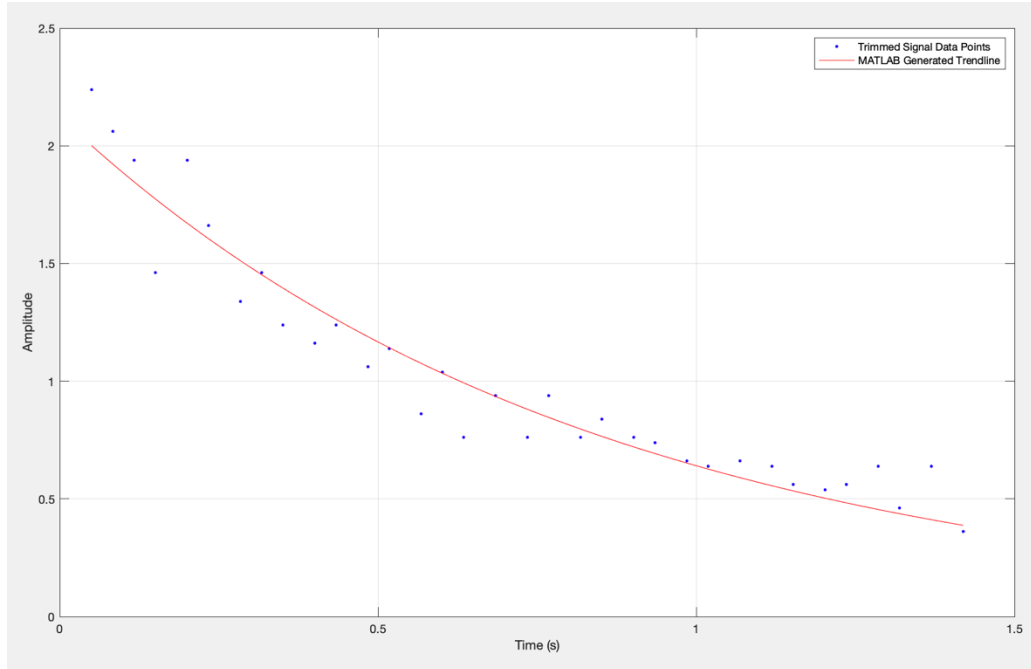


Fig. 5.6. MATLAB generated trendline to calculate silicone time constant

For the TPU specimen, the  $R^2$  value was calculated to be 0.75. The time constant was calculated to be  $0.047 \pm 0.014$  seconds. For the silicone specimen, the  $R^2$  value was calculated to be 0.92. The time constant was calculated to be  $0.83 \pm 0.09$  seconds.

Using Equation 4.7, the logarithmic decrements for both materials were calculated. The damped period was found by calculating the time difference between the third peak and second peak for each signal, as the first peak was trimmed from both signals. TPU had a damped period of 0.013 seconds, and silicone had a damped period of 0.067 seconds. Therefore, TPU had a logarithmic decrement of  $0.28 \pm 0.08$ , and silicone had a logarithmic decrement of  $0.081 \pm 0.008$ .

Using Equation 4.11, the damping ratio for each specimen was calculated. TPU had a damping ratio of  $0.04 \pm 0.02$ . Silicone had a damping ratio of  $0.013 \pm 0.007$ . As a deviation from the procedure outlined in Section 4.2.2.2, the damping ratio was used to calculate the Q factor instead of the material loss factor. The calculation was based on Equation 4.4, and the uncertainty was determined using Equation 4.3. The Q factor for TPU was calculated to be  $11 \pm 6$ , while the Q factor for silicone was calculated to be  $39 \pm 22$ . Figure 5.7 was created to compare the calculations with peer-reviewed literature values and appreciate the large uncertainties associated with each calculated Q factor. Appendix G shows sample calculations for uncertainty calculations associated with the TPU specimen.

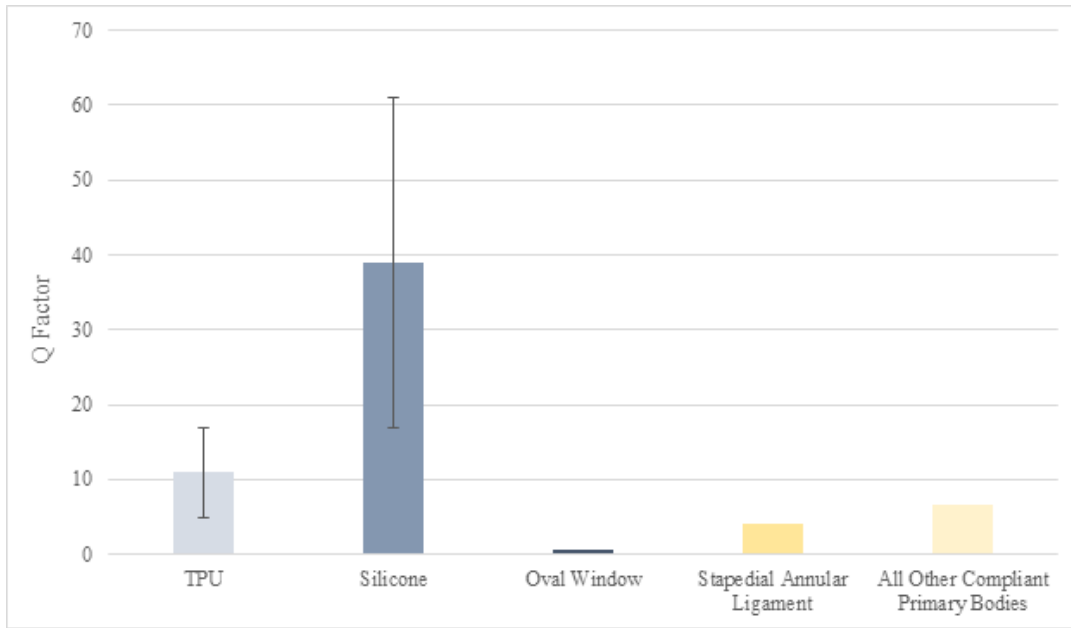


Fig. 5.7. Q Factors of both TPU and silicone with associated uncertainties versus compliant primary bodies (Homma et al., 2009; Halpin et al., 2016)

Similar to the results in Section 5.X.X, the Q factors of the chosen synthetic materials are drastically different than those of native tissue. Using Equation 4.13, the natural frequency for each material was calculated giving a value of  $77 \pm 39$  Hz for TPU, and  $15 \pm 9$  Hz for silicone. The average value for TPU falls within the specified range, 53 Hz to 80 Hz, but the upper and lower bounds fall outside of the specified range. Regardless of the standard deviation, silicone does not fall within the specified range. Like Table 5.3, Tables 5.4 through 5.6 weigh these factors in addition to factors related to mechanical properties and production. The tables subdivide the compliant primary bodies into three major groups: compliant bodies with a considerable surface area (i.e., the membranes and joints), relatively stiff bodies with a small surface area (i.e., ligaments and tendons with a Modulus above  $10^6$  Pa), and relatively soft bodies with a small surface area (i.e., ligaments and tendons with a Modulus below  $10^6$  Pa).

Table 5.4. Pugh Concept Selection Matrix for the IMJ and Membranes

Factor	Weight	TPU	Silicone
Mimics Q-Factor	5	3	1
Mimics Young's Modulus	3	5	4
Mimics Average Density	1	5	5
Within Specified Natural Frequency Range	5	3	1

Material is Readily Accessible	5	4	4
Total (Out of 95)		70	47

Table 5.5. Pugh Concept Selection Matrix for Stiffer Ligaments and Tendons (Tensor Tympani Tendon, Anterior Malleolar Ligament, Posterior Incudal Ligament)

Factor	Weight	TPU	Silicone
Mimics Q-Factor	5	3	1
Mimics Young's Modulus	3	4	4
Mimics Average Density	1	5	5
Within Specified Natural Frequency Range	5	3	1
Material is Readily Accessible	5	4	4
Total (Out of 95)		67	47

Table 5.6. Pugh Concept Selection Matrix for Softer Ligaments and Tendons (Stapedial Tendon, Lateral Malleolar Ligament, Superior Malleolar Ligament, Stapedial Annular Ligament)

Factor	Weight	TPU	Silicone
Mimics Q-Factor	5	3	1
Mimics Young's Modulus	3	3	5
Mimics Average Density	1	5	5
Within Specified Natural Frequency Range	5	3	1
Material is Readily Accessible	5	4	4
Total (Out of 95)		64	50

Based on Tables 5.4 through 5.6, TPU would be the more suitable material in all compliant primary body replications. Ligaments and tendons can be modeled as simple TPU cylinders which can be purchased from APSO parts. Membranes can be modeled as thin films which can be purchased from APSO parts, or they can be 3D printed using FDM techniques. The former option may be preferable if costs are the primary concern; the latter option may be preferable if anatomy replication is the priority (i.e., the pars tensa has a complex 3D geometry that a simple, flat film does not capture). Due to the intricate shape and adjoining surface areas with the malleus and incus, the IMJ would most likely need to be created using FDM technology. However, this preliminary discussion does not consider any limitations with the testing methods. The limitations and final recommendations are discussed in Chapters 7 and 8 respectively.

### 5.2 Verification of Static Model

The verification of the static model was mainly done through client feedback. After creating each iteration of the model, it was presented to the client, feedback was given, and a new iteration was created. After speaking with the client, all specifications were determined to be visual. Ligament length, diameter, and direction were all based on either the digital middle ear anatomy model or the  $\mu$ CT scan. The client approved these features during each iteration review.

Another form of verification was through budget checks. After each model was created, it was uploaded into the 3D printing software to get an estimate of the printing cost. After evaluating the printing cost, the unnecessary material was removed from the model. Print cost was a large factor in deciding when a model was ready to be printed.

The model had features which required tolerance. For example, the cover slides into two rectangular slots. There is a 0.1 mm space between the cover and the inside wall of the slot, which provided ample space between the two pieces.

Printing the static model also served as a form of verification for the dynamic model. When the static model was printed, an unknown feature of Geomagic was revealed. When two bodies are extruded into one another in Geomagic, the software recognizes this as a Boolean subtraction as opposed to a Boolean addition. This means that any area where two bodies overlap is empty space as opposed to filled space. After printing the static model, certain features were disconnected and had to be glued together. This initial print revealed this feature, and a process was created to prevent this from happening in the future. If the final model is uploaded to SolidWorks and each body is combined with the other bodies that it is touching, the Boolean subtraction can be changed to be a Boolean addition. This additional step in the printing process ensures that all bodies that need to be securely connected are connected.

### *5.3 Verification of Dynamic Model*

The verification of the dynamic model was also done mainly through client feedback. The measurements and spacing of the holes on the base of the model was designed to match the provided breadboard. The holes had a 25 mm center hole pattern and were size M6. The dimensions were confirmed with the client and the website of the provided breadboard, Thorlabs Optical Breadboards. The holes in ossicles and temporal bone that connect the ligaments were designed to be 3 mm, as the wires provided by the client were 1 mm in diameter. This provided 0.1 mm tolerance, like the static model print.

The successful assembly of the dynamic model confirmed the design of the digital model was correct. The base was stable and had an adequate space between the two base parts. The holes in the base of the support structure lined up properly with the optical breadboard. The M6 holes were slightly too small for the screws to fit in properly and rotate, so a drill was used to provide extra tolerance. The holes in the ossicles and temporal bone support structure were the confirmed size, 3 mm in diameter. Although the silicone cords used to replicate ligaments were also 3 mm in diameter, they were stretched and easily threaded through the holes in the ossicles and temporal bone support structure. Additionally, the design for the IMJ was verified. The malleus and incus aligned with the 3D printed IMJ and were held securely with nails and rubber bands. The main error with this feature was the IMJ material choice. The mechanism for the ISJ allowed for assembly, however, could be further improved. Both the incus and malleus were printed in PLA; therefore, the primary bodies could slip against each other and fall out of alignment. The final physical model was printed and available two days prior to the project deadline resulting in no time for troubleshooting and testing. Future recommendations are detailed in Chapter 8.

## 6.0 Design Validation

The following chapter outlines the validation for digital modeling and physical model realization. The design verification served as the validation for synthetic materials testing, reviewed in Chapters 5 and 7.

### 6.1. Digital Modeling

The first, second, and fourth project objectives were completed through digital modeling in Geomagic and SolidWorks. The static model was digitally designed and printed to satisfy objective one. This physical static model will be used as a visual aid for medical students and staff. The static model has a cover with an opening which represents the incision made while performing surgery. The opening in the cover gives the general angle and restricted view of the ossicles and ligaments that are visible during surgery. Next in the design process, the digital dynamic model was finalized, thus completing objective two. The dynamic physical model was printed and then assembled to complete objective four. This model is intended to replicate the movements and vibrations throughout the middle ear.

The completion of objectives one, two, and four were carried out through a process of creating designs digitally, reviewing the designs with the client, receiving client feedback, and creating subsequent iterations. During the first weeks of the project, the goal was to create a digital static model of the middle ear in Geomagic with specifications regarding articulation points and anatomically correct ligament lengths. Once an anatomically accurate static model was created using a  $\mu$ CT scan to extract ligament articulation points and lengths, the model was printed. The initial specifications set by the client prioritized anatomically correct diameters, lengths, articulation points, and anatomical structure for the ligaments. The ligament lengths were determined based on  $\mu$ CT scans instead of being based on literature per the client's requests. Due to a lack of literature denoting exact articulation points for ligaments in the middle ear, articulation points were based on provided  $\mu$ CT scans. After finalizing the design with the client, the static model was sent to print.

After reviewing this first dynamic iteration with the client, some specifications changed. The client expressed the desire for all ligament diameters to be constant as material stiffness changes with cross-sectional area. Additionally, some ligaments were modeled in a complicated manner to preserve the anatomical structure. The client expressed that they value ease of assembly and simplicity over visual anatomical accuracy for this specific model. The lengths and the articulation points remained the same. After the model was changed to reflect the client's feedback, the team provided an accurate price for the scaled model. The model exceeded the client's budget. The model was modified to be able to be supported by an optical breadboard to cut down on unnecessary material. Following this revision, the client expressed their satisfaction with this version of the model. The model was sent to the print shop and assembled the following week.

The design of the model also considered the factors of scaling and material selection. The prior MQP group actually modeled at an 18:1 scale. However, this model was chosen to be scaled at 15:1 to minimize model costs, material, and overall size. The cost to print at an 18:1

scale in the general area of Zürich was more expensive; therefore, it was not a feasible option to print the model on a larger scale. The final decision was made to stay within the client's budget. For the ligaments, it was possible to print with TPU, but this was more expensive. Due to the budget constraints and the question of whether TPU was the most suitable option to imitate the ligaments, it was decided to proceed with the rubber bands or silicone for the time being and to not 3D print TPU. Although soft ligaments were not able to be printed, future materials options for these parts were explored.

## 7.0 Discussion

The following chapter outlines the limitations associated with the verification and validation of each project objective. The chapter also discusses the results of design verification in context with primary literature, such as the case in synthetic materials selection.

### *7.1 Static and Dynamic Model Limitations*

The static and dynamic models were designed despite many limitations throughout the project. As the designs were finalized and priced in the print software, cost became a large design limitation. The high cost of printing in the Zürich area required additional iterations of each model to stay within the client's budget. This created a need for minimizing material, therefore changing the prior model design.

The 3D print shops and printers presented problems as well. Due to the high cost of printing, there were limited choices between print shops. The goal was to choose a print shop that had a low cost of printing and was based in the Zürich area to eliminate the need for shipping and more lead time. These two factors only led to a few choices. The options were reduced further when the size of the print bed was considered.

The fast-paced 7-week term was another difficult limitation. Paired with the budget limitation, the time that was consumed reworking the model iterations to be within budget took away from time that could have been spent testing the model at the end of the term. Additionally, the model was largely based on client feedback. As the iterations were made, certain specifications were changed based on client wants, thus creating the need for subsequent iterations.

Exact measurements and geometries of the ligaments in the middle ear are still widely unknown among researchers because of their minuscule size and difficult location. Therefore, it was difficult to compare the  $\mu$ CT scans to literature values due to the variability in current measured values. This resulted in the lack of ability to check our model dimensions accurately. So, verification of the sub-objectives relating scale in both static and dynamic models were not completed.

Another limitation was the need to learn Geomagic. Originally, SolidWorks was expected to be the main software used. After learning the amount of information that needed to be extracted from  $\mu$ CT scans and other 3D models, this assumption changed. The data that needed to be extracted from these scans and models were not able to be converted to SolidWorks. Some features in Geomagic are similar SolidWorks, but there was still a large learning curve. Certain features, such as offsets, are not available in Geomagic, and other unknowns such as Boolean subtractions were revealed during the project. This limitation was especially challenging since neither the advisors nor sponsors have a large background in creating 3D models in Geomagic. Unexpectedly working with a new software was a large limitation, but online tutorials and handbooks were useful in gaining this new skill.

## *7.2 Materials Selection in the Dynamic Physical Model*

Materials selection in the dynamic physical model informs the ease of model assembly and the accuracy of physiology replication. Therefore, this project considered the mechanical properties in addition to the sound propagation mechanisms in various test specimen. The following section contextualizes the results by comparing them to native tissue and reviews limitations that could inform future materials considerations for the dynamic physical model.

### *7.2.1 Hard Plastic Testing in Ossicular Chain Replication*

Both PLA and ABS were chosen due to their high stiffness and low cost. Additionally, both printing filaments were available in at least three local print shops, which allowed for price comparisons. From Sections 4.2.2.1 and 5.1.1, PLA was chosen over ABS due to the higher Q factor, natural frequency, and Young's Modulus.

The primary specification in deciding the hard print filament for ossicle replication was the Q factor, a dimensionless parameter which relates the energy stored versus the energy lost over one radian of vibration. A high Q factor indicates that vibration amplitude decreases slowly and, thus, sound is propagated for a longer period. It follows that in Table 5.1 the ossicular chain would have the highest Q factor among all middle ear tissues. The ossicular chain's vibrations define the sensation of hearing (Homma et al., 2009).

The Q factor can be determined from a Bode magnitude plot. Because the Bode plot considers known frequencies versus their peak amplitude, the signal inputs when testing the ABS and PLA beams needed to be reproducible and standardized. Thus, the speaker was a preferable stimulus as each signal input's frequency and duration could be measured and controlled. The automated plots clearly showed the specimen's natural frequency, but a limitation in this procedure was introduced at the end of signal processing. The resonance width on the transfer function Bode magnitude plot was needed to determine the Q factor, but this determination was not automated. Instead, the MATLAB generated plot was zoomed in, and the approximate frequencies corresponding to the full width at 6 dB re 1 V below the peak were taken in triplicate. This limitation introduced an uncertainty which was propagated through the entire analysis.

Despite the uncertainties, neither hard plastic could replicate the ossicular chain's Q factor. For the purposes of this project, PLA was chosen as the better of the two options, but it may not be the best overall material. Of course, the complex geometry of the ossicular chain demands an additive manufacturing process, which mostly limits material selection to plastics and metals. Metal printing was outside of the project scope and budget, but the results on the aluminum alloy test specimen in Section 4.2.2.1 may point to some future promise for this material family. The metal's Q factor was almost double that of either plastic, but it is not clear how this parameter would change with a more complex geometry and material processing. Additionally, the metal's Young's Modulus, density, and natural frequency are far greater than those of the ossicular chain. Depending on what property is prioritized for a dynamic physical model, metal printing may be worth exploring. There are not many shops in the Zurich area, but

some shops are in western Germany. For example, Materialise offers printing in aluminum-magnesium alloys in Munich and Bremen (Materialise, 2022).

Metal print prices are more than double those of plastic ones. Therefore, plastic printing should be exhausted before investigating metal filaments. For example, epoxy and similar resins may optimize most of the material properties discussed throughout the report. The average Young's Modulus is on the order of  $3 \times 10^9$  to  $4 \times 10^9$  Pa, and the density is comparable to both PLA and ABS (GrantaEDUPack, 2022). The current project chose to exclude epoxy from hard plastic testing due to the brittle nature and fear of crack propagation when clamping the beam in the metal support structure as shown in Figure 4.4. If the support structure can create a cantilever beam without significant crack propagation, future teams could make use of the Universtatspital Zurich laboratory's SLA printer for continued materials testing. It is suggested that resins could have a higher Q factor than their thermoplastic counterparts (Schediwiy et al., 2005), but this should be confirmed experimentally before attempting to print the ossicular chain in this material.

### *7.2.2 Soft Plastic Testing in Compliant Primary Body Replication*

Both TPU and silicone were chosen due to their compliant nature, low cost, and processability. TPU can be purchased whole-sale from an engineering supply parts website or printed using FDM technology. Similarly, silicone can be purchased whole-sale or casted into a final part. The material properties were reviewed in Section 4.2.2.2 and the sound propagation mechanisms were quantified and analyzed in Sections 4.2.2.2 and 5.1.2.

The procedure to find the displacement versus time data for the TPU and silicone strings, outlined in section 4.2.2.2, was chosen due to specimen geometry. has a few apparent limitations. When collecting the data for the TPU string, the data was taken in 2% increments which may have led to a slightly inaccurate representation of the data. This likely was the reason the calculated damping ratio and Q factor had large standard deviations. To make the data more accurate, 1% increments could have been taken instead. Additionally, both the data for TPU and silicone was collected visually using the location of the strings in respect to the ruler in the setup. This form of data collection may have resulted in the data not being as accurate compared to data collection using an accelerometer and a preprogrammed code.

The apparent lack of accuracy is shown in the high uncertainty values for the calculated damping ratios, natural frequencies, and Q factors. The values themselves also suggest some concerns in the testing procedure. Theoretically, the Q factors of these softer plastics should be less than those of hard plastics. Stated another way, the softer plastics should lose more sound energy per oscillation. It is not clear why silicone has an experimentally determined Q factor that is comparable to the ossicular chain when it has founded applications in sound insulation, e.g., caulking. Future materials testing should consider testing these softer materials as thin rectangular beams, not strings. A potential, future testing procedure could follow parts of Section 4.2.2.1 to include a pinned beam under tension where the speaker is placed below the center of the beam and the accelerometer wired in the Z axis is placed on the beam some length from the speaker. Figure 7.1 shows a potential set-up.

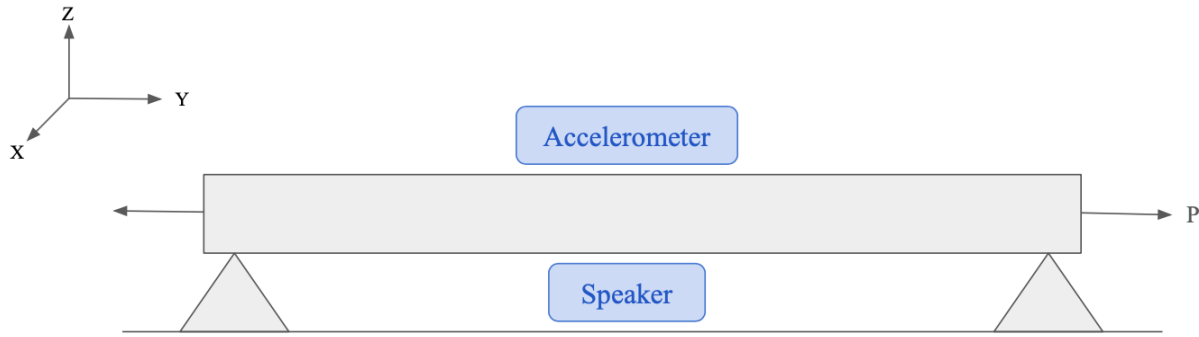


Fig. 7.1 Experimental set-up for compliant materials testing using a pinned beam under a tensile load, P

The tensile force can be approximated by knowing the strain, or the change in length over the initial length, the beam is subjected to. Assuming the strain is within the elastic deformation range of the material, the resultant stress can be calculated from the Young's Modulus. The tensile force can then be determined by dividing the stress by the beam's cross-sectional area (I. Dobrev, personal communication, February 11, 2022). The first natural frequency of the beam under a tensile force, P, can then be approximated using Equation 7.1 where E is the Young's Modulus, I is the area moment of inertia, L is the beam length, and m is the mass of the beam (Irvine, 2011).

$$f(Hz) = \frac{\pi^2}{2\pi L^2} \sqrt{1 + \frac{PL^2}{I\pi^2}} \sqrt{\frac{EIL}{m}} \quad (7.1)$$

Because it is assumed the beam is deforming along the Z-axis, the area moment of inertia can be re-expressed as one-twelfth of the beam width times the cubed beam height (I. Dobrev, personal communication, 2020). The approximated first natural frequency can be used to determine the range of inputted stimulus frequencies. After which, the procedure can follow the outlined methods and corresponding MATLAB code in Chapter 4 and Appendix B.

This test procedure was not completed due to budget and cost limitations. APSO parts does not produce TPU or silicone in the required geometry for this test. Other whole-sales engineering parts companies had a lead time of up to ten days. Printing or casting the beams would have a similar lead time at almost triple the cost. Still, the soft materials testing completed during this project is a good first step in experimentally determining relevant material properties. For example, testing these materials under tension is especially relevant to model assembly, which is reviewed in the section below.

### 7.2.3 Ligaments and Tendons in Physical Model Assembly

It is important to note that select compliant primary bodies, i.e., the ligaments, and tendons, exist under considerable tension in vivo. Therefore, the synthetic materials representing these bodies should exist under some pre-tension in the assembled, physical model. While this was not initially considered when selecting the materials, the section below compares the stiffness for silicone and TPU to those for native tissue. The section concludes with future considerations for specimen selection and geometry during model assembly.

While Sections 4.2 and 5.1 approximate stiffness as Young’s Modulus, this approximation is a serious limitation for compliant primary bodies. It does not consider material geometry and its influence on material mechanics. Assuming these compliant primary bodies experience only axial, tensile stress in the assembled model, the Modulus and specimen geometry can be used to solve for the geometry dependent stiffness,  $K$ , in Equation 7.2. In Equation 7.2,  $A$  is the cross-sectional area of the specimen,  $L$  is the length, and  $E$  is the Young’s Modulus (Cornell, 2020).

$$K = \frac{EA}{L} \quad (7.2)$$

The Young’s Modulus and anatomical dimensions of the ligaments and tendons can be referenced in Tables 4.1 and Table 3.6, respectively. From these values, the approximate axial stiffness can be calculated using Equation 7.2. The approximate values are shown in Table 7.1, below.

Table 7.1 Stiffness Values for Each Compliant Primary Body (Homma et al., 2009; De Greef, 2016; Zdilla et al., 2018; Sim & Puria, 2008, Prasad et al., 2019; Wojciechowski et al., 2020)

Primary Body	Young’s Modulus (Pa)	Average Cross-Sectional Anatomical Area (mm <sup>2</sup> )	Average Anatomical Length (mm)	Stiffness (N/mm)
Stapedial Tendon	$3.8 \times 10^5$	0.17	2.5	0.026
Tensor Tympani Tendon	$1.9 \times 10^7$	0.50	2.2	4.3
Anterior Malleolar Ligament	$1.5 \times 10^7$	0.63	2.1	4.5
Superior Malleolar Ligament	$4.9 \times 10^4$	0.049	1.3	0.0018
Lateral Malleolar Ligament	$5.0 \times 10^5$	0.24	2.0	0.060
Posterior Incudal Ligament <sup>1</sup>	$4.8 \times 10^6$	N/A	N/A	0.1
Stapedial Annular Ligament <sup>2</sup>	$4.12 \times 10^5$	N/A	N/A	0.2 - 0.5

From Table 4.1, the average Modulus for TPU is  $3.41 \times 10^7$  Pa. (Granta EDUPack, 2022). The calculated Modulus for the VMQ silicone sample is  $6.3 \times 10^5$  Pa. If the dynamic physical model is assembled at a 15:1 scale, the stiffness for each body can be calculated based on the selected material in Table 7.2, below.

Table 7.2 Stiffness Values for Each Compliant Primary Body based on Material Selection at 15:1 Scale  
(De Greef, 2016; Zdilla et al., 2018; Sim & Puria, 2008, Prasad et al., 2019; Wojciechowski et al., 2020)

Material	Primary Body	Average Cross-Sectional Area (mm <sup>2</sup> )	Average Length (mm)	Stiffness (N/mm)
TPU	Stapedial Tendon	37	38	33
	Tensor Tympani Tendon	110	33	113
	Anterior Malleolar Ligament	140	32	150
	Superior Malleolar Ligament	11	20	19
	Lateral Malleolar Ligament	53	30	61
	Posterior Incudal Ligament	N/A	N/A	Not calculated
	Stapedial Annular Ligament	N/A	N/A	Not calculated
Silicone	Stapedial Tendon	37	38	0.61
	Tensor Tympani Tendon	110	33	2.1
	Anterior Malleolar Ligament	140	32	2.7
	Superior Malleolar Ligament	11	20	0.34
	Lateral Malleolar Ligament	53	30	1.1
	Posterior Incudal Ligament	N/A	N/A	Not calculated
	Stapedial Annular Ligament	N/A	N/A	Not calculated

Table 7.2 considers the diameter at a 15:1 scale, therefore the cross-sectional area is at a 225:1 scale. As such, the axial stiffness for each ligament and tendon replicated in a synthetic material will be significantly higher than the stiffnesses for the native tissue. If the length in Table 7.2 is maintained, the average cross-sectional area and diameter for the ligaments and tendons can be calculated from the target stiffness for each native tissue in Table 7.1. Table 7.3, below, determines the new diameters for each synthetic ligament and tendon to ensure comparable stiffness.

Table 7.3 Target Cross-Sectional Area and Diameter based on Native Tissue Stiffness  
(De Greef, 2016; Zdilla et al., 2018; Sim & Puria, 2008, Prasad et al., 2019; Wojciechowski et al., 2020)

Material	Primary Body	Native Tissue Stiffness (N/mm)	Length at 15:1 Scale (mm)	Resultant Cross-Sectional Area (mm <sup>2</sup> )	Resultant Diameter (mm)
TPU	Stapedial Tendon	0.026	38	0.029	0.19
	Tensor Tympani Tendon	4.3	33	4.17	2.3
	Anterior Malleolar Ligament	4.5	32	4.23	2.3
	Superior Malleolar Ligament	0.0018	20	0.0011	0.036
	Lateral Malleolar Ligament	0.060	30	0.053	0.26
	Posterior Incudal Ligament	10	N/A	Not calculated	Not calculated
	Stapedial Annular Ligament	0.1	N/A	Not calculated	Not calculated
Silicone	Stapedial Tendon	0.026	38	1.6	1.4

Tensor Tympani Tendon	4.3	33	225	16
Anterior Malleolar Ligament	4.5	32	228	17
Superior Malleolar Ligament	0.0018	20	0.057	0.26
Lateral Malleolar Ligament	0.060	30	2.8	1.8
Posterior Incudal Ligament	10	N/A	Not calculated	Not calculated
Stapedial Annular Ligament	0.1	N/A	Not calculated	Not calculated

The worst case FDM printing tolerances are  $\pm 0.5$  mm; silicone casting has a shrinkage potential between 3% and 4% (Redwood, 2022; Silicone Dynamics, 2017). Additionally, the smallest diameter specimen available from APSO parts are 3.0 mm silicone cords and 2.5 mm inner diameter, 4.0 mm outer diameter TPU tubes (APSO, 2022). From Table 7.3, the resultant diameters for TPU are not feasible for replication or wholesale part purchase. However, the resultant diameters for silicone are most feasible for wholesale purchase from APSO parts. In this case, the stapedial tendon, superior malleolar ligament, and lateral malleolar ligament would need to be approximated as cylinders with 3 mm diameters. The minimum length scale to get a 3 mm diameter for the superior malleolar ligament is approximately 1000:1. The minimum length scale to get a 3 mm diameter for both malleolar ligaments is upwards of 30:1. For model assembly, the more suitable material for ligaments and tendons is silicone. Assembly cost should be considered when finalizing model scale, as the cost is directly proportional to model scale.

Despite TPU outscoring silicone in Pugh Concept Selection Matrices shown in Tables 5.4 through 5.6, the TPU evaluated is far too stiff for the model to move properly. At a 15:1 scale, synthetic materials with a comparable Young's Modulus will be significantly stiffer than their native tissue counterparts. To accurately replicate middle ear motion on a 15:1 scale, the Young's Modulus of the synthetic materials should be on the order of 10 to 100 times less than the native tissue counterparts. Therefore, select specifications for Objective 3 like the natural frequency and Q factor should be sacrificed for the model to meet requirements associated with model assembly in Objective 4 and with acoustic stimulation in Objective 5.

## 8.0 Conclusions and Recommendations

The following chapter outlines the conclusions and recommendations for the material selections, assembly, and instrumentation of the dynamic physical model. The primary future project work will involve iterations of this model to further improve the accuracy of middle ear physiology—and potentially pathology—replication.

### 8.1 Material Selections

Accurate primary body replication depends on appropriate material selections. As outlined in Chapters 4, 5, and 7, hard plastics were evaluated to replicate the ossicular chain while softer plastics were evaluated to replicate joints, membranes, tendons, and ligaments. From the results of hard plastic testing, reviewed in Chapter 5, PLA had a higher natural frequency, Q factor, and Young's Modulus than ABS. From the two options, PLA is the recommended material for ossicular chain replication. However, PLA's low Q factor is a limitation. It is recommended that future materials testing consider resins and other 3D printable materials with higher Q factors to better match this property of the ossicular chain.

The central recommendation around compliant primary body replication is to consider the geometry dependent stiffness over material properties. From the analysis in Chapter 7, it can be concluded the geometry-dependent stiffness of TPU, or the spring constant,  $K$ , is far greater than those of native tissues. This finding suggests the ligaments and tendons should not be replicated in TPU as the dynamic physical model would likely be too stiff to vibrate when acoustically stimulated. Instead, it is recommended the ligaments and tendons be replicated in silicone. The specific type of silicone should be verified using the procedure outlined in Section 7.2.2, and the materials tested should have undergone the same processing techniques that will be used to replicate the final model (e.g., casting, wholesale purchase). If silicone casting is not pursued due to cost constraints, it is recommended that future teams order different diameters of the silicone string tested from APSO parts to match the cross-sectional area parameters set in Table 7.3. Based on the concerns with TPU stiffness and available surface area of middle ear membranes, it is also recommended that both the pars tensa and oval window also be replicated using silicone.

Due to the complex geometry of the IMJ, it is recommended to replicate the joint using silicone casting. However due to time and budget constraints, the dynamic physical model replicated the IMJ in TPU using FDM technology. TPU is far too stiff to accurately replicate a healthy joint. TPU better mimics the stiffness seen in tympanosclerosis (Aslan et al., 2009). Common pathology modeling techniques are further reviewed in Section 8.4.

### 8.2 Dynamic Physical Model Assembly

The final recommendation for assembling includes other connection techniques. This could include using zip ties to secure the silicone cord rather than wire, with the goal of easier assembly. When assembling the model, the wire was difficult to work with. The wire requires the user to twist it multiple times to secure the silicone cord. With the limited space available for movement and the stiffness of the wire, it was difficult to wrap the wire tightly. With zip ties, the

user can easily wrap the zip tie around the silicone cord and pull it tight. This would also allow the model to be assembled with only one user, as this was not possible when using wire. Additionally, there should be soft material placed in between the incus and stapes to better replicate the ISJ. Since the stapes and incus are both 3D printed in plastic, they can easily slip against each other and pop out of alignment. A possible solution would be to place a small amount of silicone in between these two bodies. Finally, the IMJ should be printed or molded using silicone, as the TPU had an inaccurate stiffness to properly model the IMJ in a healthy state.

### *8.3 Instrumenting the Dynamic Physical Model*

The fifth project objective involves testing the assembled, dynamic physical model to replicate healthy middle ear physiology. Due to time and budget constraints, this objective was not met. The recommendations below include a preliminary testing procedure that would have been employed.

Due to the low uncertainties, quantitative input signals, and relatively standardized data processing, the primary testing procedure was adopted from the methodology outlined in Section 4.2.2.1. The Visitation FRS8M speaker, in series with the Kenmo amplifier, should be laid on its side and positioned so the polyurethane foam attached to the speaker membrane is flush with the umbo. An Adafruit ADXL335 accelerometer should be positioned at the umbo on the other side of the membrane and oriented so the positive Z-axis is pointing in the direction of sound wave propagation. The GND (ground) and  $V_{in}$  pins on the accelerometer should be wired. Though only the  $Z_{out}$  pin should be used during testing, it is recommended that the  $Y_{out}$  and  $X_{out}$  pins also be wired. Testing of the ABS and PLA beams revealed that the accelerometers are highly directionally sensitive. The experimental set-up may reveal the X or Y directions are more sensitive to the speaker's stimulus, so this wiring is recommended to prevent last minute soldering.

To measure how sound propagates through the dynamic physical model, a second ADXL335 accelerometer should be placed at the center of the stapes footplate. Again, the accelerometer should be positioned so the positive Z-axis is in the direction of sound wave propagation and wired across all axes to prevent last minute soldering. It should be noted that once the final axis is decided, both accelerometers should be measuring in the same direction and axis. Figure 8.1 indicates a schematic of the set-up by annotating the final digital model for physical model assembly. Figure 8.2 shows the block diagram of the hardware required in this test set-up. A more in-depth explanation on the block diagram can be referenced in Section 4.2.2.1, the only difference is that Fig. 8.2 depicts four input channels for the DAQ, or ADC.

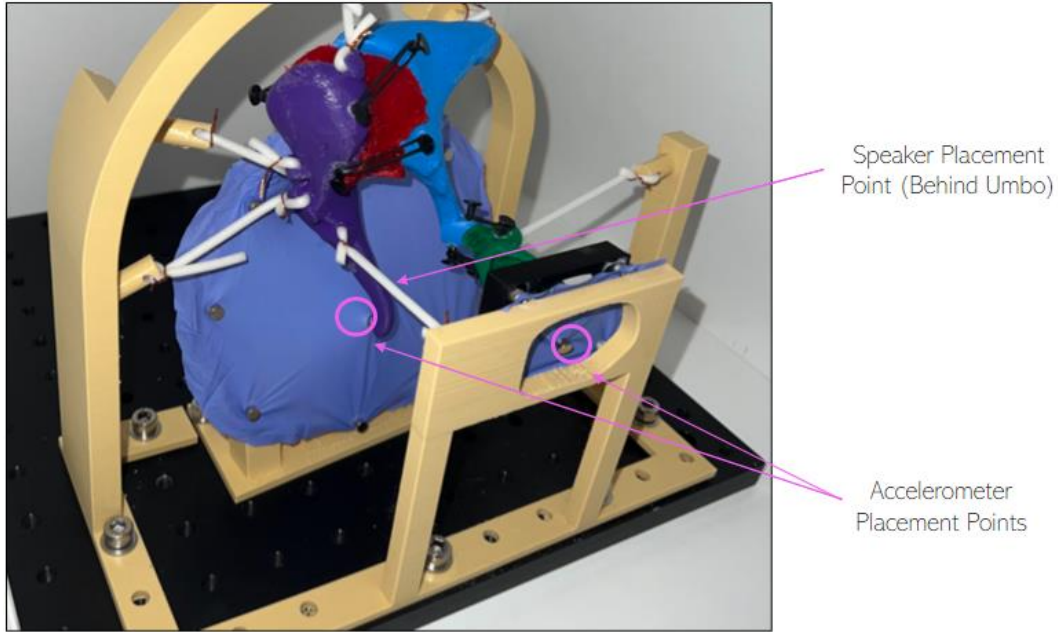


Fig. 8.1. Test set-up for acoustically stimulating the dynamic physical model

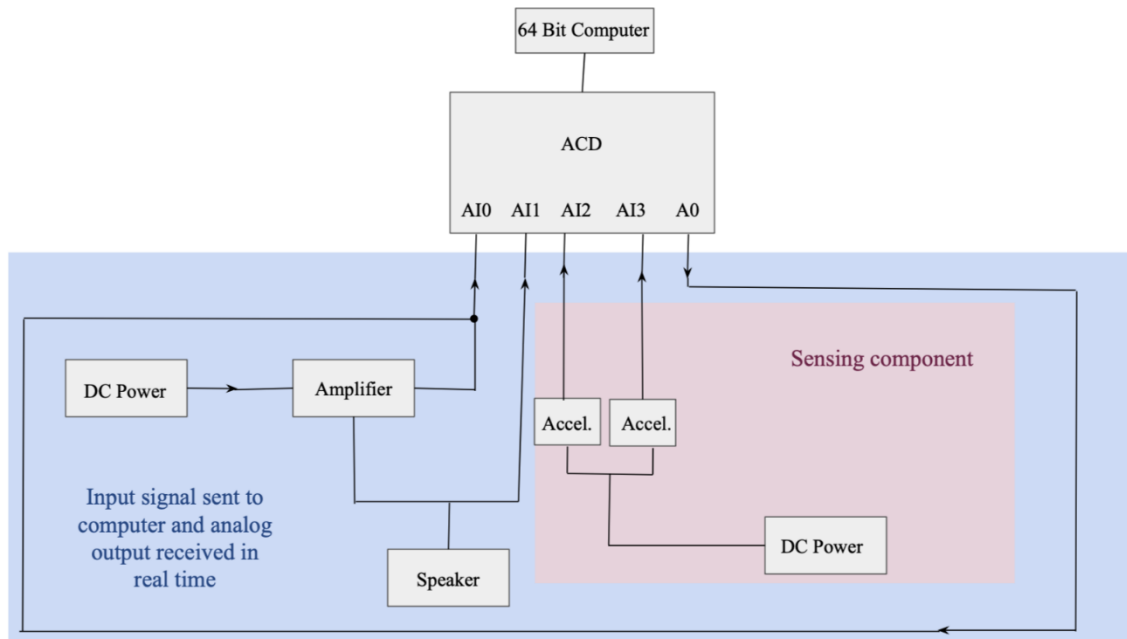


Fig. 8.2. Block diagram of the hardware needed to measure the acoustic stimulation

The MATLAB code in Appendix B can be modified to measure the acoustic stimulation. The number of input channels, specified by the variable `IN_ch_n`, should be changed from three to four. It is important to note that code input channel 1 corresponds to AI0, code input channel 2 corresponds to AI1, code input channel 3 corresponds to AI2, and code input channel 4 corresponds to AI3. After the DAQ and hardware are set-up, the first natural frequency must be entered to build the vector of signal inputs. The user-entered natural frequency cannot be simply

approximated by Equations 4.1 or 7.1. Instead, the first natural frequency will need to be estimated. It is recommended that the user try inputting frequencies between 53 Hz and 80 Hz, the specified range for the model. The natural frequency can then be approximated by looking at the transfer function's Bode magnitude plot. It should be noted that in this case, the input for the transfer function is channel AI2, or channel 3 in the code, and the output for the transfer function is channel AI3, or channel 4 in the code. It is likely that the first rounds of transfer function Bode magnitude plots will not clearly show a peak corresponding to natural frequency. The user-entered natural frequency should be further adjusted to reflect the estimated peak value, and the test procedure should be re-executed until a clear peak is reproducibly shown on the resultant plots. As for measuring the pressure drop between the umbo and stapes footplate, the amplitude values on the input Bode magnitude plot can be subtracted from the amplitude values on the output Bode magnitude plot. Because both vectors are the same size, this can be done by simply subtracting the two variables in MATLAB. The mean difference and sample standard deviation for each trial can be taken.

#### *8.4 Pathology Modeling*

For future MQP projects that are meant to build from this project, one recommended next step is to model common middle ear pathology. Since the middle ear has complex physiology with many working parts, this creates numerous possibilities for disruption in typical physiology. Disruptions include genetic disorders and the development of diseases. Oftentimes, these diseases result in conductive hearing loss and require surgical procedures to reconstruct the middle ear physiology and restore an individual's hearing. Information on the two main reasons for hearing loss, chronic otitis media and otosclerosis, and their accompanying surgical procedures can be found in Appendix H.

If a future team were to pursue modeling a diseased state middle ear, this could benefit the Universitätsspital Zürich students and staff in conceptualizing how the diseased state affects hearing in a patient. Additionally, if acoustic stimulation is paired with dynamic modeling, like in this project, results from healthy and diseased states can be compared. For example, the natural frequency of osteosclerotic ears increases by 100 Hz from healthy middle ears (Vanaja & Manjula, 2003).

#### *8.5 Broader Impacts*

This MQP project has possible broader impacts when looked at in a larger scope. These impacts could be worldwide or just locally, and they could influence the environment, society, ethics, health and safety, manufacturability, and sustainability. The impact of these 6 topics will be expanded on in the next section, but it is important to note that political ramifications and economic impacts will not be described since they are not applicable to this project.

##### *8.5.1 Environmental Impacts*

The environmental impact of this project is minimal at most. The largest concern is that both the static and dynamic middle ear models were 3D printed using plastics. Since plastics like PLA are not sustainable materials, they will not easily degrade over time. However, because just

one print of each model was made, there should not be a long-lasting environmental impact unless multiple prints are made and then left to decompose over time.

### *8.5.2 Societal Influence*

This project can have a significant societal impact, even if it is just in the scope of the University Hospital of Zurich. Both the static and dynamic models that were produced can be used for a multitude of reasons in an engineering and medical setting. First, the models can be used to further medical students and staff's understanding of the middle ear. They can be used to show correct anatomy and articulations, along with how the middle ear should act in vivo. Second, the models can be used in demonstrations for potential investors who are interested in the current, and future, middle-ear studies and experiments at the University Hospital of Zurich. Lastly, the models can be used for testing new commercial devices in 3D space to see how they would act in vivo. This gives medical staff and engineers the ability to prove that their products work on a larger scale before they implement them in clinical trials.

### *8.5.3 Ethical Concerns*

This MQP project did not have many ethical concerns since it followed HIPPA regulations. However, if the project was based on modeling a specific case or person, this would have been more concerning. In a broad scope, this project could indirectly have a long-term effect on patients affected with middle ear issues. If our models were to be used by doctors and medical students to get a better understanding of the middle ear, this could in turn help to advance their research and new devices. These devices could then further improve patients' lives. However, a population within the Deaf community are strongly opposed to the use of cochlear implants to help with hearing as they believe it disrupts their way of life (Kent, 2021). Due to this, the topic of this project may be controversial to the Deaf community.

### *8.5.4 Health and Safety Issues*

The health and safety impacts related to this project are very similar to those outlined in section 6.3.2 for societal influence. This project has the capability to have a positive impact on middle ear patients in the future. This process is also outlined above in section 6.3.3 when explaining how improving medical staff's understanding of the middle ear could improve patient's lives.

### *8.5.5 Manufacturability*

Manufacturing the final product of this project would be relatively simple and straightforward. Since the procedures for model creation and material selections are very detailed, the project could be easily replicated. If the STL files for the models are already available, then 3D printed models could be easily reproduced as FDM 3D printing shops are readily available in most areas of the world. The only limitation would be if the necessary printing filaments, e.g., PLA and TPU, were not available at the select printing shops.

### *8.5.6 Sustainability*

As mentioned in section 8.3.1, the 3D printed plastics for the final models, both static and dynamic, are not sustainable materials. Traditional plastics that are like PLA can take up to 450 years to completely decompose when placed into a landfill (Gammage, 2022). This goes to prove that our product is not necessarily sustainable, but if only one model of each is made then it should not have a major impact on the environment.

## References

- Anschuetz, L., Huwendiek, S., Stricker, D., Yacoub, A., Wimmer, W., & Caversaccio, M. (2019). Assessment of middle ear anatomy teaching methodologies using microscopy versus endoscopy: a randomized comparative study. *Anatomical sciences education*, 12(5), 507-517.
- Aslan, H., Katlimis, H., Ozturkcan, S., Ilknur, A. E., & Basoglu, S. (2009, September 22). *Tympanosclerosis and our surgical results*. European archives of oto-rhino-laryngology : official journal of the European Federation of Oto-Rhino-Laryngological Societies (EUFOS) : affiliated with the German Society for Oto-Rhino-Laryngology - Head and Neck Surgery. Retrieved February 22, 2022, from <https://pubmed.ncbi.nlm.nih.gov/19771442/>
- ASTM International. (2019). *Standard guide for silicone elastomers, gels, and foams used in medical applications part I-formulations and uncured materials*. ASTM International - Standards Worldwide. Retrieved January 20, 2022, from <https://www.astm.org/f2038-18.html>
- Bergin, M., Vlajkovic, S., Bird, P., & Thorne, P. (2013). Systematic review of animal models of middle ear surgery. *World Journal of Otorhinolaryngology*, 3(3), 71-88.
- Bikas, H., Stavropoulos, P., & Chryssolouris, G. (2015). Additive Manufacturing Methods and Modelling Approaches: A Critical Review. *Int J Adv Manuf Technol*, 83, 389. <https://doi.org/10.1007/s00170-015-7576-2>
- Brockmann, A., & Chittka, L. (2005). Perception space – The final frontier. *PLoS Biology*, 3(4), e137. doi: 10.1371/journal.pbio.0030137
- Centers for Disease Control and Prevention. (2019, October 7). *What noises cause hearing loss?* Centers for Disease Control and Prevention. Retrieved January 11, 2022, from [https://www.cdc.gov/nceh/hearing\\_loss/what\\_noises\\_cause\\_hearing\\_loss.html](https://www.cdc.gov/nceh/hearing_loss/what_noises_cause_hearing_loss.html)
- Cleveland Clinic. (2021). Epithelium: What it is, Function & Types. Cleveland Clinic. Retrieved January 14, 2022, from <https://my.clevelandclinic.org/health/articles/22062-epithelium>
- Cooper, N. P., Vavakou, A., & van der Heijden, M. (2018). Vibration hotspots reveal longitudinal funneling of sound-evoked motion in the mammalian cochlea. *Nature Communications*, 9(1), 3054. <https://doi.org/10.1038/s41467-018-05483-z>
- Cornell. (2020). *Stiffness and Size Effect*. Retrieved from <https://courses.cit.cornell.edu/mclaskey/cee3710/stimulation3/sizeEffect2020.pdf>
- De Greef, D. (2016). *The Human middle ear – A multidisciplinary study by means of tomographic imaging, stroboscopic holography, and dynamic finite element modeling*. [Doctoral dissertation, University of Antwerp] Antwerp. <https://anet.be/desktop/irua>
- Dobrev, I., Sim, J. H., Aqtashi, B., Huber, A. M., Linder, T., & Rösli, C. (2018, September 7). *Effects of middle ear quasi-static stiffness on sound transmission quantified by a novel 3-axis optical force sensor*. Hearing Research. Retrieved February 22, 2022, from <https://www.zora.uzh.ch/id/eprint/153415/>
- Elsevier B.V. (n.d.). *Tympanic cavity*. Tympanic Cavity - an overview | ScienceDirect Topics. Retrieved January 14, 2022, from <https://www.sciencedirect.com/topics/medicine-and-dentistry/tympanic-cavity>

- FDM vs. SLA: Compare the Two Most Popular Types of 3D Printers*. Formlabs. (n.d.). Retrieved January 12, 2022, from <https://formlabs.com/blog/fdm-vs-sla-compare-types-of-3d-printers/>
- Gammage, E. (2022, January 17). *How long does it take for plastic to Biodegrade?* SaveMoneyCutCarbon. Retrieved February 17, 2022, from <https://www.savemoneycutcarbon.com/learn-save/how-long-does-it-take-for-plastic-to-biodegrade/#:~:text=Why%3F,years%20to%20decompose%20in%20land%EF%AC%81>
- Gassler, J. (2019). *Anatomy of the ear, nasal cavity, pharynx, and larynx*. DeBusk College of Osteopathic Medicine. <https://dcomcme.lmunet.edu/sites/default/files/Module%203%20ENT%20Anatomy%20Gassler.pdf>
- Ghazanfar, H., Rashid, S., Hussain, A., Ghazanfar, M., Ghazanfar, A., & Javaid, A. (2018). Cadaveric dissection a thing of the past? The insight of consultants, fellows, and residents. *Cureus, 10*(4).
- Gentil, F., Parente, M. P. L., de Sousa Martins, P. A., Garbe, C. (2012). The influence of muscles activation on dynamical behavior of the tympano-ossicular system of the middle ear. *Computer Methods in Biomechanics and Biomedical Engineering, 16*(4). doi: 10.1080/10255842.2011.623674
- Gottlieb, P. (2018). Human ossicular-joint flexibility transforms the peak amplitude and width of impulsive acoustic stimuli. *J Acoust Soc Am., 143*(6), 3418-3433. doi: 10.1121/1.5039845
- GrantaEDUPack. (2022). *Ansys Database Download Homepage* from <https://www.ansys.com/products/materials/granta-edupack>
- Guelke, R., & Keen, J. A. (1951, July). *A Study of the Movements of the Auditory Ossicles Under Stroboscopic Illumination*. *J. Physiology*.
- Halpin, A. A., Elliott, S. J., & Ni, G. (2016, January 15). *Prediction of Inertial Effects Due to Bone Conduction in a 2D Box Model of the Cochlea*. AIP Conference Proceedings. Retrieved from <https://doi.org/10.1063/1.4939370>
- Hear-it. (2013, January 9). More than 700 million contract otitis media every year. Retrieved January 14, 2022, from <https://www.hear-it.org/more-than-700-million-contract-otitis-media-every-year>
- Homma, K., Du, Y. (2009). Ossicular resonance modes of the human middle ear for bone and air conduction. *J Acoust Soc Am., 125*(2), 968. doi: 10.1121/1.3056564
- Irvine, T. (2011, September 26). *Natural Frequencies of Beams Subjected to a Uniform Axial Load: Revision C*. Retrieved from [http://www.vibrationdata.com/tutorials2/beam\\_axial\\_load.pdf](http://www.vibrationdata.com/tutorials2/beam_axial_load.pdf)
- Iyer, A. (2017). Mastoid Surgery. Mastoid surgery. Retrieved January 14, 2022, from <https://www.entuk.org/mastoid-surgery>
- Jenks, C. M., Patel, V., Bennett, B., Dunham, B., & Devine, C. M. (2021). Development of a 3-Dimensional Middle Ear Model to Teach Anatomy and Endoscopic Ear Surgical Skills. *OTO open, 5*(4), 2473974X211046598.
- Kane, S., Paradise, E., Tanner, A., Torraca, T. (2020). Design and Stimulation of a Middle Ear Model to Aid with Otological Studies. *Worcester Polytechnic Institute*.

- Kent, C. (2021, June 9). *Audism and the ethics of childhood cochlear implantation*. Medical Device Network. Retrieved March 3, 2022, from <https://www.medicaldevice-network.com/analysis/audism-cochlear-implants/>
- Lee, D. H., Chan, S., Salisbury, C., Kim, N., Salisbury, K., Puria, S., & Blevins, N. H. (2010). Reconstruction and exploration of virtual middle-ear models derived from  $\mu$ CT datasets. *Hearing research*, 263(1-2), 198-203.
- Leong, A. C., & Aldren, C. (2007). 'Bones of contention': a donor register for temporal bone donation? *The Journal of Laryngology & Otology*, 121(10), 932-937.
- Lindberg, V. (2000, July 1). *Uncertainties and Error Propagation Part I of a manual on Uncertainties, Graphing, and the Vernier Caliper*. Uncertainties and Error Propagation. Retrieved February 22, 2022, from <https://www.geol.lsu.edu/jlorenzo/geophysics/uncertainties/Uncertaintiespart2.html>
- Liquid Silicone Rubber*. Protolabs. (n.d.). Retrieved January 12, 2022, from <https://www.protolabs.co.uk/services/injection-moulding/liquid-silicone-rubber/>
- Luers, J. C., & Hüttenbrink, K.-B. (2015). Surgical anatomy and pathology of the Middle Ear. *Journal of Anatomy*, 228(2), 338–353. <https://doi.org/10.1111/joa.12389>
- Materialise. (n.d.). *Locations: Germany*. Materialise. Retrieved February 22, 2022, from <https://www.materialise.com/de/about/locations/germany>
- Micro Photonics Inc. (2021, September 22). *What is MCT? an introduction*. Micro Photonics. Retrieved January 14, 2022, from <https://www.microphotonics.com/what-is-uct-an-introduction/>
- Ng, C. L., Liu, X., Chee, S. C. J., & Ngo, R. Y. S. (2015). An innovative 3-dimensional model of the epitympanum for teaching of middle ear anatomy. *Otolaryngology–Head and Neck Surgery*, 153(5), 832-837.
- Ossika, A. (2021). *Auditory ossicles*. Ken Hub. <https://www.kenhub.com/en/library/anatomy/auditory-Ossicles>
- Oxenham, A. J. (2018). How We Hear: The Perception and Neural Coding of Sound. *Annual Review of Psychology*, 69(1), 27–50. <https://doi.org/10.1146/annurev-psych-122216-011635>
- Prasad, K.C, Mohiyuddin, S. M., Anjali, P. K., ... Brindha, H. S. (2018). Microsurgical anatomy of the stapedius muscle: Anatomy revisited, redefined with potential impact in surgeries. *Indian J Otolaryngology Head Neck Surg.*, 71(1), 14-18. doi: 10.1007/s12070-018-1510-5
- Puria, S. (2013). 9 & 10. In *The Middle Ear: Science, otosurgery, and Technology* (pp. 253–304). essay, Springer.
- Physicslab: Wave fundamentals*. (n.d.). Retrieved January 14, 2022, from [http://dev.physicslab.org/Document.aspx?doctype=3&filename=WavesSound\\_Introducti onWaves.xml](http://dev.physicslab.org/Document.aspx?doctype=3&filename=WavesSound_Introducti onWaves.xml)
- Redwood, B. (2022). *Dimensional accuracy of 3D printed parts*. Hubs. Retrieved February 22, 2022, from <https://www.hubs.com/knowledge-base/dimensional-accuracy-3d-printed-parts/#fdm>
- Schediwy, S. W., Gras, S., Ju, L., & Blair, D. G. (2005, January). *High Q factor bonding using natural resin for reduced thermal noise of test masses*. AIP Publishing. Retrieved February 22, 2022, from <https://aip.scitation.org/doi/10.1063/1.1847654>

- SD3D. (n.d.) *PLA technical data sheet - SD3D printing*. Retrieved January 20, 2022, from [https://www.sd3d.com/wp-content/uploads/2017/06/MaterialTDS-PLA\\_01.pdf](https://www.sd3d.com/wp-content/uploads/2017/06/MaterialTDS-PLA_01.pdf)
- Shah, K. D., Bradoo, R. A., Joshi, A. A., & Sapkale, D. D. (2011). The efficiency of titanium middle ear prosthesis in ossicular chain reconstruction: Our experience. *Indian Journal of Otolaryngology and Head & Neck Surgery*, 65(4), 298–301. <https://doi.org/10.1007/s12070-011-0373-9>
- Sherif, H. A., & Almufadi, F. A. (2019, August 2). *Models for materials damping, loss factor, and coefficient of restitution*. ASME Digital Collection. Retrieved February 22, 2022, from <https://asmedigitalcollection.asme.org/materialstechnology/article-abstract/142/1/011006/955189/Models-for-Materials-Damping-Loss-Factor-and?redirectedFrom=fulltext>
- Silicone Dynamics. (2017, November 15). *Dimensional tolerances guide for silicone molded parts - custom silicone keypads: Silicone Dynamics, Inc.* Custom Silicone Keypads | Silicone Dynamics, Inc. Retrieved February 22, 2022, from <https://siliconedynamics.net/dimensional-tolerances-guide-for-more-functional-silicone-molded-parts/>
- Silva, A. A. (2017). Determining the speed of sound in the air by sound wave interference. *European Journal of Physics*, 38(4), 045802. <https://doi.org/10.1088/1361-6404/aa6d30>
- Sim, J. H., & Puria, S. (2008). Soft tissue morphometry of the malleus-incus complex from  $\mu$ CT imaging. *J Assoc Res Otolaryngology*, 9(1). doi: 10.1007/s10162-007-0103-x
- Sirak, K., Fernandes, D., Cheronet, O., ... Pinhasi, R. (2020). Human auditory ossicles as an alternative optimal source of ancient DNA. *Genome Research*, 30, 938. doi: 10.1101/gr.260141.119
- Sodhi, S., Singh, Z., Lal, J. (2017). Morphometric dimensions of human ear ossicles of males. *National Journal of Medical Research*, 7(1). [http://njmr.in/uploads/7-1\\_47-511.pdf](http://njmr.in/uploads/7-1_47-511.pdf)
- Sound: Characteristics, reflection of sound & hearing range. (2021, August 30). *Embibe Exams*. <https://www.embibe.com/exams/sound/>
- Tang, Z., Shen, Q., Xu, C., ... Li, S. (2017). Research on the characteristics of dynamic behavior of basilar membrane in spiral cochlea. *Journal of Vibroengineering*, 19(5), 3809-3821. doi: 10.21595/jve.2017.17911
- University of Michigan Health. (2020). Blocked eustachian tubes. Blocked Eustachian Tubes Michigan Medicine. Retrieved January 14, 2022, from <https://www.uofmhealth.org/health-library/uf9680>
- U.S. Department of Health and Human Services. (2018). Otosclerosis. National Institute of Deafness and Other Communication Disorders. Retrieved January 14, 2022, from <https://www.nidcd.nih.gov/health/otosclerosis>
- Vanaja, C. S., & Najula, P. (2003). *Middle Ear Resonant Frequency in Normal and Otosclerotic Ears: Effect of Procedural Variation*. Retrieved from <https://www.cjslpa.ca/detail.php?lang=en&ID=831>
- Waseem, M. (2020, March 9). *What is the prevalence of otitis media (om) among different age groups?* Latest Medical News, Clinical Trials, Guidelines - Today on Medscape. Retrieved January 14, 2022, from <https://www.medscape.com/answers/994656-8214/what-is-the-prevalence-of-otitis-media-om-among-different-agegroups#:~:text=Although%20OM%20can%20occur%20at,occurs%20after%20age%201%20year.>

- Wave properties: Speed, amplitude, frequency, and period—Physics / openstax.* (n.d.). Retrieved January 14, 2022, from <https://openstax.org/books/physics/pages/13-2-wave-properties-speed-amplitude-frequency-and-period>
- Withnell, R. H., & Gowdy, L. E. (2013). An analysis of the acoustic input impedance of the ear. *Journal of the Association for Research in Otolaryngology, 14*(5), 611–622. <https://doi.org/10.1007/s10162-013-0407-y>
- Wojciechowski, T., Skadorwa, T., Nève de Mévergnies, J. G., & Niemczyk, K. (2020). Microtomographic morphometry of the stapedius muscle and its tendon. *Anatomical Science International, 95*(1), 31-37.
- Zdilla, M. J., Skrzat, J., Kozerska, M., ... Wroński, S. (2018). Oval window size and shape: A  $\mu$ CT anatomical study with considerations for stapes surgery. *Otol Neurotol, 39*(5), 558-564. doi: 10.1097/MAO.0000000000001787
- Zhang, X., & Gan, R. Z. (2013, March). *Dynamic properties of human round window membrane in auditory frequencies running head: Dynamic properties of round window membrane.* Medical engineering & physics. Retrieved February 22, 2022, from <https://www.ncbi.nlm.nih.gov/pmc/articles/PMC3449020/>
- 3DPros. (2021). *Choosing infill percentage for 3D printed parts.* Retrieved February 9, 2022, from <https://www.3d-pros.com/choosing-infill-for-3d-printed-parts>

## Appendix A. Dr. Dobrev's Project Objective Rankings

	Least Important			Most Important	
<b>Digital Model of the Static Middle Ear</b>	<b>1</b>	<b>2</b>	<b>3</b>	<b>4</b>	<b>5</b>

*We define this digital model as one STL file containing all principal components of the middle ear (e.g., the tympanic membrane, a little bit of the ear canal, the ossicles, the oval window, round window, joints, ligaments, muscles, and other support structures).*

<b>Physical Model of the Static Middle Ear</b>	<b>1</b>	<b>2</b>	<b>3</b>	<b>4</b>	<b>5</b>
--	----------	----------	----------	----------	----------

*We define this static model as a durable replacement of the prior MQP model. The static model is not testable with force displacement or accelerometers. It is purely meant to show anatomy.*

<b>Digital Model of Dynamic Healthy Middle Ear</b>	<b>1</b>	<b>2</b>	<b>3</b>	<b>4</b>	<b>5</b>
--	----------	----------	----------	----------	----------

*We define this digital model as the STL files needed to print all the components of the middle ear including casts to create soft material parts.*

<b>Physical Model of the Dynamic Healthy Middle Ear</b>	<b>1</b>	<b>2</b>	<b>3</b>	<b>4</b>	<b>5</b>
---	----------	----------	----------	----------	----------

*Print all the components of the middle ear including casts to create soft material parts.*

<b>Digital Model of the Dynamic Diseased Middle Ear</b>	<b>1</b>	<b>2</b>	<b>3</b>	<b>4</b>	<b>5</b>
---	----------	----------	----------	----------	----------

*We define this model as the STL files needed to print interchangeable parts that can be switched into the healthy middle ear dynamic model.*

<b>Physical Model of the Dynamic Diseased Middle Ear</b>	<b>1</b>	<b>2</b>	<b>3</b>	<b>4</b>	<b>5</b>
--	----------	----------	----------	----------	----------

*Print the parts needed to replace healthy components in the original dynamic model to model various pathologies.*

<b>Testing the Physical Dynamic Model</b>	<b>1</b>	<b>2</b>	<b>3</b>	<b>4</b>	<b>5</b>
---	----------	----------	----------	----------	----------

*Stimulating the physical model with acoustic vibrations in both the healthy and diseased states, measuring, and analyzing the data (either with force displacement calculations or accelerometers with a corresponding code for signal acquisition).*

## Appendix B. MATLAB Code for Materials Testing in Ossicular Chain Replication

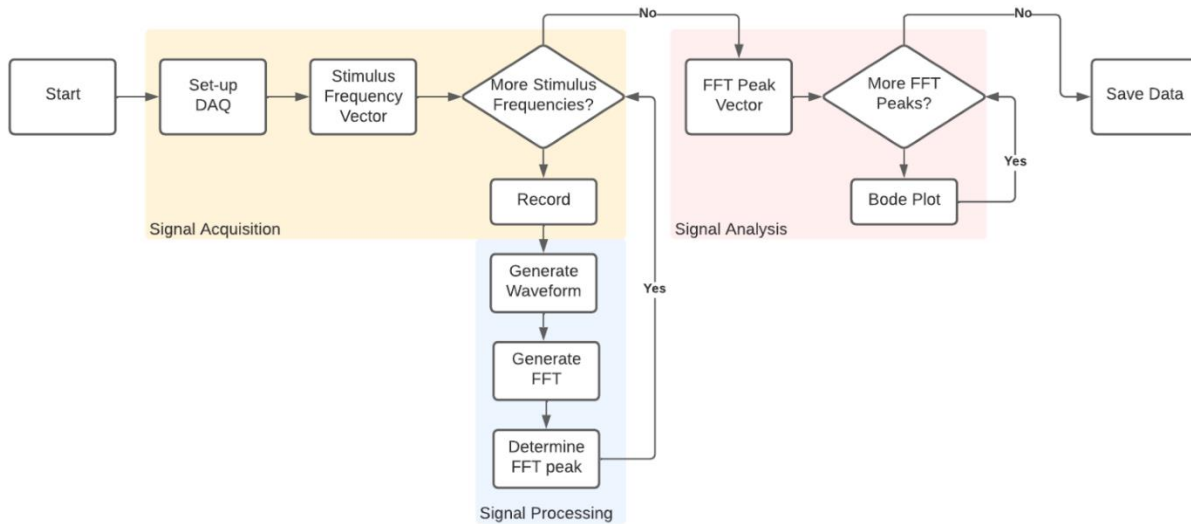


Fig. B.1. Simplified block diagram generated in Lucid chart to describe the code below

```

%Code generated by Dr. I. Dobrev, 2022
%% Clear all %%%%
close all
clc
clear all
disp(' ');
disp('All clean');
disp(' ');

%% Settings
data_dir_top = 'C:\MQP Signals\';
name_base = 'test';
cur_run = 0;%start with 0
f_s = 96000;% DAQ sampling rate

IN_ch_n=3; %number of input channels
disp('DAQ settings defined');

%% Setup Aquasition
%get a list of connected devices
devices = daq.getDevices;
%show info on the first device
devices(1)

%created DAQ session
s = daq.createSession('ni');

% Create inputs and output channels in DAQ session

%define input channels
IN_ch_index_vec = 0:(IN_ch_n-1);
addAnalogInputChannel(s,devices(1).ID, IN_ch_index_vec, 'Voltage');
  
```

```

%define output channels
addAnalogOutputChannel(s,devices(1).ID, [0], 'Voltage');

%set sampling rate and sampling type
s.Rate = f_s;%sampling rate Hz
s.IsContinuous = false;

%show DAQ session info
disp(s)

%% Define output and record

%Sampling param %%%%%%%%%%%
Sin_amp = 0.2; %V

t_s_block = 0.5;%sample time per iteration
f_res = 1/t_s_block; %frequency resolution

freq_steps = 10;%has to be an even number and you get one less

f_center = 100; %user entered natural frequency calculated from Equation 4.1
width_oct = 2;
f_min = f_center.*(2^(-width_oct));
f_max = f_center.*(2^(width_oct));

Sin_freq_before = f_min + (f_center-f_min).*sin(linspace(0,pi/2,freq_steps/2)); %ensures sample interval is smaller
when approaching the natural frequency from the right side
Sin_freq_after = fliplr(f_max - (f_max-f_center).*sin(linspace(0,pi/2,freq_steps/2)));%ensures sample interval is
smaller when approaching the natural frequency from the left side
Sin_freq = cat(2,Sin_freq_before,Sin_freq_after(2:end));

%rounds stimulus to integer Hz based on the sampling rate
Sin_freq = round(Sin_freq/f_res)*f_res; %creates the vector of stimulus frequency

iterations_n_req = 5;%number of iterations, or "trials", which are five segments taken from the recording,
normalized and overlaid on top of each other and used to calculate average waveforms and FFTs
%%%%%%%%%%

%%%%%%%%%% plotting param %%%%%%%%%%%
X_Tick = [10 20 50 100 120 150, 200];
XTickLabel = { '10', '20', '50', '100', '120', '150', '200'};
wave_plot_cycles_n = 5;
%%%%%%%%%%

%%%%%%%% variable settings %%%%%%%%%
clear Meas_Data
color_map = hsv(IN_ch_n);
iterations_n = iterations_n_req+1; %first one will be recorded but discarded later on
t_s_full = t_s_block.*iterations_n;
block_size = floor(f_s.*t_s_block);
S_n = block_size*iterations_n+1;%number of samples
%%%%%%%%

%update run number
cur_run = cur_run+1;
disp(' ');

```

```

disp(['Starting run ',num2str(cur_run)]);
start_time = tic;

for cur_freq = 1:numel(Sin_freq) %loops through each stimulus frequency

    %define time vector
    time_vec_full = linspace(0,t_s_full,S_n);
    %define stimulus signal waveform - sinusoidal
    Sin_wave = Sin_amp.*sin(2.*pi.*Sin_freq(cur_freq).*time_vec_full);
    Sin_wave = Sin_wave(:);

    disp(' ');
    disp(['Current stimulus frequency is ',num2str(Sin_freq(cur_freq)), 'Hz']);

    %queue output file
    tic
    queueOutputData(s,Sin_wave);

    % Run once per frequency

    disp('Starting aquasition.... ');

    %acquire data
    [data,time_vec,triggerTime] = startForeground(s);

    %remove first iter
    data = data((block_size+1):end,:);
    time_vec = time_vec((block_size+1):end) - t_s_block;

    disp(['Done with aquasition in ',num2str(toc,2),'s']);

    % reshape data into blocks %%%%%%%%%%%
    % block size is [time_samples_n X iter_n X Ch_n]
    wave_block = zeros(block_size,iterations_n_req,IN_ch_n);

    for cur_ch = 1:IN_ch_n
        wave_block(:, :,cur_ch) = reshape(squeeze(data(1:(end-1),cur_ch)),[block_size iterations_n_req]);
    end
    time_block = reshape(time_vec(1:(end-1)),[block_size iterations_n_req]);
    %average iterations
    wave_block_avg = median(wave_block,2);
    %%%%%%%%%%%

    %%%%%%%%%%% START of Processing %%%%%%%%%%%
    for cur_ch = 1:IN_ch_n
        for cur_iter_ind = 1:iterations_n_req

            % Extract 1 data
            waveform_1D = wave_block(:,cur_iter_ind,cur_ch);

            % calc FFT
            [FFT_spectrum_1D,f_vec_fft] = FFT_1D(waveform_1D,f_s);

            %allocate space to store fft spectrum
            if cur_iter_ind==1 && cur_ch == 1
                fft_n = numel(FFT_spectrum_1D);
            end
        end
    end
end

```

```

        %size is [FFT samples X Iterations X Channels]
        FFT_spectrum = NaN(fft_n,iterations_n_req,IN_ch_n); %generates FFT for each waveform
    end
    FFT_spectrum(:,cur_iter_ind,cur_ch) = FFT_spectrum_1D; %generates average FFT

end
end
FFT_spectrum_avg = median(FFT_spectrum,2);
%%%%%%%%%% END OF Processing %%%%%%%%%%%

%%%%%%%% collect raw data into a data structure %%%%%%%%%
Meas_Data(cur_freq).Stim_freq = Sin_freq(cur_freq);
Meas_Data(cur_freq).wave_block = wave_block;
Meas_Data(cur_freq).time_block = time_block;
Meas_Data(cur_freq).wave_block_avg = wave_block_avg;
Meas_Data(cur_freq).FFT_spectrum = FFT_spectrum;
Meas_Data(cur_freq).FFT_spectrum_avg = FFT_spectrum_avg;

%%%%%%%%%% plotting new data in detail%%%%%%%%%%

fig_name = ['Stimulus at ',num2str(Sin_freq(cur_freq)),'Hz'];
figure('name',fig_name,'units','normalized','outerposition',[0 0.05 1 0.95],'PaperPositionMode','auto','Color','w')

figure_title = [ {'Amp In'}, {'Amp Out'}, {'Accel'}] %sub-plot titles, cells must match number of input channels

for cur_ch = 1:IN_ch_n
    subplot(2, IN_ch_n, cur_ch)
    clear all_h

    %plot individual iterations
    % wave_block size is [waveform_samples_n X iter_n X Ch_n]
    cur_h = plot((time_block(:,1))*1000,(wave_block(:, :, cur_ch)),'.','Color',color_map(cur_ch,:));

    hold on
    %plot average
    % wave_block_avg size is [waveform_samples_n X 1 X Ch_n]
    all_h(cur_ch) = plot((time_block(:,1))*1000,(wave_block_avg(:, :, cur_ch)),'-','Color',color_map(cur_ch,:),'linewidth',3);
    title(figure_title{cur_ch})
    hold off

    %figure formatting
    xlim(1000*([ 0 wave_plot_cycles_n/Sin_freq(cur_freq)])); %Show the first N cycles only
    xlabel('ms');%X axis label
    ylabel({'Amplitude in [V]'})
    title([num2str(Sin_freq(cur_freq)),'Hz']) %Y axis label
    %legend({'Ch1'},'location','northeast')%Legend
    grid on

drawnow

subplot(2,IN_ch_n, cur_ch+IN_ch_n)
% %show data per channel
clear all_h

```

```

%plot individual iterations
% FFT_spectrum size is [FFT_vec_n X iter_n X Ch_n]
cur_h = semilogx(f_vec_fft,mag2db(abs(FFT_spectrum(:,:,cur_ch))),','Color',color_map(cur_ch,:));

hold on
%plot average
% FFT_spectrum_avg size is [FFT_vec_n X 1 X Ch_n]
all_h(cur_ch) = semilogx(f_vec_fft,mag2db(abs(FFT_spectrum_avg(:,:,cur_ch))),'-
','Color',color_map(cur_ch,:),'linewidth',3);
title(figure_title{cur_ch})

hold off

%figure formatting
xlim([Sin_freq(1)*0.9 Sin_freq(end)*1.2]);
ylim([-120 10]);
xlabel('Hz');%X axis label
set(gca,'XTick', X_Tick);
set(gca,'XTickLabel',XTickLabel);
ylabel({' Amplitude in [dB re. 1V]'})
grid on

drawnow
end
end%end of freq loop

disp(['Total time: ', num2str(toc(start_time),3),'s']);

%% Peaks of FFT vs Amplitude

cur_ch_out = 3; %accelerometer channel
cur_ch_in = 2; %speaker out channel

clear TF_avg

for cur_freq = 1:numel(Sin_freq)

%   cur_freq = 1

FFT_spectrum_avg = Meas_Data(cur_freq).FFT_spectrum_avg;
cur_ind = find(Sin_freq(cur_freq)<= f_vec_fft,1);
cur_ind = (cur_ind-1):(cur_ind+1);
cur_FFT_out = (squeeze(FFT_spectrum_avg(cur_ind,:,cur_ch_out)));
cur_FFT_in = (squeeze(FFT_spectrum_avg(cur_ind,:,cur_ch_in)));
[~, cur_FFT_out_max_ind] = max( abs(cur_FFT_out), [], 1);
[~, cur_FFT_in_max_ind] = max( abs(cur_FFT_in), [], 1);
cur_FFT_out_max = cur_FFT_out(cur_FFT_out_max_ind);
cur_FFT_in_max = cur_FFT_in(cur_FFT_in_max_ind);
cur_TF = cur_FFT_out_max./cur_FFT_in_max;

% cur_mag = squeeze(FFT_spectrum(cur_ind,:,cur_ch));

TF_avg(cur_freq,:) = cur_TF;
TF_avg_IN(cur_freq,:) = cur_FFT_in_max;
TF_avg_OUT(cur_freq,:) = cur_FFT_out_max;
end

```

```

figure
subplot(2,3,1)
semilogx(Sin_freq,mag2db(abs(TF_avg_IN)))
xlabel ('Hz')
ylabel ('Magnitude in [dB re. 1V]')
title ('Input Peak FFT Amplitude vs. Stimulus Frequency');
% legend('Amp In', 'Amp Out', 'Accelerometer')
grid on

subplot(2,3,4)
semilogx(Sin_freq,(angle(TF_avg_IN))./(2*pi))
xlabel ('Hz')
ylabel ('Phase in [cycles]')
% title ('Tranfer function (TF) vs stimulus freq')

subplot(2,3,2)
semilogx(Sin_freq,mag2db(abs(TF_avg_OUT)))
xlabel ('Hz')
ylabel ('Magnitude in [dB re. 1V]')
title ('Output Peak FFT Amplitude vs. Stimulus Frequency');
% legend('Amp In', 'Amp Out', 'Accelerometer')
grid on

subplot(2,3,5)
semilogx(Sin_freq,(angle(TF_avg_OUT))./(2*pi))
xlabel ('Hz')
ylabel ('Phase in [cycles]')
% title ('Tranfer function (TF) vs stimulus freq')

subplot(2,3,3)
semilogx(Sin_freq,mag2db(abs(TF_avg)))
xlabel ('Hz')
ylabel ('Magnitude in [dB re. Input]')
title ('TF = output vs input');
% legend('Amp In', 'Amp Out', 'Accelerometer')
grid on

subplot(2,3,6)
semilogx(Sin_freq,(angle(TF_avg))./(2*pi))
xlabel ('Hz')
ylabel ('Phase in [cycles]')
% title ('Tranfer function (TF) vs stimulus freq')
%%
TF_mag = abs(TF_avg);
[Q, f_max, f_delta] = Q_factor_est(TF_mag,Sin_freq,0.001);
%% Save data
tic
%disp(' ');
disp('Saving all data');
filename_mat = [data_dir_top,'\', name_base,'_data_',num2str(cur_run), '.mat'];
disp(['Saving: ',filename_mat]);

save(filename_mat,'Meas_Data','-v7.3');
disp(['Saved data structure: ', num2str(toc,3),'s']);
%%%%%%%%%% END %%%%%%%%%%%

```

## Appendix C. Data for Material Testing in Compliant Primary Body Replication

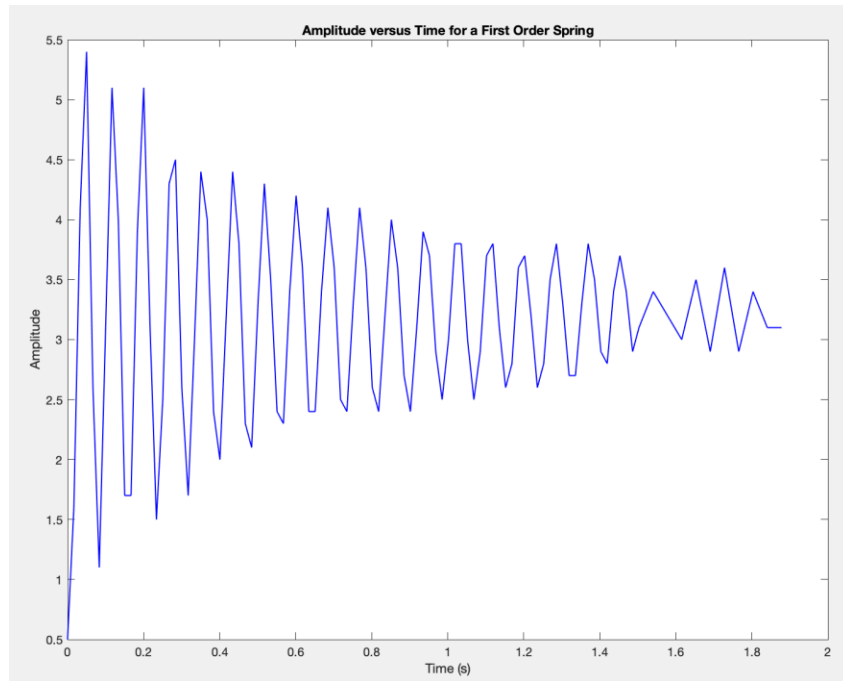


Fig.C.1. Raw data for the silicone specimen

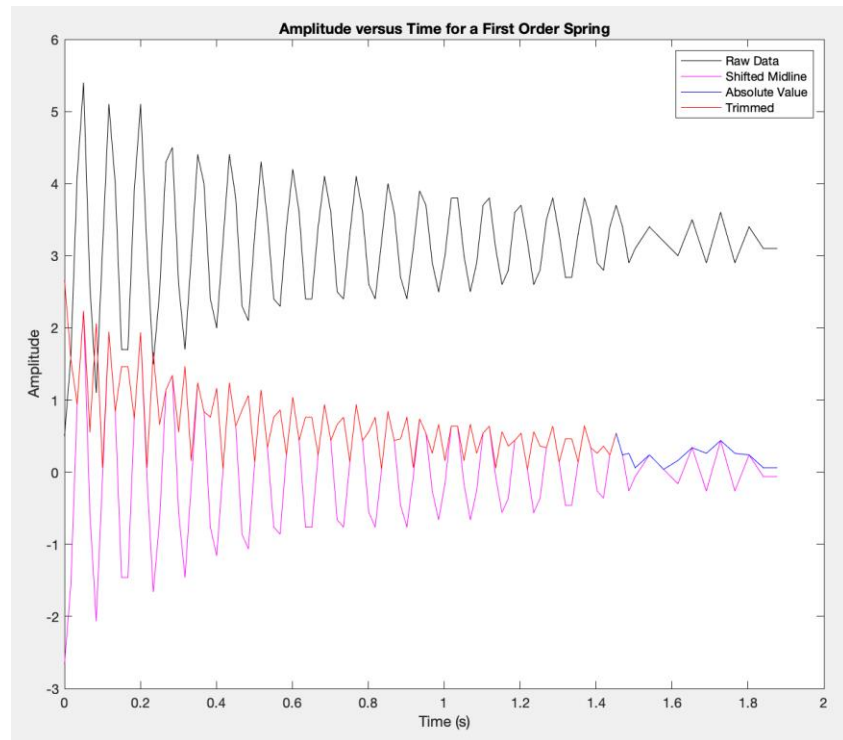


Fig.C.2. Processed data for the silicone specimen

## Appendix D. MATLAB Code for Materials Testing in Compliant Primary Body Replication

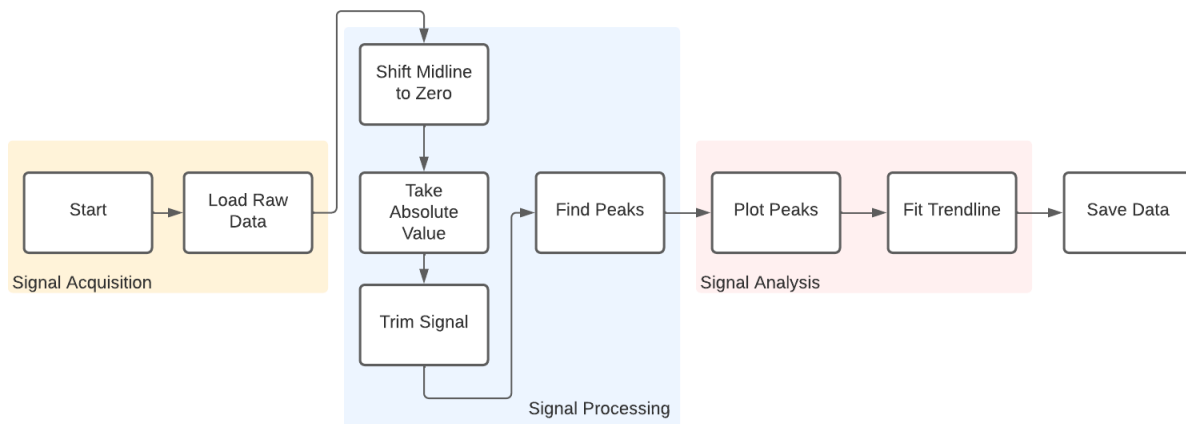


Fig. D.1. Simplified block diagram generated in Lucid chart to describe the code below

### Primary Code

```
%% Set Up
clc
clear all
close all

%% Read from Excel
[~, ~, dat] = xlsread('TPU video results.xlsx');
X_raw = dat(:,3);
X = cell2mat(X_raw);
Y_raw = dat(:,4);
Y = cell2mat(Y_raw);

%Plot Raw Data
plot(X, Y, '-b','LineWidth',1)
xlabel('Time (s)')
ylabel('Amplitude')
title('Amplitude versus Time for a First Order Spring')

%% Initial Trimming and Processing
%adapted from Dr. Ivo Dobrev, 2022
Expected_SNR = 6;

% Convert Signal from DC to AC, giving midline of 0
Y_AC = Y - mean(Y);
Y_AC_abs = abs(Y_AC);

%find beginning of signal - maximum response
[Y_max, Y_max_ind] = max(Y_AC_abs);
%remove the beginning
Y_AC_abs_trimmed1 = Y_AC_abs(Y_max_ind:end);
X_trimmed1 = X(Y_max_ind:end);

%find the end of the useful signal - maximum detectable response
```

```

Y_min = Y_max./Expected_SNR;
Y_min_ind = find(Y_AC_abs_trimmed1>Y_min,1,'last');
%remove the end
Y_AC_abs_trimmed2 = Y_AC_abs_trimmed1(1:Y_min_ind);
X_trimmed2 = X_trimmed1(1:Y_min_ind);
X_offset_ms = 1000.*X(Y_max_ind);

figure
plot(X,Y,'-k')
hold on
plot(X,Y_AC,'-m')
plot(X,Y_AC_abs,'-b')
plot(X_trimmed2, Y_AC_abs_trimmed2,'r') %Used in data analysis
title ('Amplitude versus Time for a First Order Spring')
xlabel('Time (s)')
ylabel('Amplitude')
legend('Raw Data', 'Shifted Midline', 'Absolute Value', 'Trimmed')

%% Data Analysis
%adapted from Dr. Ivo Dobrev, 2022
[pks, locs] = findpeaks(Y_AC_abs_trimmed2); %finds peaks in trimmed signal and their location along the time
vector
X_values = X_trimmed2(locs);
plot (X_values, pks)
title ('Amplitude versus Time for Peaks of Trimmed Signal')
xlabel('Time (s)')
ylabel('Amplitude')
exponential_curve_fit(X_values, pks) %MATLAB generated function from the curve fitting app which fits an
exponential decay curve to the peaks of the trimmed signal

%%%%%%%%%END%%%%%%%%%

```

## Exponential Curve Fit Function

```

function [fitresult, gof] = exponential_curve_fit(X_values, pks)
%CREATEFIT(X_VALUES,PKS)
% Create a fit.
%
% Data for 'untitled fit 1' fit:
% X Input : X_values
% Y Output: pks
% Output:
% fitresult : a fit object representing the fit.
% gof : structure with goodness-of fit info.
%
% See also FIT, CFIT, SFIT.
% Auto-generated by MATLAB on 15-Feb-2022 10:28:01
%% Fit
[xData, yData] = prepareCurveData( X_values, pks );

% Set up fitype and options.
ft = fittype( 'exp1' );
opts = fitoptions( 'Method', 'NonlinearLeastSquares' );
opts.Display = 'Off';
opts.StartPoint = [1.93390137557937 -1.02360397808716];

```

```
% Fit model to data.
[fitresult, gof] = fit( xData, yData, ft, opts );

% Plot fit with data.
figure( 'Name', 'untitled fit 1' );
h = plot( fitresult, xData, yData );
legend( h, 'Trimmed Signal Data Points', 'MATLAB Generated Trendline', 'Location', 'NorthEast' );
% Label axes
xlabel ('Time (s)')
ylabel ('Amplitude')
grid on
end
```

## Appendix E. Materials Needed for Assembly

<b>Material</b>	<b>Count</b>
5mm x 2 mm Magnets	30
Small Rubber Bands	2
Thick Rubber Bands	6
Glue	1
Wire	~30 cm
VMQ 3 mm Silicone Cord	1 m
Breadboard	1
M6 Screws and Washers	8-16

## Appendix F. Bode Plots Used in Ossicle Material Selection

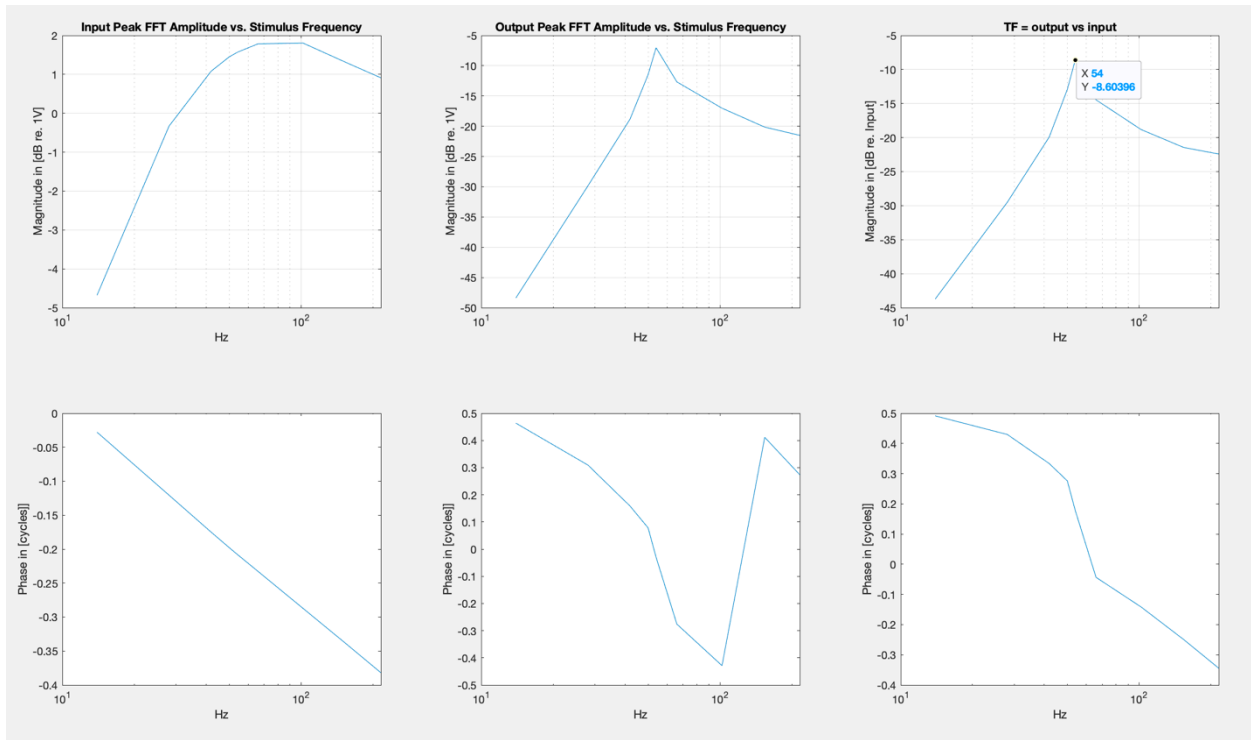


Fig. E.1. PLA Trial 1

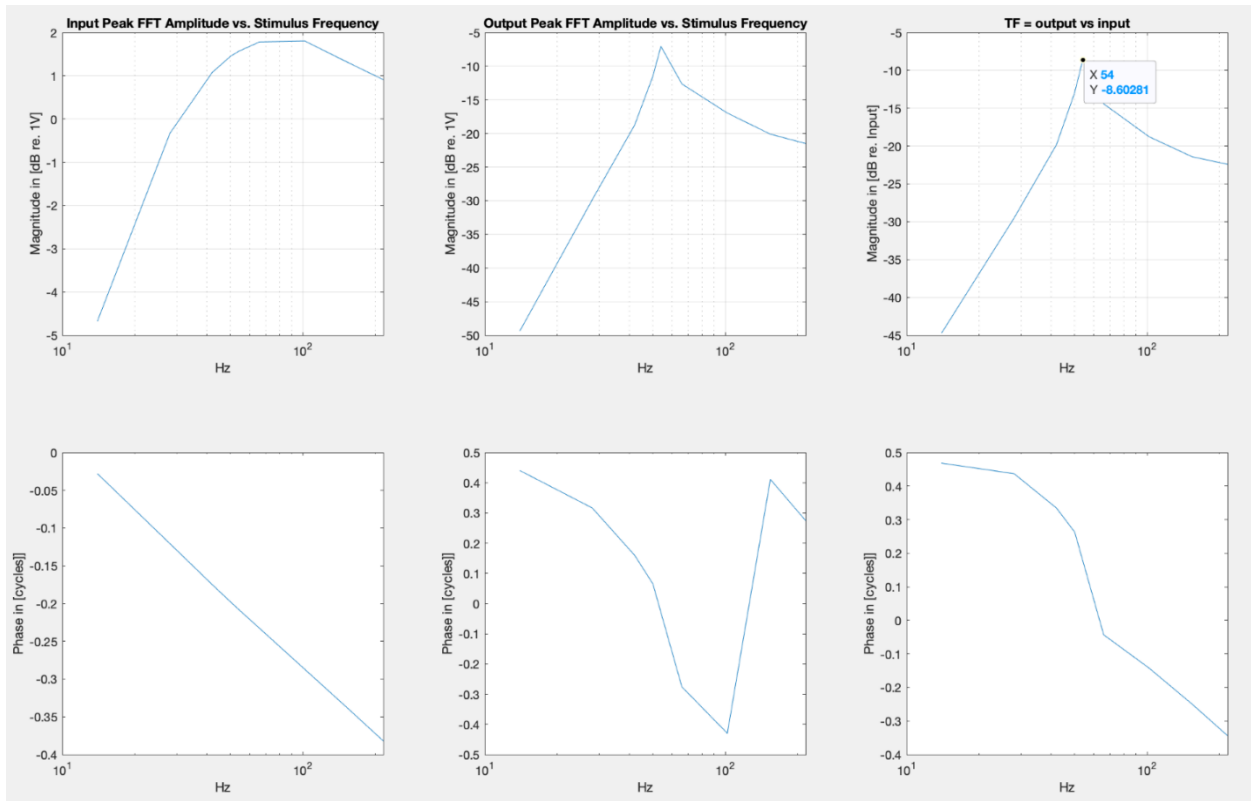


Fig. E.2. PLA Trial 2

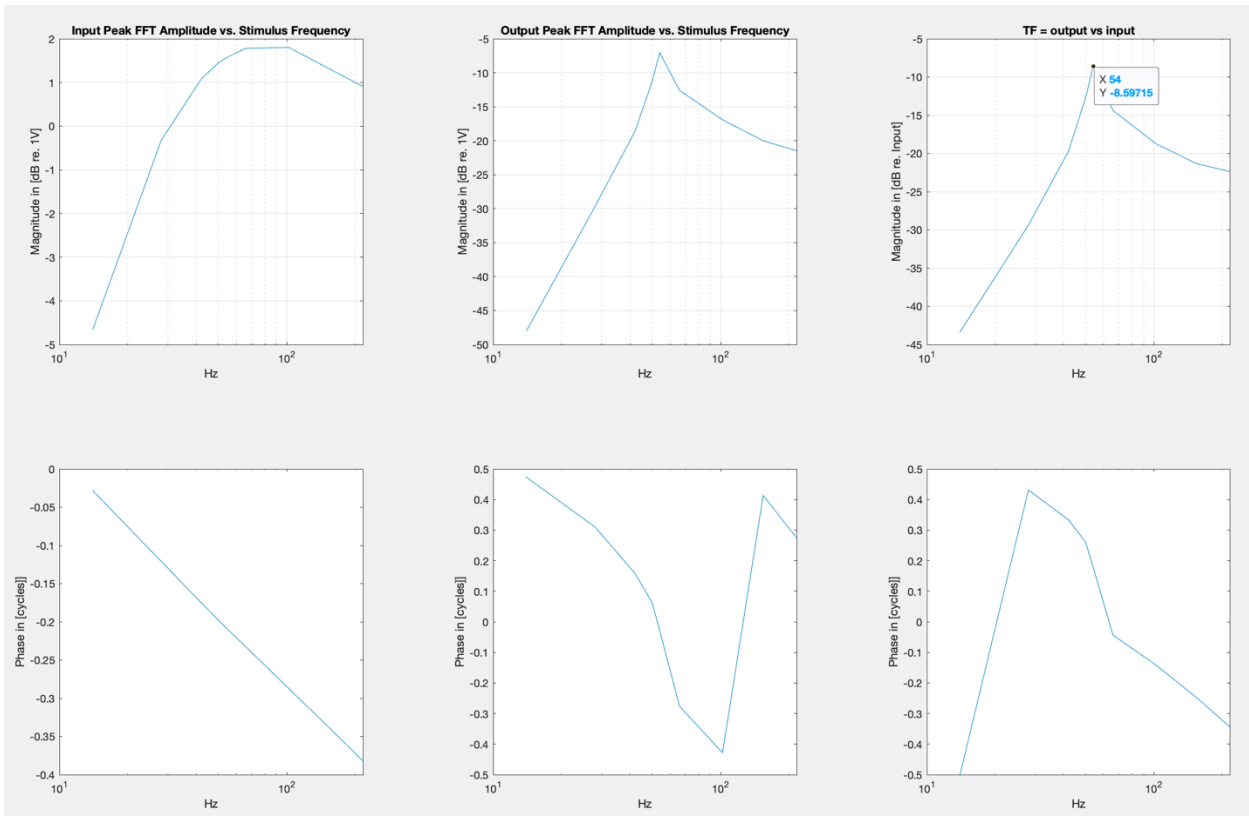


Fig. E.3. PLA Trial 3

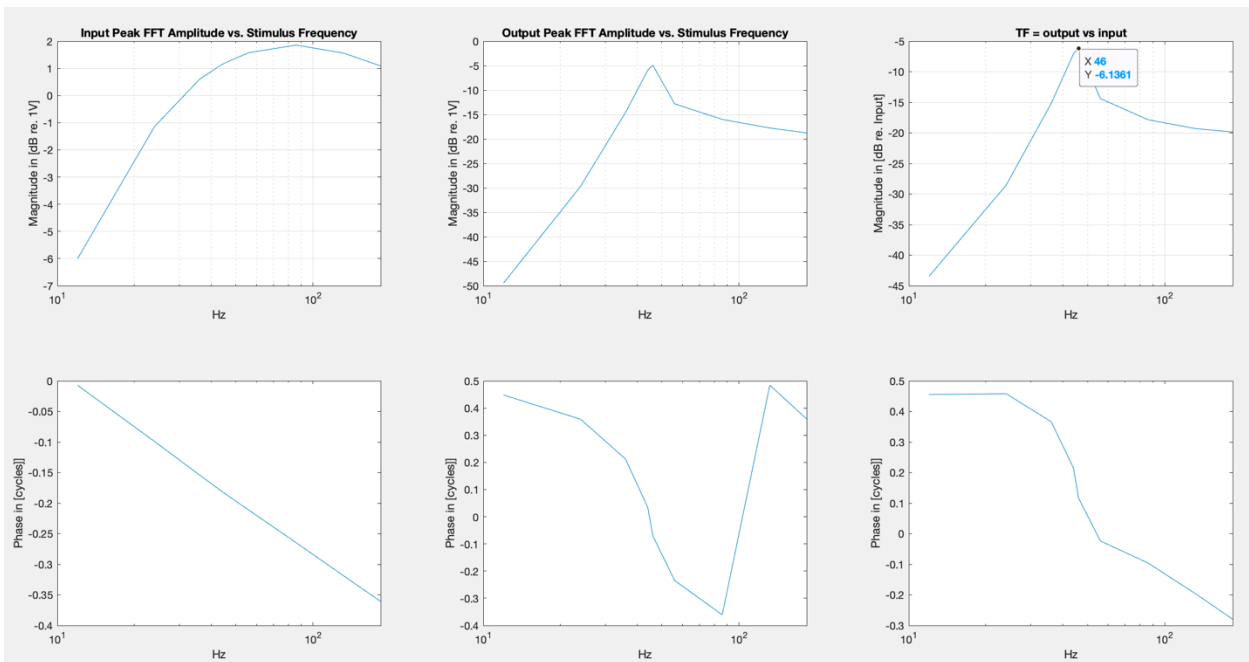


Fig. E.4. ABS Trial 1

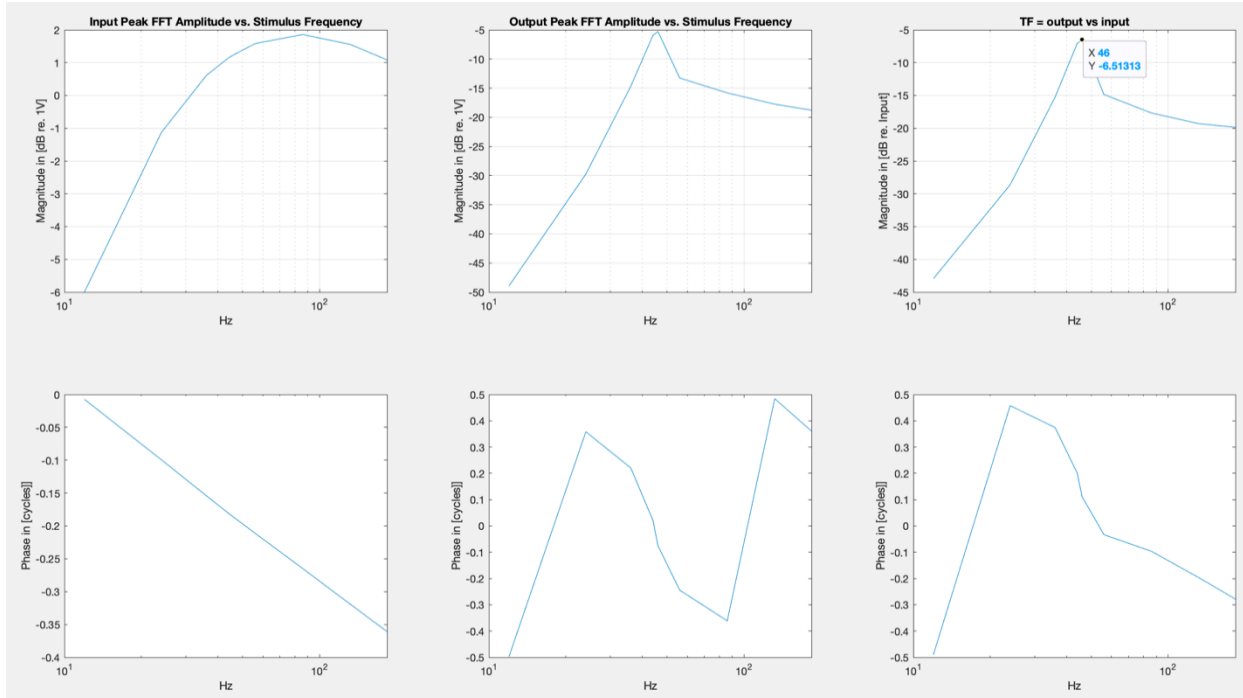


Fig. E.5. ABS Trial 2

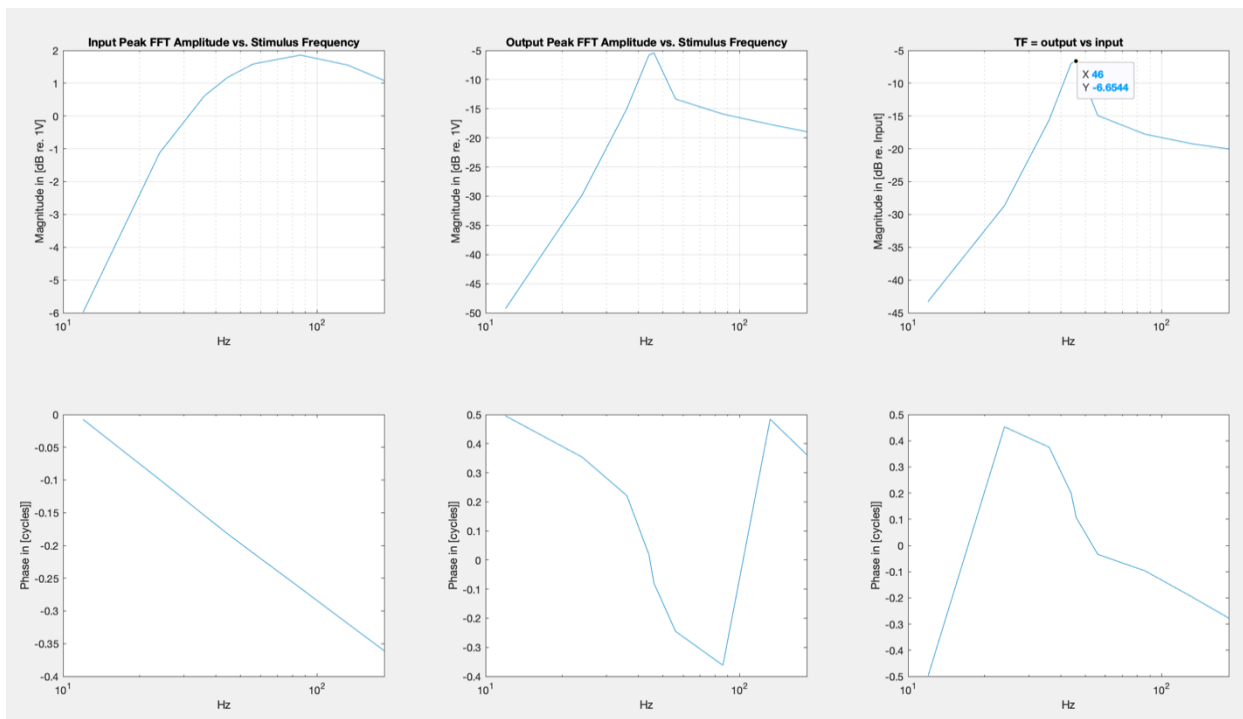


Fig. E.6. ABS Trial 3

## Appendix G. Sample Uncertainty Calculations

The following calculations follow the uncertainty analysis for the TPU specimen tested using force-displacement video capture. The calculated time constant was  $0.047 \pm 0.014$  seconds, and the period was 0.013 seconds. From Burwell and Strang, the logarithmic decrement can be calculated (1952).

$$\delta = \frac{P}{\tau} = \frac{0.013s}{0.047s} = 0.28$$

The uncertainty is propagated using the equation below, which can be used when two variables are simply multiplied or divided (Lindberg, 2000).

$$\frac{\Delta\delta}{\delta} = \sqrt{\left(\frac{\Delta P}{P}\right)^2 + \left(\frac{\Delta\tau}{\tau}\right)^2}$$

Because there is no associated uncertainty with the damped period, the first term under the square root goes to zero. The uncertainty equation can be simplified and re-expressed with the calculated values.

$$\frac{\Delta\delta}{0.28} = \sqrt{\left(\frac{0.014}{0.47}\right)^2} \quad \therefore \Delta\delta = 0.08$$

The uncertainty of the logarithmic decrement is then propagated when calculating the damping ratio, shown in the equation below (Burwell & Strang, 1951).

$$\zeta = \frac{\delta}{\sqrt{(2\pi)^2 + \delta^2}} = \frac{0.28}{\sqrt{(2\pi)^2 + 0.28^2}} = 0.04$$

Because there are no simple mathematical operations (e.g., addition, multiplication), the uncertainty must be calculated using partial derivatives as shown in Lindberg's general equation below which X, W, and Y are independent variables of the function Z (2000).

$$\Delta z^2 = \left(\frac{\partial f}{\partial w}\right)^2 \Delta w + \left(\frac{\partial f}{\partial x}\right)^2 \Delta x + \left(\frac{\partial f}{\partial y}\right)^2 \Delta y$$

Because the only variable to solve for the damping ratio is the logarithmic decrement, the uncertainty analysis can be simplified in the set of equations below.

$$\begin{aligned} \Delta\zeta^2 &= \left(\frac{\partial\zeta}{\partial\delta}\right)^2 \Delta\delta \\ \Delta\zeta^2 &= \left(\frac{4\pi^2}{(4\pi^2 + \delta^2)\sqrt{4\pi^2 + \delta^2}}\right)^2 \Delta\delta \\ \Delta\zeta^2 &= \left(\frac{4\pi^2}{(4\pi^2 + 0.28^2)\sqrt{4\pi^2 + 0.28^2}}\right)^2 0.08 \quad \therefore \Delta\zeta = 0.02 \end{aligned}$$

The damping ratio is used to find the Q factor in the equation below (Burwell & Strang, 1951).

$$Q = \frac{1}{2\zeta} = \frac{1}{2(0.04)} = 11$$

Similar to the uncertainty calculation for the logarithmic decrement, the uncertainty can be calculated for Q as follows (Lindberg, 2000).

$$\frac{\Delta Q}{Q} = \sqrt{\left(\frac{\Delta \zeta}{\zeta}\right)^2}$$

$$\frac{\Delta Q}{11} = \sqrt{\left(\frac{0.02}{0.04}\right)^2} \quad \therefore \Delta Q = 6$$

Therefore, the final answer with propagated uncertainty is  $Q = 11 \pm 6$ .

## Appendix H. Common Diseases

Chronic otitis media (COM) is a disease affecting 709 million people worldwide, with 80-90% of cases in children under 6 years old (Waseem, 2020; Hear-it, 2013). COM causes chronic inflammation of the middle ear and mastoid, the bony area directly behind the ear (Iyer, 2017; Puria, 2013). This inflammation can result in the partial or total loss of the ossicles and/or tympanic membrane (TM), which results in hearing loss under 60-70 dB (Puria, 2013). For comparison, a human's whisper creates about 30 dB of sound, a normal conversation creates about 60 dB, and a car horn 16 feet away creates about 100 dB (Centers for Disease Control and Prevention, 2019).

COM can develop in two ways: COM with cholesteatoma and COM without cholesteatoma. Cholesteatoma is an abnormal skin growth behind the eardrum that gradually expands and creates pressure on other middle ear structures, which eventually can lead to the destruction of the structures (Luers & Hüttenbrink, 2015). COM with cholesteatoma is indicated by a perforation in the TM and COM without cholesteatoma by a perforation in the pars tensa (Puria, 2013). Ears with both types of COM often have a dysfunctional Eustachian tube, the tube that connects the middle ear to the back of the throat, and abnormal static pressure—two major reasons for the loss of hearing (University of Michigan Health, 2020; Puria, 2013). Severe COM can result in tympanosclerosis, which involves progressive fixation and stiffening of primary bodies around the tympanic membrane ([Aslan et al., 2009](#)). COM is the most common disease to develop out of all the possible middle ear diseases, so it is crucial to understand the varying surgical treatments that are currently available.

Another common disease is otosclerosis, which affects more than 3 million Americans (Cleveland Clinic, 2021). Otosclerosis is a genetic disorder that affects the optic capsule bones at the area anterior to the oval window (Puria, 2013). This disorder develops a lesion in the oval window area that leads to the progressive fixation of the stapes, therefore also resulting in conductive hearing loss (Puria, 2013). Unlike COM, the physiology of the middle ear and mastoid remain unaffected and functioning. This means that the main challenge when completing a surgical procedure is eliminating the mechanical fixation of the stapes and allowing for the typical fluid movement.

### *Surgical Procedures and Clinical Treatments*

Since COM and otosclerosis can affect most aspects of the middle ear, there are numerous surgical procedures and accompanying treatments tailored to repair the middle ear and restore hearing in patients. These procedures, which are further discussed in the following sections, can either aim to repair just one part of the middle ear or multiple aspects at once.

#### *Tympanoplasty*

When the middle ear is affected by chronic otitis media, a surgical procedure is typically needed to reconstruct the tympanic membrane and/or the ossicles. This procedure is called tympanoplasty and it has two main subtypes: myringoplasty and ossiculoplasty. Myringoplasty, more commonly known as TM reconstruction, aims to repair the TM by using tissue grafts

(Puria, 2013). These grafts are inserted using an overlay technique which can create a high risk for covering the epithelium, the body tissue covering all internal and external surfaces of the body, and developing scarring (U.S. Department of Health and Human Services, 2018; Luers & Hüttenbrink, 2015).

Ossiculoplasty, more commonly known as ossicular reconstruction, repairs one or more of the damaged ossicles. The ossiculoplasty procedure often utilizes the implementation of prosthetics to restore a functioning middle ear. If the ossicles are missing or too diseased to be reused, synthetic implants are introduced to reconstruct the ossicular chain (Puria, 2013). If the stapes is present in the chain, a prosthesis is placed from the TM to the head of the stapes, termed a partial ossicular replacement prosthesis (PORP) (Puria, 2013). If the stapes is not present, a prosthesis is placed between the TM and the stapes footplate, termed a total ossicular replacement prosthesis (TORP). PORPs and TORPs are typically made of titanium or hydroxyapatite. However, titanium is favored for prostheses because it has low stiffness, is lightweight, and is biocompatible (Luers & Hüttenbrink, 2015; Puria, 2013). Titanium also has a greater ability to effectively restore and transmit sound compared to hydroxyapatite (Shah et al., 2011).

### *Mastoidectomy*

Tympanoplasty is typically performed in conjunction with mastoidectomy—a surgical procedure where the mastoid is opened, and mastoid air cells are drilled away to remove middle ear infection (Puria, 2013). COM is often the cause of these infections, and there are two types of mastoidectomies: canal wall-up and canal wall-down. Canal wall-up removes the mastoid air cells while still preserving the posterior wall and is performed when the mastoid cavity is large (Luers & Hüttenbrink, 2015; Puria, 2013). Canal-wall down completely removes the posterior bony canal wall and is performed when the mastoid cavity is very narrow (Luers & Hüttenbrink, 2015).

### *Stapedectomy*

The last major surgical procedure for the middle ear is a stapedectomy. This procedure is done when a damaged stapes is removed and then replaced by an artificial prosthesis. Stapedectomies aim to restore conductive hearing loss in patients that have a fixed stapes due to otosclerosis (Puria, 2013). Similar to the other procedures, there are two main types: a total stapedectomy and a stapedotomy. A total stapedectomy is when the entire stapes footplate is removed. A stapedotomy is when a small opening of about 0.5mm is created in the footplate and a piston-like prosthesis is implanted into the opening (Luers & Hüttenbrink, 2015). The other side of the prosthesis is connected to the long process of the incus, and once the attachment is secured, the ossicular chain will move together and create vibrations in the prosthesis to be converted into sound (Luers & Hüttenbrink, 2015).

Prosthetic implants for a stapedectomy, specifically the stapedotomy, are typically made of titanium and Teflon. While Teflon is relatively inert, it is not resorbed by the body and has the ability to extrude, therefore making titanium an overall more suitable material (Puria, 2013). Studies have found that larger diameter prosthetics are more effective in restoring conductive

hearing loss (Puria, 2013). All in all, the surgical procedures and implants discussed have proven to be successful in reconstructing the middle ear anatomy and restoring conductive hearing in patients.